3-22-2012

Augmenting the Global Positioning System with Foreign Navigation Systems and Alternative Sensors

Christopher B. Killion

AUGMENTING THE GLOBAL POSITIONING SYSTEM WITH FOREIGN NAVIGATION SYSTEMS AND ALTERNATIVE SENSORS

THESIS

Christopher B. Killion, Second Lieutenant, USAF

AFIT/GE/ENG/12-24

DEPARTMENT OF THE AIR FORCE
AIR UNIVERSITY

AIR FORCE INSTITUTE OF TECHNOLOGY

Wright-Patterson Air Force Base, Ohio

The views expressed in this thesis are those of the author and do not reflect the official policy or position of the United States Air Force, the Department of Defense, or the United States Government.

AFIT/GE/ENG/12-24

AUGMENTING THE GLOBAL POSITIONING SYSTEM WITH FOREIGN NAVIGATION SYSTEMS AND ALTERNATIVE SENSORS

THESIS

Presented to the Faculty

Department of Electrical and Computer Engineering

Graduate School of Engineering and Management

Air Force Insitute of Technology

Air University

Air Education and Training Command

in Partial Fulfillment of the Requirements for the

Degree of Master of Science in Electrical Engineering

Christopher B. Killion, B.S.E.E.

Second Lieutenant, USAF

March 2012

AFIT/GE/ENG/12-24

AUGMENTING THE GLOBAL POSITIONING SYSTEM WITH FOREIGN NAVIGATION SYSTEMS AND ALTERNATIVE SENSORS

Christopher B. Killion, B.S.E.E.
Second Lieutenant, USAF

Approved:

/signed/	5 March 2011
Lt Col Michael J. Stepaniak, PhD (Chairman)	Date
/signed/	5 March 2011
Meir Pachter, PhD (Committee Member)	Date
/signed/	5 March 2011
John F. Raquet, PhD (Committee Member)	Date

Abstract

The United States Global Positioning System, with its great accuracy, receives extensive use by civilians and military organizations throughout the world. However, in areas with limited or partially obstructed views of the sky, such as amongst tall buildings or imposing geographic features, a position solution can be difficult or impossible to obtain as the limited view of the sky decreases the number of visible satellites. Augmenting the GPS constellation by receiving signals from foreign satellite navigation systems as well using measurements from inertial and barometric sensors can increase the availability of a position solution in a degraded reception environment.

This thesis investigates combining the GPS system with the Galileo, GLONASS, and Compass foreign navigation systems, a barometric altimeter, and inertial sensors. Data for the GPS and GLONASS systems were collected and the data for the Galileo and Compass systems were simulated. A model of downtown Dayton, OH was constructed and various combinations of the systems were tested throughout the model to measure the availability of a position solution. An algorithm was also created to investigate augmenting GPS with the minimum necessary number of foreign satellites. A simulation was then setup for an autonomous aerial vehicle flight through the model using a Kalman Filter to combine the various sensors with GPS.

Augmenting GPS showed great improvements in availability throughout the model of downtown Dayton. Furthermore, augmenting the GPS system with foreign systems allowed the autonomous aerial vehicle to successfully navigate in the simulation whereas using only GPS, the vehicle was unable to navigate successfully. This opens up the urban environment to more robust navigation solutions for people on the ground as well as allows for unmanned aerial vehicles to expand their area of operation.

Table of Contents

List of Figures

List of Tables

List of Abbreviations

Augmenting the Global Positioning System with Foreign Navigation Systems and Alternative Sensors

1 Introduction

1.1 Motivation

Information plays a major role in any conflict. In battle, commanders desire as much accurate and timely information as possible. Accurate position information of both friendly and enemy forces, as well as equipment and potential targets drives strategy and plans on the battlefield. In today's world of advanced technology, the United States Armed Forces heavily rely on the Global Positioning System (GPS) to obtain precise position information. Concurrently with the development of GPS, conflicts have shifted from the open battlefields of years past to the confines of urban population centers. These urban centers impede the use of GPS. Tall or closely spaced buildings create "urban canyons" which block the view of the sky (and therefore the line of sight to the orbiting satellites) rendering the GPS receivers unable to achieve a position solution. This loss of position information may mean that ground troops do not know where exactly they are located and cannot call for precision ordinance, or it may mean that a small unmanned aerial vehicle can no longer perform it's mission of autonomously flying through a neighborhood collecting intelligence and mapping the area.

GPS receivers require four visible satellites to compute their locations. If there are not four visible satellites, then no positioning information is available. Not only must there be an adequate amount of satellites, but they must have proper geometry, that is, they must be spaced out over the sky. If there are four visible satellites but they are clustered in

a small area of the sky, then the position solution produced will be erroneous and unusable. This exemplifies the issues of GPS in an urban environment. Buildings can block large portions of the sky limiting the number of satellites in view as well as concentrating the satellites in view to a small portion of the sky.

GPS is just one global navigation satellite system (GNSS). Russia has an operational system called GLONASS and the European Union and China have plans for their own systems, Galileo and Compass, respectively. When all these systems become operational, there will be over 100 navigation satellites in orbit. If a receiver could use satellites from all the constellations instead of only GPS, then users in urban environments could have a more reliable and robust source of positioning information.

Currently, there are civil receivers that process signals from all the GPS and GLONASS satellites in view. These, however, do not utilize the encrypted military signal from GPS or have the ability to minimize the number of non-GPS satellites used.

GPS is a good system but has faults and shortcomings in certain situations which augmentation, both by other systems and alternative sensors, could relieve.

1.2 Problem Statement

GPS gives unprecedented performance and accuracy in determining the location of a receiver. This technology has given the military the ability to drop munitions in all weather conditions with accuracy that has never before been achieved as well as opened doors to autonomously-navigating unmanned vehicles on land and in the air. However, the United States Armed Forces are currently using only standalone GPS for their satellite navigation which limits receivers to approximately 30 satellites. However, the National Space Policy from 2010 directed that foreign GNSSs could be used to augment GPS [33]. These receivers could benefit from augmentation in the form of other countries' and organizations' navigation satellites as well as a barometric altimeter and inertial sensors optimized by Kalman filtering.

This thesis investigates the advantages of augmenting GPS with foreign satellite navigation systems as well as a barometric altimeter and Kalman filtering while in an urban environment consistent with degraded reception and accuracy. Availability of an acceptable position solution is the metric by which various augmentation techniques and styles will be compared.

1.3 Thesis Overview

Chapter 2 gives a general background and overview of the current and planned GNSSs, barometric-altimeters, and presents some related research. In Chapter 3, the simulation, assumptions, scenario, position estimation, dilution of precision, and weighted least squares are discussed. Chapter 4 presents and analyzes the outcomes of the simulation. Chapter 5 discusses the results of the research as well as possible outcomes from the effort and recommendations for further research.

2 Background

2.1 Overview

The purpose of this chapter is to present information relevant to this research effort. An overview of satellite navigation is covered in Section 2.2. Sections 2.3 to 2.6 discuss the individual satellite navigation systems of GPS, GLONASS, Compass and Galileo. Then, barometric altimeters are reviewed in Section 2.7 Finally a literature review concludes the chapter in Section 2.9.

2.2 Satellite Navigation

Satellite navigation, at its core, consists of very basic principles. The distance between two points can be determined if something travels in a straight line between the two points and the time it took to traverse the distance and the speed it traveled are both known. Intuitively, this makes sense. If a vehicle travels for one hour at a speed of 60 miles per hour between points A and B, then points A and B must be 60 miles apart. Satellite navigation uses and expands upon this principle.

To determine the location of a receiver using a satellite constellation, the scenario changes. To simplify the initial explanation, the two-dimensional case will be considered. Instead of knowing the locations of points A and B and trying to find the distance between them, only the location of point A, the satellite, is known. The satellite transmits a signal which travels, ideally, in a straight line at the speed of light from the satellite to the receiver. The receiver detects and decodes the signal and discerns how long it took the signal to travel from the satellite to the receiver. Because the traverse time and speed are known, the distance between the satellite and the receiver is known. By itself, this information does not uniquely locate the receiver. This information confines the receiver's location to a circle surrounding the satellite where the radius of the circle is the distance

calculated by the time of transit of the signal, but the specific location of the receiver on the circle is yet unknown. This is shown in Figure 2.1.

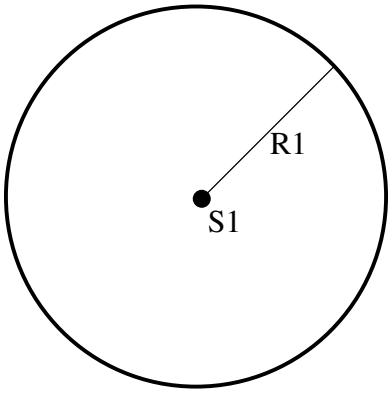

Figure 2.1: Circle of possible locations around a single satellite.

To establish a more accurate position, the receiver acquires another measurement from a different satellite. This new measurement also confines the receiver location to a circle surrounding the second satellite. With two measurements in hand, the receiver knows that its location must be on *both* circles. These circles will intersect at two points which are the possible locations of the receiver. This is demonstrated in Figure 2.2.

A third measurement is included from yet another satellite to uniquely define the location of the receiver. The circle of location from this third satellite will intersect with only one of the two previous intersections thereby resolving the location of the receiver which can be seen in Figure 2.3.

To expand this to the three-dimensional, real world scenario, the possible locations from each satellite are limited not to a circle, but to a sphere where the radius is the distance calculated by the time of transit of the signal. The intersection of the spheres of the first and second satellites forms a circle. The sphere from the third satellite intersects this circle at two points and now in three dimensions a fourth satellite could be

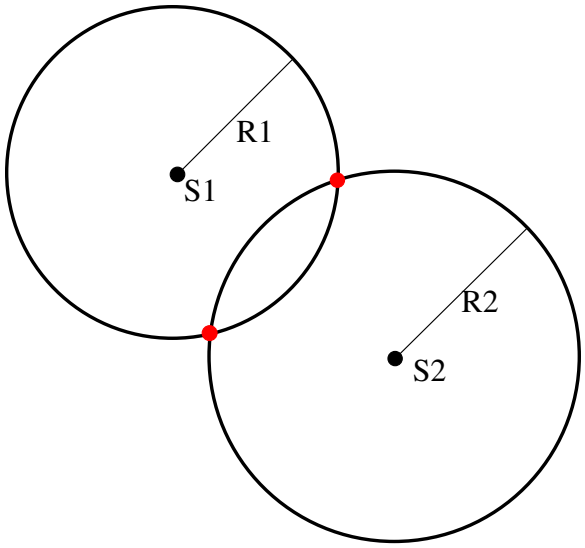

Figure 2.2: Two possible locations with two satellites.

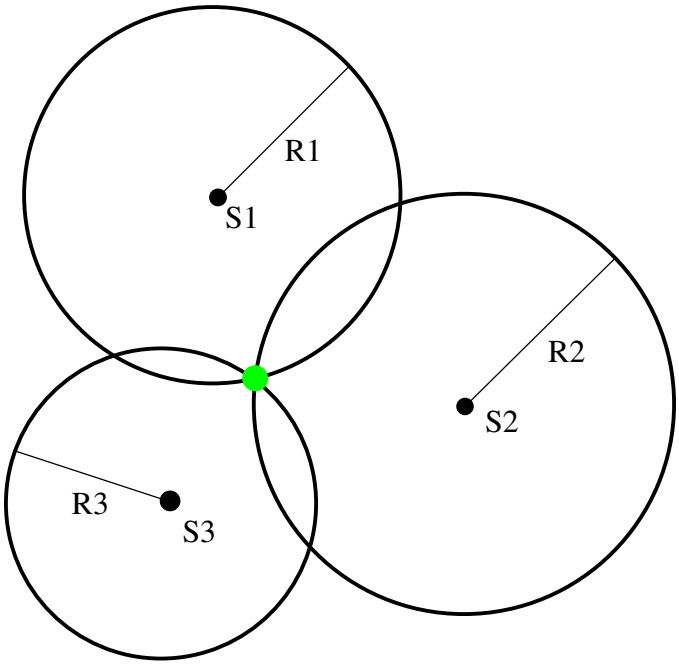

Figure 2.3: Uniquely defined position of the receiver with three satellites.

incorporated whose sphere of location intersects one of the two points to uniquely determine the location of the receiver. In practice, because of the altitude of the satellites, before the fourth satellite is added, one intersection point will be close to Earth while the

other will be a great distance away and can be ruled out immediately. A fourth satellite is still required, however, to account for the bias between GPS system time and the low quality clock in the user's receiver, as will be discussed later.

All of the discussion up to this point has been under the assumption that there are no errors in the calculation of the radii from the satellites. When errors are considered, the location of the receiver is confined not to a single point in space but to a volume where the receiver resides anywhere inside. Again, for simplicity, the two-dimensional case will be explored.

In reality, the range to a satellite will not be exact and will have an error associated with it. This is shown in Figure 2.4 with the calculated radius drawing the black circle but the circle of the true radius could be anywhere between the red circles.

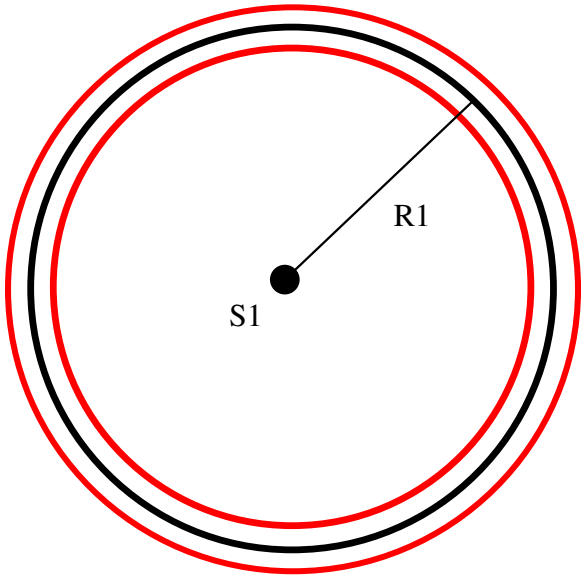

Figure 2.4: Distance from a satellite with errors.

When the measurement from the second satellite is included, also with errors, the result shows that the receiver could be inside two possible areas.

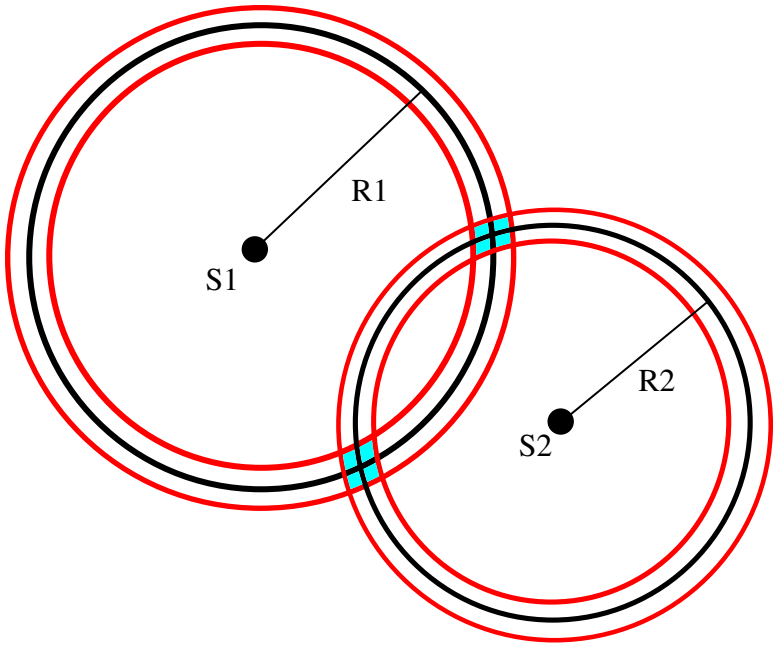

Figure 2.5: Location of receiver could be in two possible areas.

The addition of the third receiver locates the receiver within a single area as in Figure 2.6. This explanation, again, scales directly to the three-dimensional situation only with spheres and the final location residing somewhere inside a volume instead of circles and the final location residing somewhere inside an area.

As can be seen from Figures 2.4 through 2.6, the amount of error in the final position solution (the size of the area or volume) depends closely upon the accuracy of the range measurements to the satellites. However, range error is not solely responsible for the position errors. The constellation geometry also plays a role in determining how large the final area/volume is in which the receiver is located. The effect of the constellation geometry on position accuracy is characterized by a term called the dilution of precision (DOP).

The ideal geometry is to have the satellites spaced out evenly around the receiver. This geometry was used in Figures 2.1 through 2.6. In the two-dimensional case with three satellites, the ideal geometry contains all three satellites spaced 120° apart in

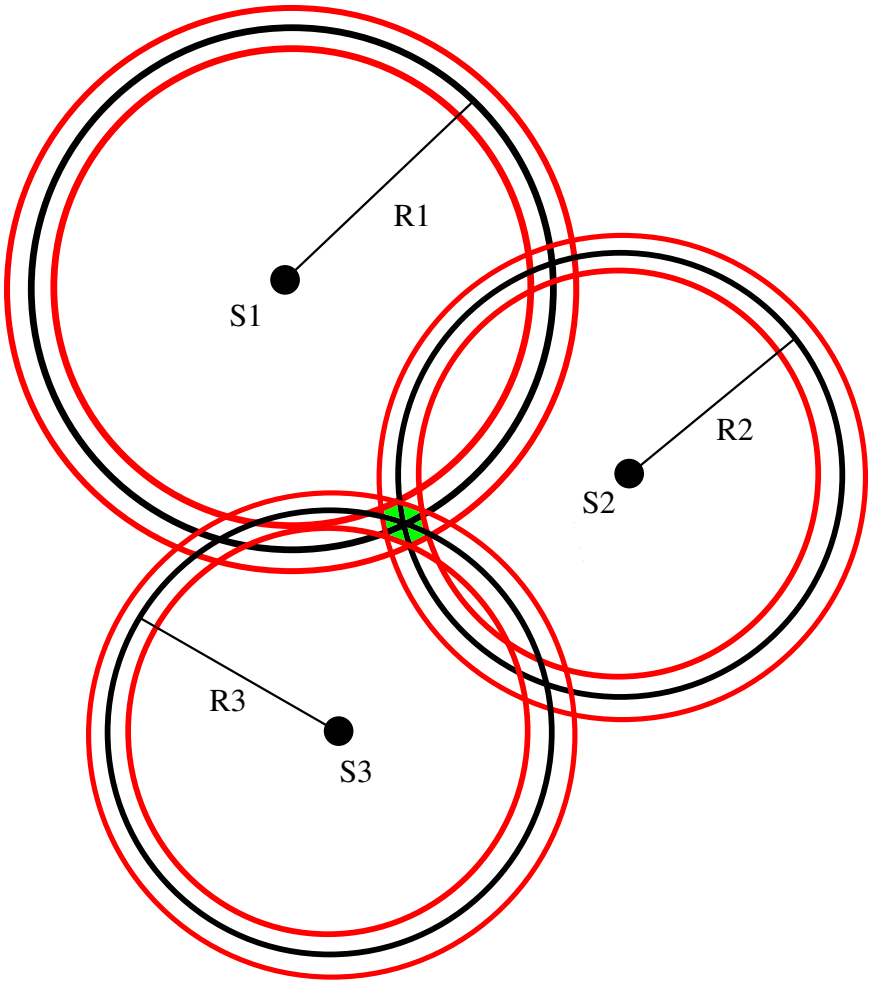

Figure 2.6: Receiver located within a single area.

azimuth around receiver. In the three-dimensional case, the ideal geometry in free space consists of three satellites spaced 120° apart in azimuth around receiver at an elevation angle of −19.47° below the local level plane of the receiver and the fourth satellite at zenith [20]. Unfortunately, since satellite navigation requires a line of sight from the receiver to the satellite, the optimal four-satellite constellation geometry cannot be achieved with a receiver on the ground. The best attainable geometry is three satellites equally spaced in azimuth at 0° elevation on the local level horizon and the fourth satellite at zenith. For practical purposes, a satellite must be at least 5° above the horizon.

Figure 2.7 illustrates the situation with three collinear satellites. Even with the same satellite range error as before, the geometry expands the area where the receiver could reside. This DOP from the satellite constellation geometry has the effect of multiplying the range errors.

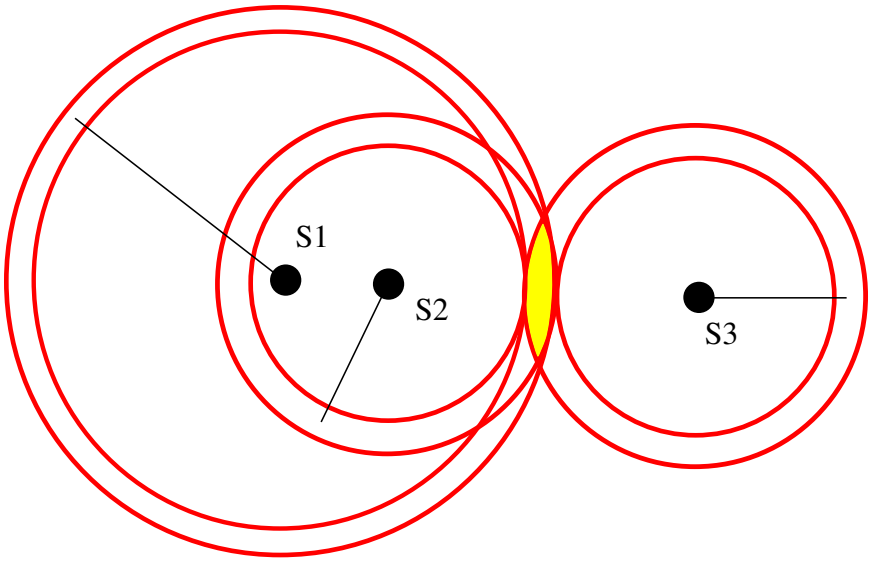

Figure 2.7: Constellation geometry inflates the error with range errors held constant.

To know how long the signal took to traverse the distance from the satellite to the receiver, the satellite encodes in the signal certain information letting the receiver know when it transmitted the signal. Upon detection, the receiver compares the time of transmission (according to the satellite) with the time of reception (according to the receiver). One major drawback to this idea is that to work properly and accurately, the receiver and the satellite clocks must be synchronized *exactly* as even a 1 μs difference in the clocks will result in the range being off by approximately 300 m. Fortunately, the solution to this problem is quite easy. The satellites all have highly accurate atomic clocks which are synchronized with a master clock on the ground. Therefore, if the receiver has a clock error, then that error will be on the measurements from every single satellite and

will be the same for all of them. In other words, if the receiver has a 2 μs clock error, then the ranges from the receiver to all the satellites will be wrong by exactly 600 m. The receiver clock error goes into the system of equations as well so there are now four unknowns and a fourth satellite is required to solve the system of equations. This system is solvable so whether the receiver clock error is 1 ns or 10 s, the receiver can still accurately calculate its position and also its clock error. Therefore, satellite navigation systems also afford the receiver extremely accurate time.

Satellite navigations systems do not rely on two-way communication between the satellite and the receiver. Instead, the systems solely rely only on the signal transmitted by the satellite. This means that there is no limit to the amount of receivers that can use a satellite navigation constellation at any time. Unfortunately, satellites do not have an endless supply of power so the transmitted signals are not very strong. As a result, after the trip from the satellite to the receiver, the power levels received are miniscule. Accordingly, satellite signals can be jammed, both intentionally and unintentionally, very easily thereby disrupting the navigation services.

As mentioned earlier, there must be a line of sight between the satellite and the receiver. Consequently, inside buildings or under dense foliage, satellite navigation services will range from severely limited to completely unavailable. Tall buildings or geographic obstructions such as mountains or valley walls block the line of sight to the satellite decreasing the number of visible satellites and also limiting the visible satellites to a smaller portion of the sky which causes DOP issues to arise due to the poor visible satellite geometry.

2.3 GPS

The origins of GPS date back to the 1960s. With the dawn of the space age, the United States launched the first satellite positioning system, TRANSIT. TRANSIT used the received doppler shifts from the signals of the satellites passing overhead to locate the

receiver on the earth [5]. TRANSIT demonstrated the possibility of satellite navigation and further DoD advancements led to GPS. TRANSIT used the received doppler shifts from the satellites' signals to determine location whereas GPS uses the signals' time of arrival to determine location. TRANSIT had several shortcomings including long periods between available position updates and inaccuracies resulting from a non-stationary user [25]. GPS resolves both of these deficiencies as well as has greater accuracy. From the beginning, the United States Department of Defense (DoD) primarily used the system but the civilian sector has increasingly depended on GPS.

2.3.1 Performance and Signals. There are two distinct services provided by the GPS satellites: standard positioning service (SPS) and precise positioning service (PPS). Before 1 May 2000, the SPS included selective availability (SA) which intentionally degraded the accuracy of the position solution. The performance of SPS, transmitted only on the L1 frequency, with SA turned on gave erratic errors in position and limited accuracy to approximately 100 m. With SA deactivated, the SPS accuracy improved to around 10 m. The PPS accompanies the SPS but only select users have access to this signal. The PPS transmits on both the L1 and L2 frequencies giving dual-frequency receivers the ability to filter out atmospheric errors. PPS also uses a faster code chipping rate which yields greater accuracy. The P-code, as the PPS code is referred to, usually gets encrypted by the satellite into a form called the Y-code. This cannot be deciphered without an encryption key which limits the use of the PPS to only authorized receivers[14]. More information on the two services is included in Table 2.1. The accuracies/errors given in the table are the root mean square (RMS) errors for the 95% global average (performance will exceed these standards 95% of the time).

GPS satellites use radio transmissions in their one-way communication with receivers. Even though there are over 30 GPS satellites continuously orbiting the Earth,

Table 2.1: Attributes of C/A Code and P Code[14, 15]

	C/A Code	P Code
Chipping Rate $\left(\frac{\text{chips}}{\text{sec}}\right)$	1.023×10^6	10.23×10^6
Chipping Period	977.5 ns	97.7 ns
Chip Range	293 m	29.3 m
Code Repeat Interval	1 ms	1 Week
Position Accuracy (95%)	6.0 m	2.6 m
Velocity Accuracy (95%)	0.006 m/s	0.006 m/s
Time Error Specification (95%)	40 ns	40 ns

they all transmit their signals on the two frequencies shown in Table 2.2. To keep signals

Table 2.2: GPS Frequencies

$L1$ = 1575.42 MHz
$L2$ = 1227.60 MHz

from individual satellites distinguishable, the system uses code division multiple access (CDMA). Each satellite has its own unique "code". This ranging code gets modulated right onto the navigation message which contains all the pertinent information. The receiver knows the specific code for each satellite and searches the incoming signals to find a match. Once it finds the code it is looking for, it can decipher the signal and know which satellite it came from as well as all the information needed from that satellite to aid in position calculations. This CDMA scheme not only conserves bandwidth and makes receivers simpler by only having to listen to one or two frequencies, but also enables the receiver to pull the very faint signals from the satellites out of the mass of background noise and other satellites signals at that frequency.

On the ground, the power received in the signals from the satellites are at a minimum -158.5 dBW for the L1 frequency and -160.0 dBW for the L2 frequency [13]. This makes GPS extremely susceptible to both intentional and unintentional jamming. The CDMA helps overcome this tiny amount of received power yet the GPS signals remain extremely vulnerable to being covered up and washed out.

2.3.2 Space Segment. The DoD decided upon 24 (expandable to 32) satellites in a medium earth orbit (MEO) in 1973. The first satellite went to space in 1978 and the system as a whole was fully operation in 1995 [25]. GPS satellites reside in six orbital planes spaced 60° apart at an inclination of $55^\circ \pm 3^\circ$ in nearly circular orbits (eccentricity= 0 ± 0.02) [15]. The satellites orbit at an altitude of approximately $20,182$ km [19].

2.3.3 Ground Segment. There is more to GPS than just satellites orbiting the Earth sending out radio transmissions. There exists a vast control segment on the ground, operated by the US Air Force, that monitors the satellites' health and orbits, keeps accurate system time, and creates the satellite ephemerides [25].

There are seventeen monitoring stations spread around the Earth which track the satellites and report back to the Master Control station located at Schriever Air Force Base in Colorado. From here, updates and corrections to the ephemerides and orbits are commanded which are then transmitted back up to the satellites through four ground antennas located at various longitudes around the Earth. With the antennas and monitoring stations situated all around the Earth, all satellites in the constellation are in view of at least one ground station and antenna at all times.

2.3.4 User Segment. The third segment of the system, along with the space segment and control segment, is the individual user. Originally designed for use by the military, GPS has expanded its horizons to the civilian market as well. Users today can be

anything from warships and multi-billion dollar military aircraft to hikers with small hand-held receivers. The applications of GPS are endless and cheap, small, and accurate receivers foster accessibility to the masses. For the purposes of this paper, the user is assumed to be a military user with more stringent accuracy and authentication requirements.

2.4 Galileo

The impetus for Galileo came from Europe's desire for independence from GPS, which is controlled by the United States DoD, and also to profit from the satellite navigation market. The system from the beginning had visions of civilian control and interoperability with the currently operational satellite navigation systems, GPS and GLONASS. To this end, the European Union (EU), along with separate contributions from Germany, France, Great Britain and Italy will fund Galileo [5].

2.4.1 Performance and Signals. Galileo will broadcast many signals across the frequency spectrum. Table 2.3 outlines the signals used by Galileo. The E5a and E5b

Table 2.3: Galileo signals [5, 6]

Signal	Center Frequency	Bandwidth	Minimum Power Received
E1	1575.42 MHz	40.92 MHz	−157 dBW
E5a	1176.45 MHz	41.035 MHz	−155 dBW
E5b	1207.14 MHz	41.035 MHz	−155 dBW
E6	1278.75 MHz	40.92 MHz	−155 dBW

signals actually are two halves of the E5 band which is 92.07 MHz wide. The E1 signal coincides with the GPS L1 signal. In efforts to avoid interference, the E1 channel will be

modulated with new and different techniques [5]. The satellites themselves employ a CDMA scheme much like GPS.

With the abundance of signals transmitted by the Galileo satellites, the system will offer many services to its users. The Open Service (OS) is free to all users and will broadcast on the E1 and E5 channels allowing for dual frequency atmospheric corrections to be made. OS is similar to the standard GPS service. The commercial service (CS) will require users to pay to receive this service. CS will be broadcast on the E1, E5, and E6 signals. It will have a faster data rate than the OS allowing for greater accuracy and transmission of correction data. The safety of life (SoL) service will provide integrity monitoring and availability guarantees. The SoL will be useful in situations such as landing an airplane in instrument conditions where accurate navigation is of the utmost importance. It will be broadcast on the E1 and E5 signals. The public regulated service (PRS) will be available only to authorized users, mainly, public servants, and will incorporate anti-spoofing and anti-jamming technology. The PRS will be broadcast on the E1 and E6 signals. There will also be a search and rescue service (SAR) which will aid in the location of emergency distress signal transmitters [5].

Due to technological and design improvements, Galileo is slated to have slightly better performance than GPS. Table 2.4 summarizes the performance of the system for the PRS on the E1 signal.

2.4.2 Space Segment. The design of the Galileo constellation calls for a total of 30 satellites composed of 27 operational and three active spare satellites. The orbits are scheduled to be circular orbits at an inclination of 56° and an altitude of $23,223$ km above the surface of the earth. The satellites will be evenly distributed between three orbital planes [6]. As of this writing, there are only two satellites in orbit which are undergoing in-orbit validation testing. In 2010 the European Space Agency (ESA) negotiated a

Table 2.4: Galileo Performance [16, 8]

	C/A Code
Chipping Rate $\left(\frac{\text{chips}}{\text{sec}}\right)$	10.23×10^6
Chipping Period	97.7 ns
Chip Range	29.3 m
Code Repeat Interval	100 ms
Position Accuracy (95%)	2 m

contract to have 14 satellites delivered by the year 2014 [8]. Galileo is scheduled to reach initial operational capability by 2015 and full operational capability by 2020 [7].

2.4.3 Ground Segment. Galileo will monitor the satellites with a vast ground support network. There will be two control centers, one located in Germany and one located in Italy. The network will also include five monitoring/control stations and five uplink stations giving coverage all around the world [16]. The control centers will have a ground control segment (GCS) and a ground mission segment (GMS). The GCS will cover constellation management, including satellite telemetry and uplink communication, ranging, and health monitoring. The GMS will cover navigation data, timing, and data integrity as well as monitoring the search and rescue payload [8].

2.4.4 User Segment. Although there are no users currently because the constellation is not operational, Galileo is designed with both operational independence and interoperability with GPS and GLONASS in mind. This means that it can be used as a standalone system or with the other systems to gain better accuracy or a solution in difficult receiving environments.

2.5 GLONASS

Shortly after the United States announced the development of GPS, the Soviet Union announced the development of their own satellite navigation system: the Global Navigation Satellite System (GLONASS). The program came to fruition in the 1980s and 1990s under the control of the Russian Military Space Forces [19]. Although 26 GLONASS satellites orbited in 1995, the constellation fell into disrepair with the hard times in Russia to the point where only 8 operational satellites orbited in 2001. Beginning in 2001 the program was revamped and in 2007 Russian president Vladimir Putin declared the system open for use without limitation [5].

2.5.1 Performance and Signals. Like GPS, GLONASS also broadcasts both a standard and a precise service. However, unlike GPS, GLONASS uses a system where every satellite gets its own frequency, known as frequency division multiple access (FDMA). The frequency spectrum is broken down into two sub-bands from which the GLONASS channels derive their specific frequencies. The channels are outlined in Table 2.5. There are more satellites than available channels so two satellites may use the

Table 2.5: GLONASS Frequencies [16]

$f_{kL1} = 1602 \text{ MHz} + k * 0.5625 \text{ MHz}$
$f_{kL2} = 1246 \text{ MHz} + k * 0.4375 \text{ MHz}$
where $k = -7... + 6$

same channel if they are in antipodal spots of the same orbital plane [16, 19]. Originally, GLONASS transmitted the precise signal on both the L1 and L2 channels and the standard service only on the L1 channel but with the launch of the newer GLONASS-M satellites, the standard service will also be broadcast on L2. In the interest of inter-constellation

cooperation, future satellites will broadcast a CDMA signal as well [16]. Table 2.6 further describes the GLONASS service. Because the satellites broadcast on different

Table 2.6: Attributes of standard service and precise service [5, 19, 29, 31]

	Standard Service	Precise Service
Chipping Rate ($\frac{\text{chips}}{\text{sec}}$)	511×10^3	5.11×10^6
Chipping Period	1.96 μs	196 ns
Chip Range	587.1 m	58.7 m
Code Repeat Interval	1 ms	1 s
Position Accuracy	7 m	N/A
Velocity Accuracy($\frac{\text{meters}}{\text{sec}}$)	0.15	0.15
Time Error Specification	1 μs	1 μs

frequencies, the system only has two different ranging codes, one for the precise service and one for the standard service. The receiver determines which satellite it is listening to simply by the frequency of the signal. The power received from these signals will be, at a minimum, -161 dBW for the L1 sub-band and -167 dBW for the L2 sub-band [31].

2.5.2 Space Segment. As of July 2011, GLONASS has 23 operational satellites in orbit at 19, 100 km above the Earth with a goal of having a total of 24 satellites in orbit which would constitute the 21 satellites plus the 3 active spares needed for uninterrupted global coverage. The satellites orbit in 3 orbital planes each with inclinations of 64.8°. The constellation is designed so that the satellite ground tracks will repeat every 8 sidereal days so the satellites overhead each day will vary but the values of DOP will repeat on a daily basis [31].

2.5.3 Ground Segment. The ground segment for GLONASS controls and oversees the constellation. There is one system control center located in Moscow and 10 tracking stations located across Russia. The control segment looks after the health or the satellites and monitors their orbits. It also determines their ephemerides and maintains GLONASS time. Each satellite contains laser reflectors which allows laser and radar tracking accurate to 2 cm in range and 2″ in angle by the tracking stations [5].

2.5.4 User Segment. The user segment of GLONASS mirrors that of GPS. The system is used heavily by both the military and also civilians over a broad range of applications. Due to the satellites each transmitting on a separate frequency, the receivers are more complicated and costly than their GPS counterparts [19].

2.6 Compass

China is now embarking on its second generation of satellite navigation systems. Beidou-1 was China's first satellite navigation system which launched in the 2000s with regional coverage in mind, not global. This system had many similarities to the failed US Geostar system [16]. The new system, Compass, or Beidou-2, marks China's entrance to the GNSS stage. The first satellite launched in 2007 and the system is expected to be fully operational by the year 2020 [12].

2.6.1 Performance and Signals. Compass designers plan to incorporate two levels of accuracy into the system, open service and authorized service. The authorized service will be used by the Chinese government and its military. The services will be transmitted on the frequencies outlined by Table 2.7. The minimum power received for all the signals will be −163 dBW [11].

In December 2011, China released an interface control document for the Compass system. What is known about the performance and signals is displayed in Table 2.8. The

Table 2.7: Compass signals [16, 11]

Signal	Center Frequency	Bandwidth
B1	1561.098 MHz	4.092 MHz
B1-2	1589.742 MHz	4.092 MHz
B2	1207.14 MHz	24 MHz
E6	1268.52 MHz	24 MHz

chipping rates were uncovered by examining the signal of the test satellites currently in orbit and confirmed by the release of the interface control document.

Table 2.8: Attributes of Compass [16, 11]

Chipping Rate $\left(\frac{\text{chips}}{\text{sec}}\right)$	2.046×10^6 and 10.23×10^6
Position Accuracy	10.0 m
Velocity Accuracy	0.2 m/s
Time Error	50 ns

2.6.2 Space Segment. By the time the system is running at full operational capability, there will be a total of 35 Compass satellites. 30 of these will be in MEO at an altitude of $21,490$ km and the other five will be in geostationary orbit (GEO) providing regional coverage to China at al altitude of $35,786$ km. The satellites in GEO will be located at the longitudes of $55°E$, $80°E$, $110°E$, $140°E$, and $160°E$ [27].

2.6.3 Ground Segment and User Segment. Once completed, the ground segment will consist of a master station and upload stations. There are currently no users as the constellation is not operable but once finished, the system will work as a standalone system or in cooperation with existing satellite navigation systems [27].

2.7 Altimeter

Barometric altimeters (baro-altimeters) are instruments which give a height above sea level. A baro-altimeter, in its simplified form, is nothing more than an air pressure gauge with a display that is calibrated not with millibars or inches of mercury, but feet above sea level. In an airplane, staying at a constant height above mean sea level (MSL) is a very important aspect of safe navigation. Baro-altimeters measure the amount of air that is above the sensor, which varies predictably with height above MSL.

Baro-altimeters measure the static air pressure, that is, the force exerted by the ambient, non-moving air. This proves to be a very useful piece of information. Static pressure varies in a known and predictable manner as you move from sea level up through the atmosphere. With this knowledge, a baro-altimeter can read the static pressure at its current altitude, compare the reading to sea level pressure, and know its altitude above mean sea level.

Unfortunately, the atmosphere constantly moves and changes, thereby varying the sea level pressure. However, most altimeters have the ability to accept a calibration for the value of the sea level pressure at their location at that time which will correct the baro-altimeter to show its MSL altitude.

The known and predictable manner that static pressure changes with altitude is somewhat complicated as well. Equation 2.1 shows the relationship between static pressure, p, and altitude above sea level, h,

$$p = p_0 \left(1 - \frac{L * h}{T_0}\right)^{\frac{g*M}{R*L}} \tag{2.1}$$

where p_0 is the standard sea level pressure, L is the temperature lapse rate, T_0 is the standard sea level temperature, g is the Earth's gravitational acceleration at sea level, M is the molar mass of dry air, and R is the universal gas constant. Equation 2.2 substitutes all

the constants into Equation 2.1 which simplifies to

$$p = 29.92\left(1 - \frac{h}{145449.25}\right)^{-5.26} \tag{2.2}$$

At altitudes under 20,000 ft MSL, the equation can be closely approximated by a linear equation given in Equation 2.3.

$$p = 29.09 - 0.0008 * h \tag{2.3}$$

Figure 2.8 shows the plot of the Standard Day Pressure versus Altitude MSL along with its linear approximation.

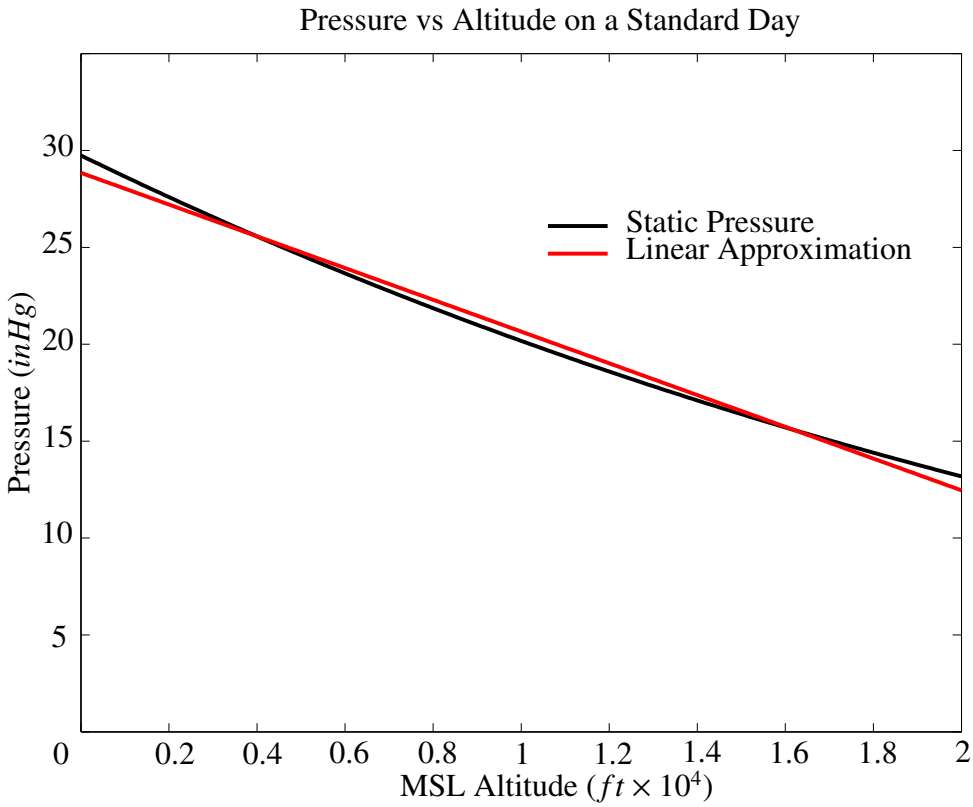

Figure 2.8: Standard day static pressure vs altitude and its linear approximation.

2.8 Kalman Filtering

Kalman filters have been used since the 1960s to give an optimized estimate of the state variables in a system [3]. More specifically, a Kalman filter is an algorithm that estimates the states of a system (for example position and velocity of an object) as well as keeps track of the covariance of the estimates. The algorithm is recursive, needing only the state estimate from the previous point in time, and uses a model of the system dynamics to estimate the values of the states at the next time step. Measurements of the states, which often are corrupted by some amount of noise, are taken into the filter and compared against the filter's projection of the states. The filter then weights the projection and the measurements based on their error statistics and blends them to obtain an optimal estimate of the states. The algorithm then continues in a loop projecting ahead the estimates and incorporating measurements when available. Much more detailed and extensive information regarding Kalman filters can be found in [3, 21, 22]. In this thesis, a Kalman filter is used to combine GNSS position solutions with inertial and barometric sensor readings.

2.9 Related Research

Moudrak, et al. looked at the interoperability of the GPS and Galileo systems [26]. More specifically, they examined the timing aspects. They note how there will be time offset between the two system times which will cause a bias in the position and time solutions. To overcome the obstacle, they looked at a five-unknown least-square solution as well as a four-unknown least-square solution with the time offset broadcast to the receiver (with uncertainty in the time offset). Their results showed that the five-unknown solution has greater accuracy than the four-parameter solution with the broadcast time offset as long as the time offset uncertainty is greater than 5 ns.

Eissfeller, Ameres, Kropp, and Sanroma gave an overview and compared the performance of GPS, Galileo, and GLONASS [5]. The state that GLONASS and Galileo are moving towards interoperability with GPS. They say combining the GNSS systems will yield in better geometry and increased availability.

Kaya and Saritas discuss their design of a computer simulation for DOP. They derive the equations for DOP and give a metric for DOP values [17].

Richard Langley gives a detailed overview of GPS accuracy. He delves into the effects of good and poor geometry. He outlines how the values of DOP are inversely proportional to the volume of the tetrahedron whose five corners are the locations of the four satellites and the receiver. A larger volume signifies and better (smaller) DOP value. He also details the geometry for the theoretical best four-satellite constellation as well as the best possible geometry for a receiver on the surface of the Earth [20].

Misra, Burke and Pratt give a general overview of GPS as well as talk about the measurements, models, and errors. They delve into error mitigation and sub-meter positioning accuracy [24].

Dutt et al. studied DOP and how it relates to satellite constellation geometry [4]. They uncover the relationship between tetrahedron volume and DOP values. They find the best four satellites which give the lowest DOP of all the visible satellites but find that including all the visible satellites helps to lower the DOP value over the DOP value from just the optimal four.

Yarlagadda, Ali, Al-Dahir and Hershey mathematically derive the DOP equations. Then they investigate absolute bounds on geometric dilution of precision (GDOP). They prove the minimum values for GDOP and position dilution of precision (PDOP) as $\sqrt{2}$ and 1.323, respectively [35].

Kihara examined a policy for selecting the satellites to provide the best accuracy. He showed modest improvements in accuracy, with real satellite location data, using the

satellites which gave the best horizontal dilution of precision (HDOP) to calculate the horizontal position and the satellites which delivered the best vertical dilution of precision (VDOP) to calculate the vertical position as opposed to using the same set of four satellites with the best overall GDOP to calculate the entire position solution [18].

Sairo, Akopian, and Takala cover weighting the DOP matrices. This is integral for combining different GNSS systems as not all produce the same level of accuracy. This is taken into account when calculating DOP and the weighting matrix will appropriately account for the accuracy discrepancies between the systems. Furthermore, they prove that weighted DOP monotonically decreases with respect to the number of satellites [30].

Bo and Shao look into selecting the satellites to track in a combined GPS and Galileo receiver. They note that with the vast increase in visible space vehicles with a combined receiver will mean the receiver cannot always track all the satellites in view. Therefore, they execute an algorithm which takes into account weighting the DOP matrix to get the most accuracy out of the combined GPS-Galileo constellation and receiver [2].

McKay and Pachter examine optimizing geometry for GPS navigation. They find that the condition number of the visibility matrix, also known at the H matrix, is a good measure of the geometry of the constellation at hand. The condition number of H sets an upper bound on the error amplification due to the geometry of the constellation [23].

Hegarty and Chatre give an exhaustive overview of all the currently operational and planned global satellite navigation systems including GPS, GLONASS, Galileo, and Compass. They discuss the use of GNSS, predominantly GPS, in the field of aviation detailing the need for as high of accuracy and availability as possible [16]. They champion the use of interoperability of between all of the systems.

The European Space Agency has published many technical documents the specifications of the planned Galileo satellite navigation system. The interface control document is the most detailed among the documents and it details every conceivable detail

of the signals transmitted by the satellites as well as other pertinent detail about the system such as the plan for the constellation [7, 6, 8].

Mutlu studied augmenting GPS with foreign GNSS when a uniform elevation mask blocks the view of the sky. He found that augmenting GPS increases the availability of a position solution and that the dilution of precision depends on the time offset between the systems [27].

Oktay looked at augmenting the GPS system with pseudolites to provide precise positioning in an urban environment. Augmenting the GPS constellation with a pseudolite enhanced availability and accuracy of a position solution so long as the pseudolite was placed close to the horizon [28].

Gao et al. launched a study to characterize the signal transmitted by the newly launched Compass-M1 satellite. They undertook this effort in an attempt to understand the signal structure, its codes, and its code structure. With a description of the signal, they can determine the information necessary to design a receiver to acquire and track the satellite as well as investigate possibile future interoperability with other systems or determine if there will be interference issues. After detecting the signal with a high gain antenna, they published their findings on the characterization of the Compass-M1 signal [9].

Yong and Lingjuan set up a simulation to compare the GDOP of a position solution with only the optimum four satellites in use or all visible satellites in use. They proved in theory that the all-in-view GDOP value is always equal to or less than the GDOP for the optimum four satellites showing increasing the number of satellites in view helps improve the GDOP value. Furthermore they showed that weighting the GPS satellites based on satellite elevation and signal to noise ratio (SNR) in the DOP calculation increased accuracy and smoothed fluctuations in DOP when satellites rose or set [36].

Langley gives an update of GLONASS. He describes the technical basics of the system by giving details on the control, space, and user segment. He says that the system

has less accuracy than GPS and still does not have a full compliment of satellites in orbit yet. He states that in urban canyons and other visibility-restricted locations, accuracy and availability will increase with the advent of combining GLONASS and GPS [19].

Previous research examined availability when combining multiple GNSSs while increasing the uniform elevation mask angle but did not look into using an actual city model. Also they did not implement a Kalman filter combining inertial measurements with an augmented GPS constellation. Furthermore, augmenting the GPS constellation with only the minimum number of foreign satellites was not examined. This research will examine availability in a simulated city environment as well as simulate an autonomous aerial vehicle navigating around the city model using a Kalman filter incorporating inertial and GNSS measurements.

2.10 Summary

This chapter started by examining the basics of how GNSS works in Section 2.2. It then gave a general overview of the current and planned global satellite navigation systems in Sections 2.3 - 2.6. Then, it looked at barometric altimeters in Section 2.7 and Kalman filters in Section 2.8. Finally, it delved into pertinent research and related works in Section 2.9.

3 Methodology

3.1 Overview

Chapter 3 goes over the simulation used in this research. It starts by outlining the scenario upon which this research is based, then it delves into the assumptions made as well as describes the simulation. In Section 3.5, finding position and velocity from pseudorange measurements is discussed. Following this, Sections 3.6 and 3.7 discuss calculating the DOP and weighted least squares. In Section 3.8 the method of combining multiple systems together is examined. Then, Section 3.9 discusses the method of choosing augmentation satellites. Section 3.11 closes out the chapter with details of the UAV simulation.

3.2 Scenario

In recent times, the hotbeds of military actions often lie in heavily populated urban areas or steep mountainous regions. Unfortunately, modern technology that military forces depend on, like GPS, can suffer significant setbacks when operating in these environments. Buildings block the line of sight from the receiver to many satellites when the buildings are either very tall, very close together, or combinations of the two, as can geographic features. This blockage means that the receiver may not have enough satellites in view to provide a position solution, or the geometry of the satellites in view yields an inaccurate position solution. Accordingly, soldiers on the ground would have to operate with degraded navigation information or possibly lose the location information of both friendly and enemy forces. While they would be able to continue the mission, other users, such as an autonomous unmanned aerial vehicle (UAV), may not have sufficient navigation information to continue operation.

In this scenario, a PPS GPS user operates in an urban environment. The simulated city around the user obstructs the view to parts of the sky. Availability of an acceptable position solution will be calculated using only GPS, and then again while augmenting GPS with various combinations of GLONASS, Galileo, and Compass satellites. The scenario also investigates selective augmentation rather than all-in-view augmentation to meet positioning requirements so that dependence on others systems can be minimized.

There are interchangeable city models that can be plugged into the simulation. These models come from work by Dr. Richard Ellefsen. He studied cities all over the world and came up with seven urban terrain zones (UTZ) that make up different parts of a city which are described in Table 3.1 [34] . The characteristics of these zones are summarized in Table 3.2. Oktay used Ellefsen's data to evaluate pseudolite performance in a uniform

Table 3.1: Urban Terrain Zone Descriptions [34]

UTZ	Description
1	Attached and closely spaced inner-city buildings
2	Widely spaced high-rise office buildings
3	Attached houses
4	Closely spaced industrial/storage buildings
5	Widely spaced apartment buildings
6	Detached houses
7	Widely spaced industrial/storage buildings

city [28]. This work improves upon the model by creating an approximation of a three block by three block section of downtown Dayton, OH so that results from a more realistic, non-uniform location could be obtained. In Figure 3.1, the lighter the area on the model, the taller the building. For comparison, a UTZ model is included in Figure 3.3.

Table 3.2: Urban Terrain Zone Characteristics [34]

UTZ	Footprint (m^2)	Avg. Height (m)	Avg. Separation (m)
1	2000	30	5
2	4000	45	30
3	500	6	20
4	4000	9	25
5	1000	20	50
6	100	6	15
7	10000	9	70

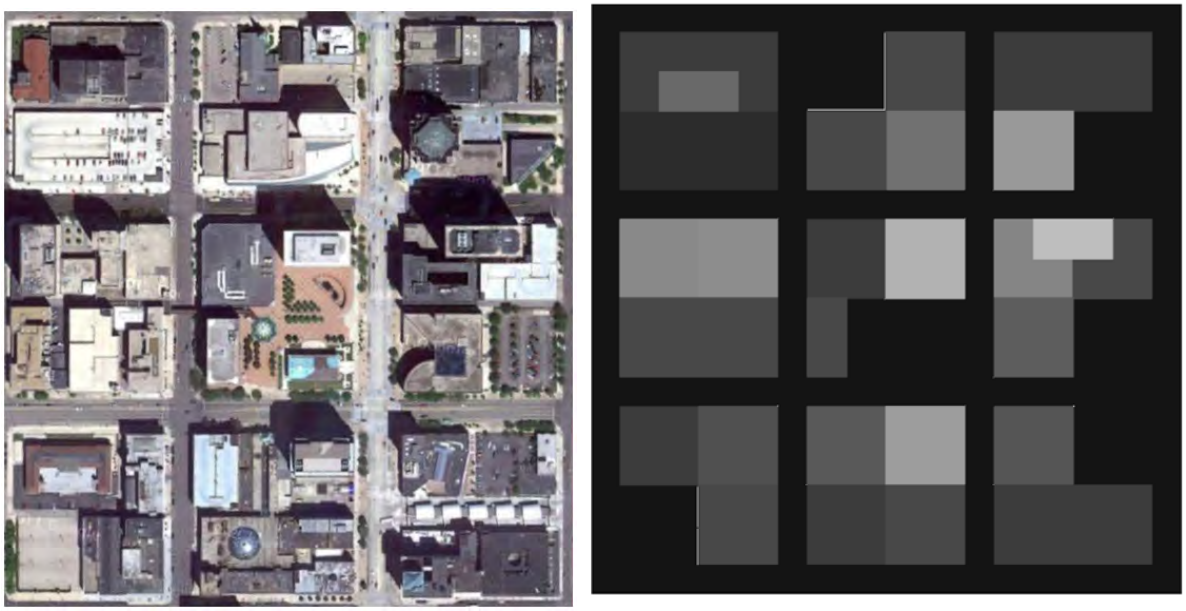

(a) Dayton, OH

(b) Model of Dayton, OH

Figure 3.1: Overhead view of downtown Dayton, OH and the model

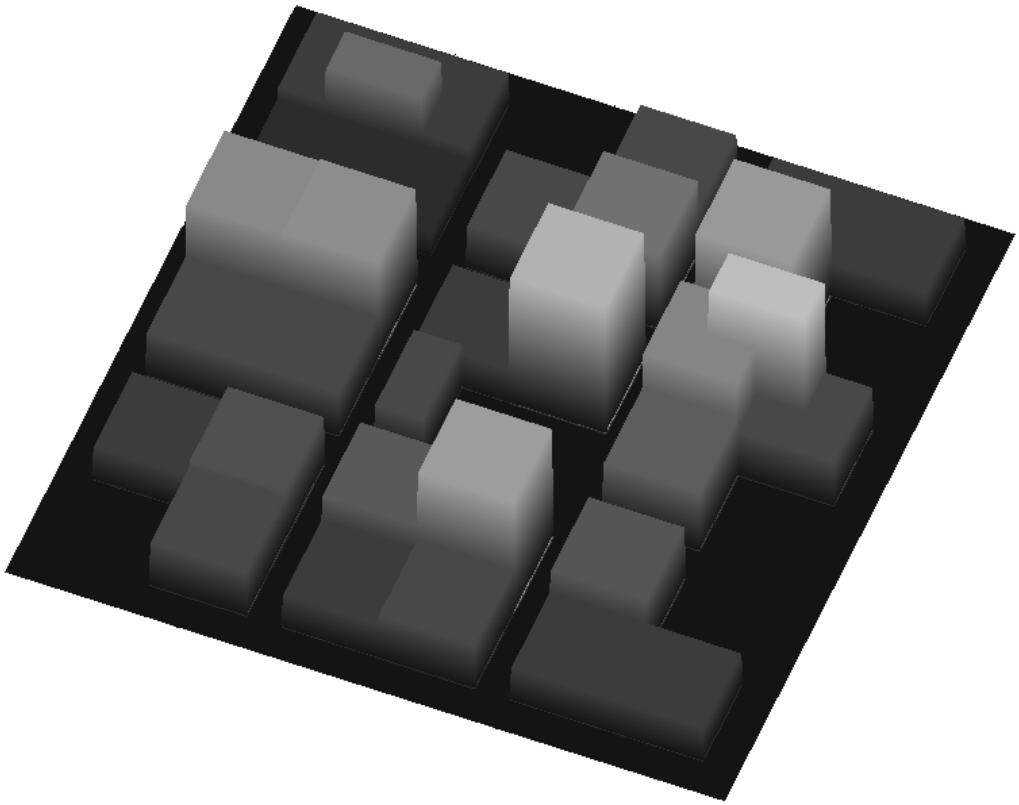

Figure 3.2: Alternate view of the Dayton city model

The scenario examines availability at a single location in the city over the course of a day to identify augmentation gains compared to the baseline of only using GPS. Also, a UAV flight is simulated through the city models to determine how autopilot-controlled flight and navigation are affected by the urban environment, with its associated loss of satellites in view, and augmentation.

3.3 Assumptions

There are four GNSS systems that are examined in this body of work: GPS, Galileo, GLONASS, and Compass. These all have different characteristics and specifications that a

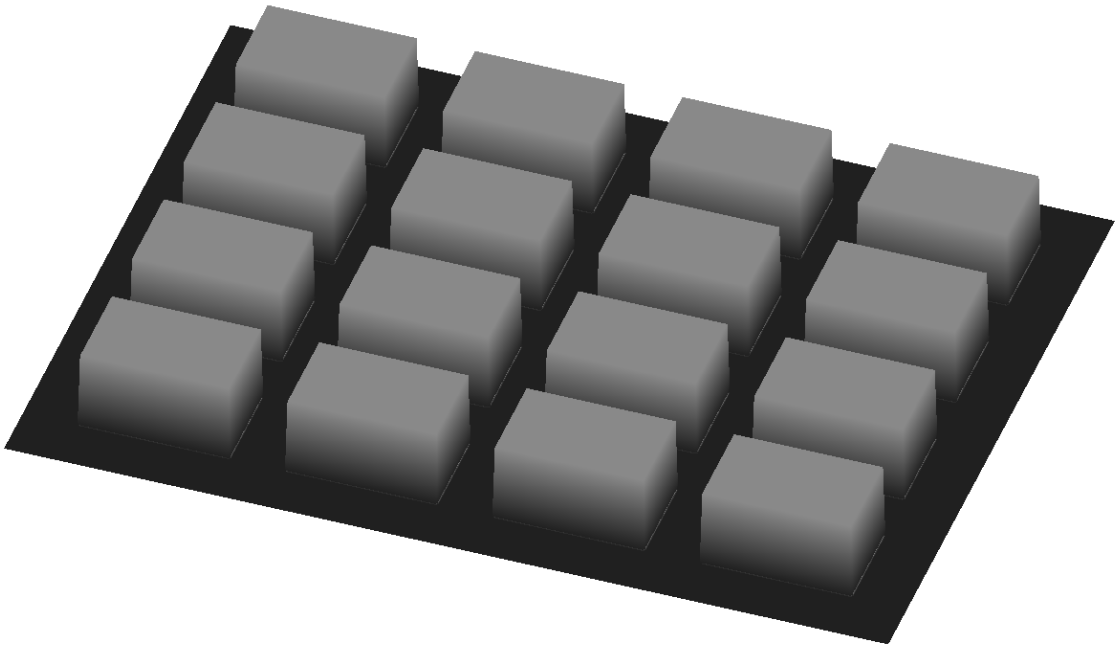

Figure 3.3: View of the UTZ city model

receiver must account for when solving for an actual position solution but they are beyond the scope of this thesis. Instead, this thesis focusses on PDOP calculation so simplifying assumptions can be made. It is assumed that:

- The errors within a system are lumped into a single user equivalent range error (UERE) which varies between the different systems but is constant for satellites within a given system.
- The Galileo constellation has 27 satellites evenly spaced in 3 orbital planes with an inclination of 56° and a radius of 29, 601 km.
- The Compass constellation has 30 MEO satellites evenly spaced in 3 orbital planes with an inclination of 56° and a radius of 29, 601 km. It also has 5 GEO satellites at 35, 780 km.
- All of the GNSS reference frames are matched.

- The time offsets between the systems are known.
- The sea level pressure at the receiver is known.

3.4 Simulation

Real data for both the GPS and GLONASS systems was collected from reference stations in downtown Dayton at the Ohio Department of Transportation reference station and the Russian Federal Space Agency [1], respectively . Using this data, the satellite locations over a 24 hour period on 4 July 2011 were calculated. GPS ephemeris data was collected and used to calculate the positions of the GPS satellites at five-minute intervals. The GLONASS data contained the earth-centered earth-fixed (ECEF) coordinates of the satellites but only at an interval of once every 15 minutes. The 15 minute data was interpolated using Matlab® to get data in five-minute intervals. The data for the Galileo and Compass satellites was obtained by way of a simulation of Walker constellations using Satellite Tool Kit (STK).

A Walker constellation is a constellation of satellites in circular orbits with the same altitude and inclination where the following notation describes the constellation: $i : t/p/f$. In this notation, i is the inclination of the orbits in degrees, t is the total number of satellites in the constellation, p is number of orbital planes, and f describes the phasing between the orbital planes. For example, the Galileo constellation can be described as a Walker constellation of the form $56^\circ : 27/3/1$ as it has 27 satellites in three orbital planes all with a 56° inclination.

The ECEF satellite locations over a 24 hour period were determined in five-minute intervals for Galileo and Glonass from the STK simulation. With the satellite location information for all the constellations known, the data was converted from the ECEF coordinate frame to the latitude, longitude, altitude (LLA) coordinate frame using Matlab®. With this data, the azimuth angle, elevation angle, and range to the all of the

satellites was then calculated. Any location could be used to calculate this but Dayton, OH, with LLA coordinates (39.8°N, 84.2°W, 195m), was chosen as the location for this simulation.

The city was simulated in Matlab® by creating a matrix where the location in the matrix, say for instance row 3 and column 4, equates to a physical location in the city 4m in the x-direction and 3m in the y-direction from the origin. The value at that location in the matrix defines the height at that location in the "city". The city model was built using the profiles from Dr. Ellefsen's research. "Streets" have a height of 0m and the "buildings" have the appropriate height for the city model chosen. To build the more realistic Dayton city model, Google Maps was used to measure the size of the blocks and streets of downtown Dayton as well as to locate and measure the horizontal dimensions the buildings. The actual building height data helped to create an approximate model of downtown Dayton for use in the simulation.

The city model elevation mask needed to be created next. This mask is a 1×360 vector where the location in the vector corresponds to azimuth angle and the value at that location in the vector defines the elevation mask angle for that azimuthal direction. Any satellite with an elevation angle below the elevation mask angle in a particular azimuthal direction will have a line of sight to the satellite that is obstructed by buildings. To find the values for the elevation mask, the elevation (α) and azimuth (θ) angles from a point in the city (where the receiver resides) to every other point in the city were calculated using Equation 3.1.

$$\begin{aligned} \theta &= \tan^{-1}\left(\frac{Y - y_{rec}}{X - x_{rec}}\right) \\ \alpha &= \tan^{-1}\left(\frac{Z - z_{rec}}{\sqrt{(X - x_{rec})^2 + (Y - y_{rec})^2}}\right) \end{aligned} \tag{3.1}$$

With this done for every point in the city model, the azimuth angles were rounded to the nearest 5° and the maximum elevation angle was recorded for this 5° section of azimuth directions. Ideally this would be done with rounding to the nearest degree but the city

model, which is constructed from individual points, not lines, did not have enough fidelity to yield a smooth and accurate elevation mask. With the maximum elevation angle for each 5° section known, the data was interpolated by a factor of five to result in an elevation mask with 1° fidelity. Figure 3.4 compares the interpolated mask against the non-interpolated mask.

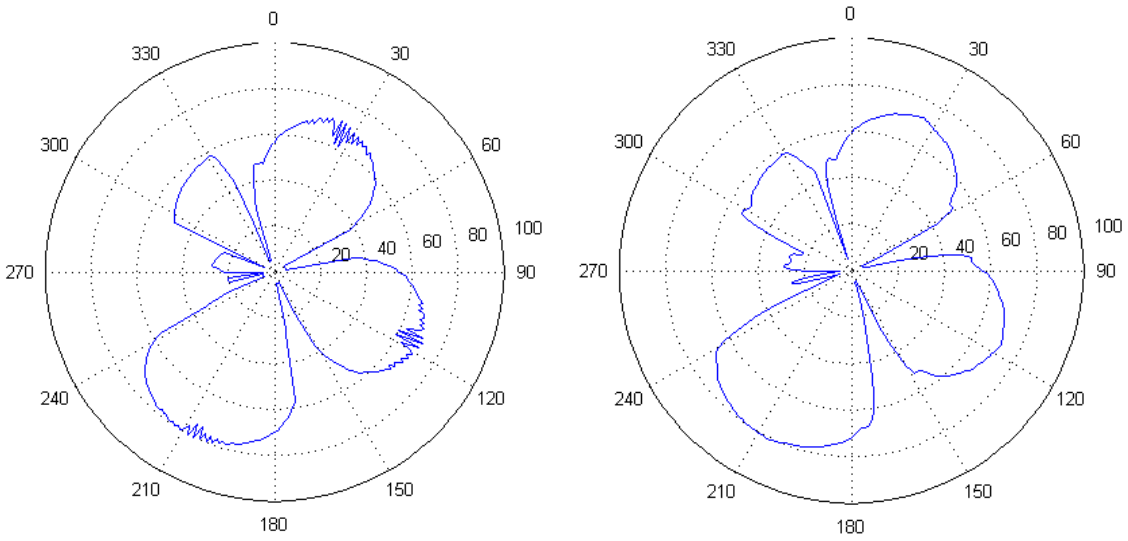

(a) Rough mask

(b) Interpolated mask

Figure 3.4: Comparison of the interpolated mask and the rough mask

The polar plot of the elevation mask angle can also be viewed with the scale set so that 90° is at the origin and 0° is at the edges, such as in Figure 3.5. This gives the same effect as a looking through a wide-angle lens that is set on the ground and pointed straight up. In this case, the elevation mask angle traces the visible edges of the tops of the buildings. The satellites are displayed on the mask angle plot. The green colored satellites are visible and the gray satellites are obstructed by the buildings.

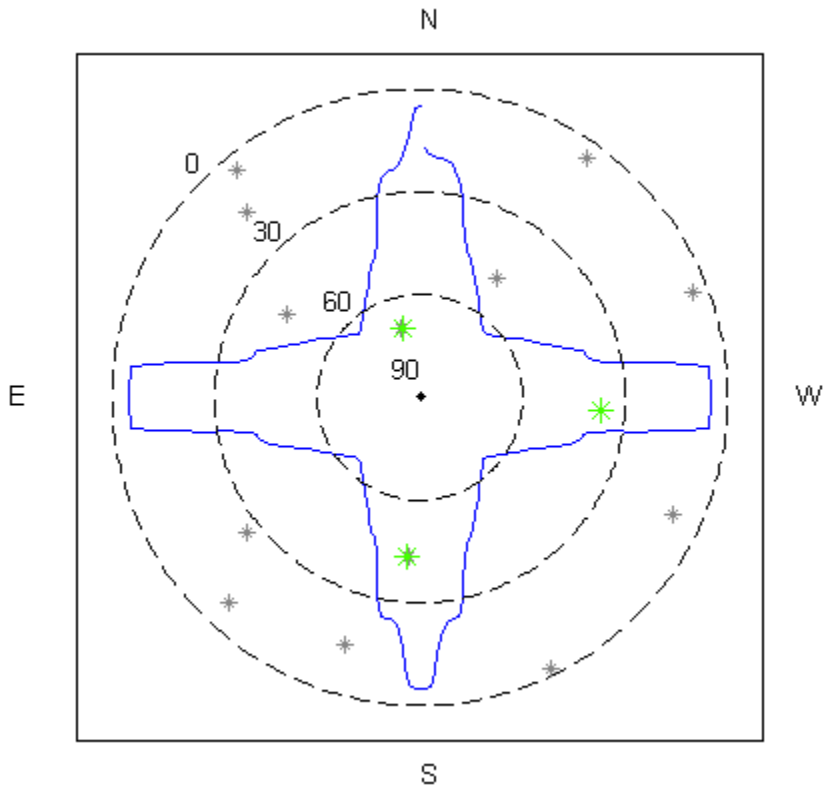

Figure 3.5: Comparison of the interpolated mask and the rough mask

With the elevation mask built and the satellite locations known, the elevation angles of the satellites could be compared to the elevation angles in the mask to see which satellites are visible. The DOP at each time step was then calculated using only the visible satellites. This is done for a single location in the city over the course of 24 hours with various constellations in use. This gives the ability to compare the results between using solely GPS, or GPS augmented with any combination of a barometric altimeter and foreign GNSSs.

Additionally, a simulation was also set up so that the receiver location moved around the city while the satellites remain in fixed locations overhead. This simulation represents a small UAV navigating autonomously through the city relying on satellite navigation and an inertial navigation system (INS) to find its way to waypoints between the buildings.

The barometric altimeter, GNSSs, and INS measurements go through a Kalman Filter which combines them and delivers the best estimate of the vehicle's position. The ability to navigate will be directly dependent on the quality of the INS and the availability of a GNSS based position solution. The availability will increase as foreign GNSSs augment GPS. The results of this simulation were analyzed to determine how effective GPS/INS alone was in autonomously navigating in an urban environment versus the addition of foreign satellite navigation services.

3.5 PVT Calculation

A satellite navigation receiver relies on the signals received from orbiting satellites to determine its position. It accomplishes this feat by knowing when the satellites transmitted the signal, when it received the signal, and the location of the satellites from where the signals originated. In an ideal world, the receiver can calculate the range to the satellite based solely on the time it took the signal to travel. However, due to the receiver clock error, which is the discrepancy between between the satellite and receiver clocks, the time of travel measurement has error leading to an error in the range calculation. The calculated range to the satellite with the error is known as the pseudorange. Fortunately this does not cause a problem because the receiver clock error is the same on all the measurements from all the satellites so it can be solved for and removed. The vectors between the location of the receiver (x_r, y_r, z_r) and the k^{th} satellite, where $k = 1, 2, 3, 4, ..., n$, are shown in Cartesian coordinates in Figure 3.1.

The pseudorange measurements from four satellites give the receiver the ability to determine its location as well as the receiver clock error. Equation 3.2 defines a generic pseudorange measurement

$$\rho_k = \| x_k - x_r \| + ct_r \tag{3.2}$$

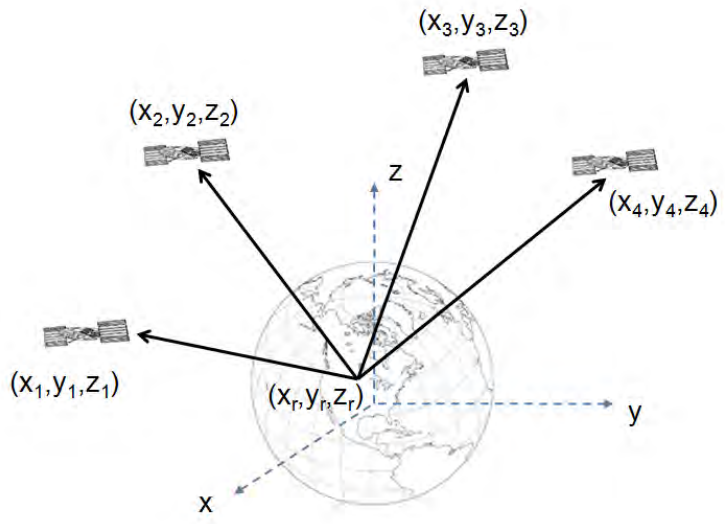

Figure 3.6: Receiver to satellite vectors

where ρ_k is the pseudorange between the receiver and the k^{th} satellite, x_k is the position vector of the kth satellite, and x_r is the receiver position vector. Equation 3.3 expands Equation 3.2.

$$\begin{aligned}\rho_k &= \sqrt{(x_k - x_r)^2 + (y_k - y_r)^2 + (z_k - z_r)^2} + ct_r \\ &= f(x_r, y_r, z_r, t_r)\end{aligned} \tag{3.3}$$

The four unknowns in Equation 3.3 ($x_r,\ y_r,\ z_r,$ and ct_r) clearly show why four satellites are needed.

To solve the k pseudorange equations, they are first linearized around an approximate user position and then iterated until the solution converges. If the receiver location is approximately known $(\hat{x}_r, \hat{y}_r, \hat{z}_r)$, the true location (x_r, y_r, z_r) can be found from small

displacements $(\Delta x_r, \Delta y_r, \Delta z_r)$. The solution then takes the form

$$\begin{aligned} x_r &= \hat{x}_r + \Delta x_r \\ y_r &= \hat{y}_r + \Delta y_r \\ z_r &= \hat{z}_r + \Delta z_r \\ t_r &= \hat{t}_r + \Delta t_r \end{aligned} \tag{3.4}$$

where the position is the sum of the approximate position and the displacement. After each iteration, the displacement becomes smaller as the approximate position hones in on the true position.

The pseudorange can now take the form

$$f(x_r, y_r, z_r, t_r) = f(\hat{x}_r + \Delta x_r, \hat{y}_r + \Delta y_r, \hat{z}_r + \Delta z_r, \hat{t}_r + \Delta t_r). \tag{3.5}$$

Expanding about the approximate point using a Taylor series expansion results in Equation 3.6.

$$\begin{aligned} &f(\hat{x}_r + \Delta x_r, \hat{y}_r + \Delta y_r, \hat{z}_r + \Delta z_r, \hat{t}_r + \Delta t_r) = \\ &\quad f(\hat{x}_r, \hat{y}_r, \hat{z}_r, \hat{t}_r) + \frac{\partial f(\hat{x}_r, \hat{y}_r, \hat{z}_r, \hat{t}_r)}{\partial \hat{x}_r}\Delta x_r + \frac{\partial f(\hat{x}_r, \hat{y}_r, \hat{z}_r, \hat{t}_r)}{\partial \hat{y}_r \Delta y_r} + \\ &\quad \frac{\partial f(\hat{x}_r, \hat{y}_r, \hat{z}_r, \hat{t}_r)}{\partial \hat{z}_r}\Delta z_r + \frac{\partial f(\hat{x}_r, \hat{y}_r, \hat{z}_r, \hat{t}_r)}{\partial \hat{t}_r}\Delta t_r + \ \mathit{Higher\ Order\ Terms} \end{aligned} \tag{3.6}$$

Because the goal is to linearize the pseudorange equation, the higher order, nonlinear terms are discarded. The partial derivatives from Equation 3.6 are

$$\begin{aligned} \frac{\partial f(\hat{x}_r, \hat{y}_r, \hat{z}_r, \hat{t}_r)}{\partial \hat{x}_r} &= -\frac{x_k - \hat{x}_r}{\hat{r}_k} \\ \frac{\partial f(\hat{x}_r, \hat{y}_r, \hat{z}_r, \hat{t}_r)}{\partial \hat{y}_r} &= -\frac{y_k - \hat{y}_r}{\hat{r}_k} \\ \frac{\partial f(\hat{x}_r, \hat{y}_r, \hat{z}_r, \hat{t}_r)}{\partial \hat{z}_r} &= -\frac{z_k - \hat{z}_r}{\hat{r}_k} \\ \frac{\partial f(\hat{x}_r, \hat{y}_r, \hat{z}_r, \hat{t}_r)}{\partial \hat{t}_r} &= \ c \end{aligned} \tag{3.7}$$

where $\hat{r}_k$ is the magnitude of the vector from the approximate receiver position to the satellite position shown in Equation 3.8.

$$\hat{r}_k = \sqrt{(x_k - \hat{x}_r)^2 + (y_k - \hat{y}_r)^2 + (z_k - \hat{z}_r)^2} \tag{3.8}$$

Substituting Equations 3.4 and 3.7 into Equation 3.6 yields

$$\rho_k = \hat{\rho}_k - \frac{x_k - \hat{x}_r}{\hat{r}_k}\Delta x_r - \frac{y_k - \hat{y}_r}{\hat{r}_k}\Delta y_r - \frac{z_k - \hat{z}_r}{\hat{r}_k}\Delta z_r + c\Delta t_r. \tag{3.9}$$

Rearranging Equation 3.9 with the known quantities on the left and the unknown quantities on the right gives

$$\hat{\rho}_k - \rho_k = \frac{x_k - \hat{x}_r}{\hat{r}_k}\Delta x_r - \frac{y_k - \hat{y}_r}{\hat{r}_k}\Delta y_r - \frac{z_k - \hat{z}_r}{\hat{r}_k}\Delta z_r + c\Delta t_r. \tag{3.10}$$

Assigning new variables to simplify the equation, the following equations are introduced:

$$\begin{aligned} \Delta\rho &= \hat{\rho}_k - \rho_k \\ a_{xk} &= \frac{x_k - \hat{x}_r}{\hat{r}_k} \\ a_{yk} &= \frac{y_k - \hat{y}_r}{\hat{r}_k} \\ a_{zk} &= \frac{z_k - \hat{z}_r}{\hat{r}_k} \end{aligned} \tag{3.11}$$

where (a_{xk}, a_{yk}, a_{zk}) are unit vectors which point from the approximate receiver position to the k^{th} satellite.

Alternatively, the unit vectors which point from the approximate receiver position to the k^{th} satellite can be defined in terms of their azimuth (θ) and elevation (α) angles from the receiver in a local level coordinate frame. This is particularly useful in this simulation as the satellites' locations are described by these angles already. Equation 3.12 outlines the alternative method.

$$\begin{aligned} a_{xk} &= \cos(\alpha_k)\sin(\theta_k) \\ a_{yk} &= \cos(\alpha_k)\cos(\theta_k) \\ a_{zk} &= \sin(\alpha_k) \end{aligned} \tag{3.12}$$

Putting these new variables into Equation 3.10 yields:

$$\Delta\rho_k = a_{xk}\Delta x_r + a_{yk}\Delta y_r + a_{zk}\Delta z_r - c\Delta t_r. \tag{3.13}$$

The linearized system of equations is now ready to be solved for Δx_r, Δy_r, Δz_r and Δt_r using the measurements from all k satellites.

$$\begin{aligned}
\Delta\rho_1 &= a_{x1}\Delta x_r + a_{y1}\Delta y_r + a_{z1}\Delta z_r - c\Delta t_r \\
\Delta\rho_2 &= a_{x2}\Delta x_r + a_{y2}\Delta y_r + a_{z2}\Delta z_r - c\Delta t_r \\
\Delta\rho_3 &= a_{x3}\Delta x_r + a_{y3}\Delta y_r + a_{z3}\Delta z_r - c\Delta t_r \\
&\vdots \\
\Delta\rho_k &= a_{xk}\Delta x_r + a_{yk}\Delta y_r + a_{zk}\Delta z_r - c\Delta t_r
\end{aligned} \tag{3.14}$$

These k linear equations can be written in matrix notation as

$$\begin{bmatrix} \Delta\rho_1 \\ \Delta\rho_2 \\ \Delta\rho_3 \\ \vdots \\ \Delta\rho_k \end{bmatrix} = \begin{bmatrix} a_{x1} & a_{y1} & a_{z1} & -1 \\ a_{x2} & a_{y2} & a_{z2} & -1 \\ a_{x3} & a_{y3} & a_{z3} & -1 \\ \vdots & \vdots & \vdots & \vdots \\ a_{xk} & a_{yk} & a_{zk} & -1 \end{bmatrix} \begin{bmatrix} \Delta x_r \\ \Delta y_r \\ \Delta z_r \\ c\Delta t_r \end{bmatrix} \tag{3.15}$$

or more compactly as

$$\boldsymbol{\Delta\rho} = \mathbf{H}\boldsymbol{\Delta x} \tag{3.16}$$

where

$$\boldsymbol{\Delta\rho} = \begin{bmatrix} \Delta\rho_1 \\ \Delta\rho_2 \\ \Delta\rho_3 \\ \vdots \\ \Delta\rho_k \end{bmatrix}, \mathbf{H} = \begin{bmatrix} a_{x1} & a_{y1} & a_{z1} & -1 \\ a_{x2} & a_{y2} & a_{z2} & -1 \\ a_{x3} & a_{y3} & a_{z3} & -1 \\ \vdots & \vdots & \vdots & \vdots \\ a_{xk} & a_{yk} & a_{zk} & -1 \end{bmatrix}, \text{ and } \boldsymbol{\Delta x} = \begin{bmatrix} \Delta x_r \\ \Delta y_r \\ \Delta z_r \\ c\Delta t_r \end{bmatrix}.$$

Here, the $\boldsymbol{\Delta\rho}$ is the pseudorange difference vector, $\mathbf{H}$ is the measurement matrix and $\boldsymbol{\Delta x}$ is the receiver position displacement vector.

If there are less than 4 visible satellites, the system of equations is under-determined and there is not enough information available to solve for $\mathbf{\Delta x}$. If there are exactly 4 satellites visible, there is one unique solution that solves the system of equations which can be found using Equation 3.17.

$$\mathbf{\Delta x} = \mathbf{H^{-1}} \Delta\rho \tag{3.17}$$

If there are more than 4 satellites visible, there will not be a unique solution as the system of equations is overdetermined. The best solution in this scenario would be to find an answer that minimizes the error between all of the possible solutions and the chosen solution. This chosen solution represents the best fit to all of the possible solutions. This "best fit" solution is calculated by the method of least squares, which assumes the measurements are independent and have equal variances, shown in Equation 3.18.

$$\mathbf{\Delta x} = (\mathbf{H^T H})^{-1} \mathbf{H^T} \Delta\rho \tag{3.18}$$

As mentioned earlier, Equation 3.18 can be iterated until $\mathbf{\Delta x}$ becomes suitably small by adding $\mathbf{\Delta x}$ to the previous solution estimate and calculating a new $\Delta\rho$ which is then plugged back into Equation 3.18.

3.6 Dilution of Precision

As previously discussed, the geometry of the visible satellites plays a large role in the accuracy of the position solution. Ideally, the satellites would be spaces out in azimuth at relatively low elevation angles with a single satellite overhead at zenith. In an urban canyon, this type of geometry would be very difficult to achieve as the buildings block out most of the low elevation satellites leaving most of the visible satellites clustered overhead in a relatively small area of the sky. This clustering of satellites yields very poor DOP values.

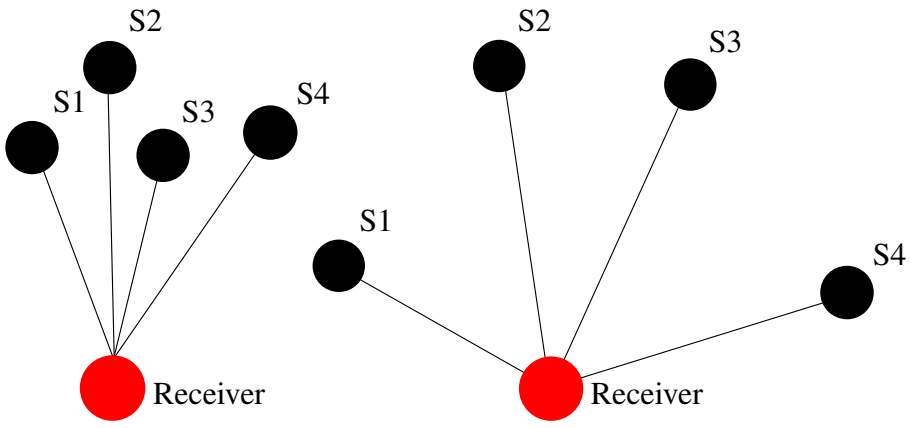

(a) Poor DOP (b) Good DOP

Figure 3.7: Good and bad satellite geometry

The starting point for calculating the DOP is the measurement covariance matrix. Let this matrix be defined according to Equation 3.19.

$$\text{Cov}\{\Delta\rho\} = \begin{bmatrix} \sigma_{\rho_1}^2 & \sigma_{\rho_1\rho_2} & \cdots & \sigma_{\rho_1\rho_k} \\ \sigma_{\rho_2\rho_1} & \sigma_{\rho_2}^2 & \cdots & \sigma_{\rho_2\rho_k} \\ \vdots & \vdots & \ddots & \vdots \\ \sigma_{\rho_k\rho_1} & \sigma_{\rho_k\rho_2} & \cdots & \sigma_{\rho_k}^2 \end{bmatrix} \tag{3.19}$$

The diagonal terms of the covariance matrix are the variances of the measurements from the individual satellites and the off-diagonal terms of the matrix are the covariances between all of the different measurements' errors. However, we make simplifying assumptions about this covariance matrix:

- All of the measurement errors follow a Gaussian distribution with a mean of zero
- All of the measurements from satellites of a single constellation have the same variance equal to the square of the constellation's UERE
- All of the measurement errors are uncorrelated

After implementing these assumptions the covariance matrix simplifies to:

$$\text{Cov}\{\mathbf{\Delta}\rho\} = \mathbf{I}\sigma^{\mathbf{2}}_{\mathbf{UERE}} \tag{3.20}$$

Now, according to Equation 3.18, $\mathbf{\Delta x}$ is a random variable which depends on $\mathbf{\Delta}\rho$. We can take the covariance of Equation 3.18 and get

$$Cov\{\mathbf{\Delta x}\} = \mathbf{Cov}\{(\mathbf{H^T H})^{-1}\mathbf{H^T}\mathbf{\Delta}\rho\} \tag{3.21}$$

Because $\text{Cov}\{\mathbf{A\Delta}\rho\} = \mathbf{A}\,\text{Cov}\{\mathbf{\Delta}\rho\}\mathbf{A^T}$, it follows that

$$\begin{aligned}\text{Cov}\{\mathbf{\Delta x}\} =&(\mathbf{H^T H})^{-1}\mathbf{H^T}\,\text{Cov}\{\mathbf{\Delta}\rho\}\mathbf{H}(\mathbf{H^T H})^{-1}\\ =&(\mathbf{H^T H})^{-1}\mathbf{H^T H}(\mathbf{H^T H})^{-1}\sigma^{\mathbf{2}}_{\mathbf{UERE}}\\ =&(\mathbf{H^T H})^{-1}\sigma^{\mathbf{2}}_{\mathbf{UERE}}\end{aligned} \tag{3.22}$$

The DOP matrix is defined as $(\mathbf{H^T H})^{-1}$, depends completely on the satellite geometry, and relates the errors in the measurements to an error in receiver position. Normally at this point, the errors are in the ECEF coordinate frame which has little significance to the end user. To get from ECEF to a local-level coordinate frame (such as ease, north, up), a direction cosine matrix would be used to convert the errors. However, in this simulation the local level azimuth and elevation angles were used to construct the measurement matrix so the errors are already expressed in the local-level frame!

Because $\mathbf{\Delta x}$ has four constituents, the result of this operation is a 4×4 matrix that takes the form

$$\text{Cov}\{\mathbf{\Delta x}\} = \begin{bmatrix} \sigma^2_E & \sigma_{NE} & \sigma_{UE} & \sigma_{ct_rE} \\ \sigma_{EN} & \sigma^2_N & \sigma_{UN} & \sigma_{ct_rN} \\ \sigma_{EU} & \sigma_{NU} & \sigma^2_U & \sigma_{ct_rU} \\ \sigma_{Ect_r} & \sigma_{Nct_r} & \sigma_{Uct_r} & \sigma^2_{ct_r} \end{bmatrix} \tag{3.23}$$

Equation 3.24 rewrites the DOP matrix for convenience's sake.

$$(\mathbf{H^T H})^{-1} = \begin{bmatrix} D_{11} & D_{12} & D_{13} & D_{14} \\ D_{21} & D_{22} & D_{23} & D_{24} \\ D_{31} & D_{32} & D_{33} & D_{34} \\ D_{41} & D_{42} & D_{43} & D_{44} \end{bmatrix} \tag{3.24}$$

According to the rewritten matrix, the GDOP is calculated using the formula

$$GDOP = \sqrt{D_{11} + D_{22} + D_{33} + D_{44}} \tag{3.25}$$

Consequently, the component errors are related to the UERE via the GDOP by

$$\sqrt{\sigma_E^2 + \sigma_N^2 + \sigma_U^2 + \sigma_{ct_r}^2} = GDOP \times \sigma_{UERE} \tag{3.26}$$

It is clearly seen that the value of GDOP amplifies the measurement errors onto the position solution.

Several other measures of DOP exist including, PDOP, HDOP, VDOP and Time Dilution of Precision (TDOP). The DOP measures are defined as:

$$\begin{aligned} PDOP &= \sqrt{D_{11} + D_{22} + D_{33}} \\ HDOP &= \sqrt{D_{11} + D_{22}} \\ VDOP &= \sqrt{D_{33}} \\ TDOP &= \sqrt{D_{44}} \end{aligned} \tag{3.27}$$

These too are relatable to the UERE via

$$\begin{aligned} \sqrt{\sigma_E^2 + \sigma_N^2 + \sigma_U^2} &= PDOP \times \sigma_{UERE} \\ \sqrt{\sigma_E^2 + \sigma_N^2} &= HDOP \times \sigma_{UERE} \\ \sigma_U &= VDOP \times \sigma_{UERE} \\ \sigma_{ct_r} &= TDOP \times \sigma_{UERE} \end{aligned} \tag{3.28}$$

The lower the value of DOP, the more accurate the final position solution. For this research PDOP was chosen as the metric of judgement as it characterizes the

three-dimensional accuracy of the final position solution. Furthermore, the calculations previously described assume that all the measurements have the same variance which is acceptable if all the measurements come from properly functioning satellites from a single constellation. However, different GNSS constellations have different UERE values and hence, different measurement variances. This problem is solved by using the weighted least-squares method which is tackled in Section 3.7.

3.7 Weighted Least Squares

To get representative simulation results when combining multiple GNSSs for a position solution, the least squares calculations must account for the accuracy differences between the different GNSSs. This is accomplished by using a technique known as weighted least squares where the measurements from the satellites of each constellation are given an appropriate weight based on the overall system accuracy. The weights are put into the weighting matrix, **W**, which is then included in Equation 3.18 [20]. With the inclusion of the weighting matrix, Equation 3.18 becomes

$$\mathbf{\Delta\hat{x}} = (\mathbf{H^T W H})^{-1}\mathbf{H^T W \Delta}\rho \tag{3.29}$$

and the DOP equation becomes

$$DOP = (\mathbf{H^T W H})^{-1} \tag{3.30}$$

As mentioned earlier, **W** comes from system accuracies. It can be written as

$$\mathbf{W} = \mathbf{R}^{-1} \tag{3.31}$$

where **R** is a covariance matrix. Assuming that the $\Delta\rho$ from all of the satellites are independent and follow a Gaussian distribution, the covariance matrix **R** for m GPS and n

GLONASS satellites is

$$\mathbf{R} = \begin{bmatrix} \frac{\sigma^2_{1GPS}}{\sigma^2_{GPS}} & 0 & & \cdots & & 0 \\ 0 & \ddots & 0 & & & \\ & 0 & \frac{\sigma^2_{mGPS}}{\sigma^2_{GPS}} & 0 & & \vdots \\ \vdots & & 0 & \frac{\sigma^2_{1GLO}}{\sigma^2_{GPS}} & 0 & \\ & & & 0 & \ddots & 0 \\ 0 & & \cdots & & 0 & \frac{\sigma^2_{nGLO}}{\sigma^2_{GPS}} \end{bmatrix} \tag{3.32}$$

Notice if there are k satellites total, then the matrix will be $k \times k$ with only the diagonal elements being non-zero. The variances are normalized by the GPS variance. This means that the **R** matrix will default to the identity matrix if only GPS satellites are used or if the systems from which the satellites come from have equal variances.

The variances used in this research are outlined in Table 3.3.

Table 3.3: GNSS Variances

GPS	6.76 m
GLONASS	19.89 m
Galileo	4 m
Compass	25 m

As an example, the **R** matrix for three GPS satellites and two GLONASS satellites is

$$\mathbf{R} = \begin{bmatrix} 1 & 0 & 0 & 0 & 0 \\ 0 & 1 & 0 & 0 & 0 \\ 0 & 0 & 1 & 0 & 0 \\ 0 & 0 & 0 & 2.94 & 0 \\ 0 & 0 & 0 & 0 & 2.94 \end{bmatrix} \tag{3.33}$$

3.8 Combining Systems

Combining pseudorange measurements from multiple system systems requires only slight modification of the **H** matrix which is derived from the $\mathbf{\Delta}\rho$ equations in 3.14. Pseudorange measurements take the same form whether they are from a GPS satellite or another system's satellite. The only difference between the two will be a different clock error for a different system's satellite compared to a clock error for a GPS satellite. This is because the different GNSSs' system times are not synchronized. The pseudorange equations for m GPS satellites and n GLONASS satellites are written as

$$\begin{aligned}
\Delta\rho_{1GPS} &= a_{x1GPS}\Delta x_r + a_{y1GPS}\Delta y_r + a_{z1GPS}\Delta z_r - c\Delta t_{rGPS} \\
&\vdots \\
\Delta\rho_{mGPS} &= a_{xmGPS}\Delta x_r + a_{ymGPS}\Delta y_r + a_{zmGPS}\Delta z_r - c\Delta t_{rGPS} \\
\Delta\rho_{1GLO} &= a_{x1GLO}\Delta x_r + a_{y1GLO}\Delta y_r + a_{z1GLO}\Delta z_r - c\Delta t_{rGLO} \\
&\vdots \\
\Delta\rho_{nGLO} &= a_{xnGLO}\Delta x_r + a_{ynGLO}\Delta y_r + a_{znGLO}\Delta z_r - c\Delta t_{rGLO}
\end{aligned} \tag{3.34}$$

The new set of $\Delta\rho$ equations can now be written in matrix form shown in Equation 3.35.

$$\begin{bmatrix} \Delta\rho_{1GPS} \\ \vdots \\ \Delta\rho_{mGPS} \\ \Delta\rho_{1GLO} \\ \vdots \\ \Delta\rho_{nGLO} \end{bmatrix} = \begin{bmatrix} a_{x1GPS} & a_{y1GPS} & a_{z1GPS} & -1 & 0 \\ \vdots & \vdots & \vdots & \vdots & \vdots \\ a_{xmGPS} & a_{ymGPS} & a_{zmGPS} & -1 & 0 \\ a_{x1GLO} & a_{y1GLO} & a_{z1GLO} & 0 & -1 \\ \vdots & \vdots & \vdots & \vdots & \vdots \\ a_{xnGLO} & a_{ynGLO} & a_{znGLO} & 0 & -1 \end{bmatrix} \begin{bmatrix} \Delta x_r \\ \Delta y_r \\ \Delta z_r \\ c\Delta t_{rGPS} \\ c\Delta t_{rGLO} \end{bmatrix} \tag{3.35}$$

Now if the time offset between the systems is not known, then $c\Delta t_{rGLO}$ would be a fifth unknown that would have to be solved for. However, it is assumed that the offset is

known in this simulation. The time offset is defined as

$$\Delta t_{GPS-GLO} = c\Delta t_{GPS} - c\Delta t_{GLO} \tag{3.36}$$

This offset gets added to the bottom of the $\mathbf{\Delta}\rho$ matrix as a measurement so the new system of equations becomes

$$\begin{bmatrix} \Delta\rho_{1GPS} \\ \vdots \\ \Delta\rho_{mGPS} \\ \Delta\rho_{1GLO} \\ \vdots \\ \Delta\rho_{nGLO} \\ \Delta t_{GPS-GLO} \end{bmatrix} = \begin{bmatrix} a_{x1GPS} & a_{y1GPS} & a_{z1GPS} & -1 & 0 \\ \vdots & \vdots & \vdots & \vdots & \vdots \\ a_{xmGPS} & a_{ymGPS} & a_{zmGPS} & -1 & 0 \\ a_{x1GLO} & a_{y1GLO} & a_{z1GLO} & 0 & -1 \\ \vdots & \vdots & \vdots & \vdots & \vdots \\ a_{xnGLO} & a_{ynGLO} & a_{znGLO} & 0 & -1 \\ 0 & 0 & 0 & 1 & -1 \end{bmatrix} \begin{bmatrix} \Delta x_r \\ \Delta y_r \\ \Delta z_r \\ c\Delta t_{rGPS} \\ c\Delta t_{rGLO} \end{bmatrix} \tag{3.37}$$

The final row of $\mathbf{H}$ takes the time bias between GPS and GLONASS into account. Now, the $\mathbf{R}$ matrix must also be amended. In an ideal world, the time offset would be exactly known, however, this is not always the case. To take into account the inaccuracies in the time offset value, the covariance of the error in seconds multiplied by the speed of light, c, gives the time offset covariance in units of meters so it can be normalized by the GPS covariance. The new $\mathbf{R}$ matrix is

$$\mathbf{R} = \begin{bmatrix} \frac{\sigma^2_{1GPS}}{\sigma^2_{GPS}} & 0 & & \cdots & \cdots & & 0 \\ 0 & \ddots & 0 & & & & \\ & 0 & \frac{\sigma^2_{mGPS}}{\sigma^2_{GPS}} & 0 & & & \vdots \\ \vdots & & 0 & \frac{\sigma^2_{1GLO}}{\sigma^2_{GPS}} & 0 & & \vdots \\ \vdots & & & 0 & \ddots & 0 & \\ & & & & 0 & \frac{\sigma^2_{nGLO}}{\sigma^2_{GPS}} & 0 \\ 0 & & \cdots & \cdots & & 0 & \frac{c\sigma^2_{\Delta t_{GPS-GLO}}}{\sigma^2_{GPS}} \end{bmatrix} \tag{3.38}$$

Adding satellites from a third constellation follows the same pattern. If p Galileo satellites were to be added to the previous constellation consisting of m GPS and n

GLONASS satellites, then the matrix form of the $\Delta\rho$ equation including the known time offset becomes

$$\begin{bmatrix} \Delta\rho_{1GPS} \\ \vdots \\ \Delta\rho_{mGPS} \\ \Delta\rho_{1GLO} \\ \vdots \\ \Delta\rho_{nGLO} \\ \Delta\rho_{1GAL} \\ \vdots \\ \Delta\rho_{pGAL} \\ \Delta t_{GPS-GLO} \\ \Delta t_{GPS-GAL} \end{bmatrix} = \begin{bmatrix} a_{x1GPS} & a_{y1GPS} & a_{z1GPS} & -1 & 0 & 0 \\ \vdots & \vdots & \vdots & \vdots & \vdots & \vdots \\ a_{xmGPS} & a_{ymGPS} & a_{zmGPS} & -1 & 0 & 0 \\ a_{x1GLO} & a_{y1GLO} & a_{z1GLO} & 0 & -1 & 0 \\ \vdots & \vdots & \vdots & \vdots & \vdots & \vdots \\ a_{xnGLO} & a_{ynGLO} & a_{znGLO} & 0 & -1 & 0 \\ a_{x1GAL} & a_{y1GAL} & a_{z1GAL} & 0 & 0 & -1 \\ \vdots & \vdots & \vdots & \vdots & \vdots & \vdots \\ a_{xpGAL} & a_{ypGAL} & a_{zpGAL} & 0 & 0 & -1 \\ 0 & 0 & 0 & 1 & -1 & 0 \\ 0 & 0 & 0 & 1 & 0 & -1 \end{bmatrix} \begin{bmatrix} \Delta x_r \\ \Delta y_r \\ \Delta z_r \\ c\Delta t_{rGPS} \\ c\Delta t_{rGLO} \\ c\Delta t_{rGAL} \end{bmatrix} \tag{3.39}$$

and the $\mathbf{R}$ matrix becomes

$$\mathbf{R} = \begin{bmatrix} \frac{\sigma^2_{1GPS}}{\sigma^2_{GPS}} & 0 & \cdots & & & & & & & \cdots & 0 \\ 0 & \ddots & 0 & & & & & & & & \vdots \\ \vdots & 0 & \frac{\sigma^2_{mGPS}}{\sigma^2_{GPS}} & 0 & & & & & & & \\ & & 0 & \frac{\sigma^2_{1GLO}}{\sigma^2_{GPS}} & 0 & & & & & & \\ & & & 0 & \ddots & 0 & & & & & \\ & & & & 0 & \frac{\sigma^2_{nGLO}}{\sigma^2_{GPS}} & 0 & & & & \\ & & & & & 0 & \frac{\sigma^2_{1GAL}}{\sigma^2_{GPS}} & 0 & & & \\ & & & & & & 0 & \ddots & 0 & & \\ & & & & & & & 0 & \frac{\sigma^2_{pGAL}}{\sigma^2_{GPS}} & 0 & \vdots \\ \vdots & & & & & & & & 0 & \frac{c\sigma^2_{\Delta t_{GPS-GLO}}}{\sigma^2_{GPS}} & 0 \\ 0 & \cdots & & & & & & & \cdots & 0 & \frac{c\sigma^2_{\Delta t_{GPS-GAL}}}{\sigma^2_{GPS}} \end{bmatrix} \tag{3.40}$$

The process continues just the same for adding satellites from a fourth constellation to the equations.

The simulation of the barometric altimeter takes a slightly different form. For DOP calculations, the baro-altimeter was modeled as a satellite that sits directly overhead the receiver and does not move from zenith so it only measures the vertical channel. Furthermore, the barometer measurements do not depend on time to calculate altitude. Using Equation 3.12 and the elevation angle to the simulated baro-altimeter satellite of $\alpha_{BA} = 90°$, the $\Delta\rho_{BA}$ equation for this "satellite" looks like

$$\Delta\rho_{BA} = \cos(\alpha_{BA})\sin(\theta_{BA})\Delta x_r + \cos(\alpha_{BA})\cos(\theta_{BA})\Delta y_r + \sin(\alpha_{BA})\Delta z_r \tag{3.41}$$

When 90° is plugged in for α_{BA}, the equation simplifies drastically to

$$\Delta\rho_{BA} = \Delta z_r \tag{3.42}$$

This can now be added to the bottom of the $\boldsymbol{\Delta\rho}$ matrix equation.

$$\begin{bmatrix} \Delta\rho_{1GPS} \\ \vdots \\ \Delta\rho_{mGPS} \\ \Delta\rho_{1GLO} \\ \vdots \\ \Delta\rho_{nGLO} \\ \Delta\rho_{1GAL} \\ \vdots \\ \Delta\rho_{pGAL} \\ \Delta t_{GPS-GLO} \\ \Delta t_{GPS-GAL} \\ \Delta\rho_{BA} \end{bmatrix} = \begin{bmatrix} a_{x1GPS} & a_{y1GPS} & a_{z1GPS} & -1 & 0 & 0 \\ \vdots & \vdots & \vdots & \vdots & \vdots & \vdots \\ a_{xmGPS} & a_{ymGPS} & a_{zmGPS} & -1 & 0 & 0 \\ a_{x1GLO} & a_{y1GLO} & a_{z1GLO} & 0 & -1 & 0 \\ \vdots & \vdots & \vdots & \vdots & \vdots & \vdots \\ a_{xnGLO} & a_{ynGLO} & a_{znGLO} & 0 & -1 & 0 \\ a_{x1GAL} & a_{y1GAL} & a_{z1GAL} & 0 & 0 & -1 \\ \vdots & \vdots & \vdots & \vdots & \vdots & \vdots \\ a_{xpGAL} & a_{ypGAL} & a_{zpGAL} & 0 & 0 & -1 \\ 0 & 0 & 0 & 1 & -1 & 0 \\ 0 & 0 & 0 & 1 & 0 & -1 \\ 0 & 0 & 1 & 0 & 0 & 0 \end{bmatrix} \begin{bmatrix} \Delta x_r \\ \Delta y_r \\ \Delta z_r \\ c\Delta t_{rGPS} \\ c\Delta t_{rGLO} \\ c\Delta t_{rGAL} \end{bmatrix} \tag{3.43}$$

The accuracy of the baro-altimeter can be set based on the chosen covariance, in meters^2, that is used in the **R** matrix. If set to 0 the baro-altimeter exactly knows the altitude, if it is set to ∞ (or otherwise a very large number), then it does not know the altitude at all.

3.9 Method of Choosing Satellites

Augmentation of the GPS constellation is not always necessary. If the receiver is in an open field or in a location where an acceptable GPS-only position solution is available, then augmentation from the other constellations is not needed. Furthermore, since the United States controls GPS, the performance characteristics are known and the system can be trusted. This may not be the case for foreign systems, however, so minimum dependence on the foreign GNSSs is attractive to military users and other users who require precision in difficult reception environments.

The simulation contains an augmentation algorithm which first tries to obtain a position solution with acceptable PDOP. For this research, a PDOP $\leq$ 6 is defined as the threshold for acceptability. Only if the GPS-only solution is either unacceptable or unavailable does the algorithm augment the GPS constellation with foreign satellites. The algorithm is described in Figure 3.8.

When augmenting, if there are fewer than 4 GPS satellites visible, the simulation will automatically add the necessary number of non-GPS satellites to get a total of 4. This method selectively augments the GPS constellation with the minimum number of non-GPS satellites necessary to get an acceptable PDOP. This means that the simulation will stop augmenting the constellation once the PDOP meets the threshold. This may lead to settling for a PDOP of 4.8 with selective augmentation using only one foreign satellite rather than using all the satellites in view for a PDOP of 3.6, for instance, but the solution still meets the requirement and the dependence on foreign systems is limited. Selective

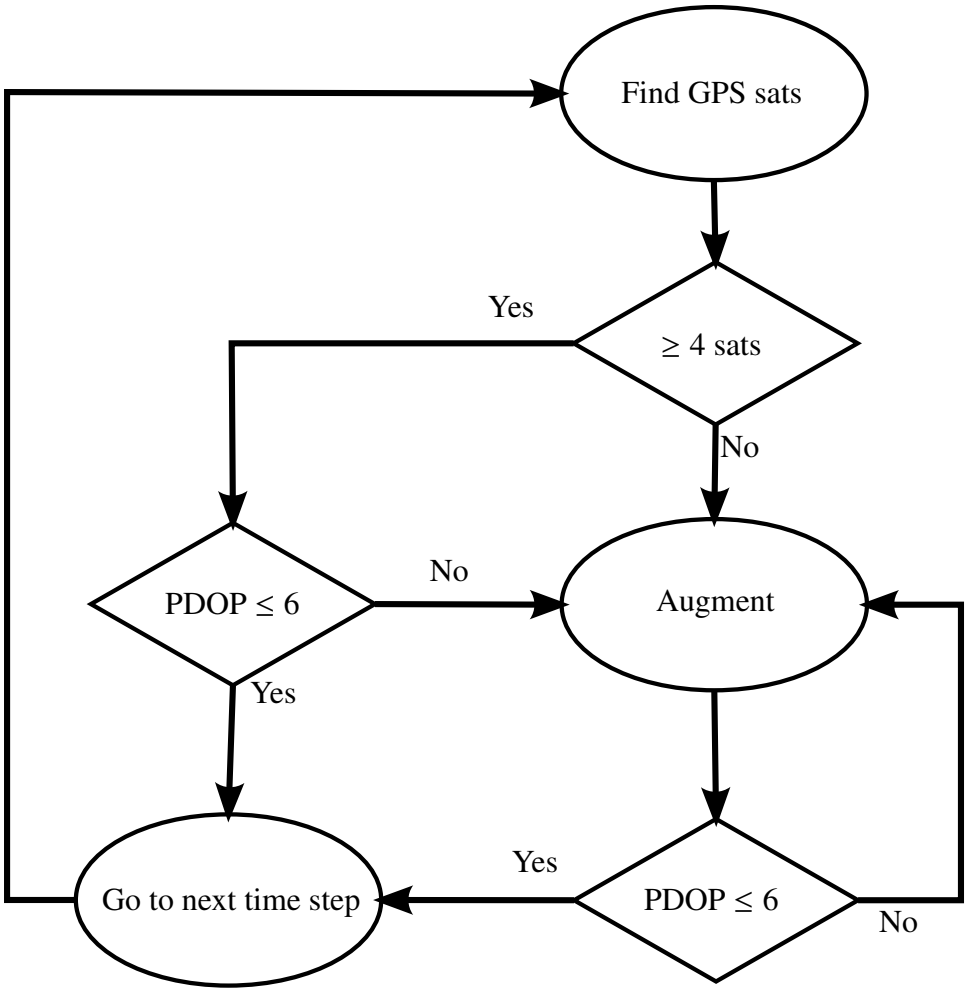

Figure 3.8: Satellite augmentation algorithm

augmentation defaults to all-in-view when all the satellites have been added to try and meet the threshold. The availability using selective augmentation will always be identical to the availability using an all-in-view selection scheme, though the PDOP could be slightly worse yet still below the threshold.

Any time a satellite needs to be added, the one that yields the best PDOP will be used. To find out which satellite is the best, a brute force method was implemented. Each visible satellite is tested with the current constellation and the PDOP is calculated. The satellite that gives the best PDOP is used. If augmenting with one satellite does not give an acceptable PDOP, or more than one satellite was required to get to the minimum of 4,

then all combinations of two satellites from those that are visible will be tested and the best pair will be used, and likewise for higher numbers of satellites.

Instead of using the brute force method and testing all possible combinations of satellites, the geometry of the current constellation could be examined and the location of the best satellite predicted. The simulation could then quickly augment the current constellation with the satellite that is closest to this optimal location bypassing the need to try numerous combinations. However, even using the brute force method, the simulation runs very quickly. In fact, it only slowed down when there were approximately 25 or more foreign satellites in view to search through, though, when this was the case, GPS provided a quality solution on its own so no augmentation was necessary. As augmentation is only required when visible satellites are scarce, the situation naturally limits the number of possible combinations of foreign satellites making the brute force method timely and satisfactory.

3.10 Altimeter Accuracy

All of the equations given in Chapter 2 assume a "standard atmosphere". This is the average pressure, density, and temperature at various altitudes. The standard day at sea level has a temperature of 59° F and a pressure of 29.92 inHg. When examining Dayton, OH for comparison to the standard atmosphere, data for all of 2001 was collected. The average sea level pressure recorded in Dayton, OH was 30.07 inHg with a standard deviation of 0.19 inHg. Pressure changes over the course of a day as well, and on average, the difference between the minimum and maximum pressure recorded each day was 0.19 inHg. When plotted, the average sea level pressure recorded each day takes on a Gaussian-like distribution seen in Figure 3.9.

If the altimeter follows the linear approximation, Equation 2.3 says that altitude will vary by $1,250$ ft for each one inch change in the pressure. From the data sample, the daily

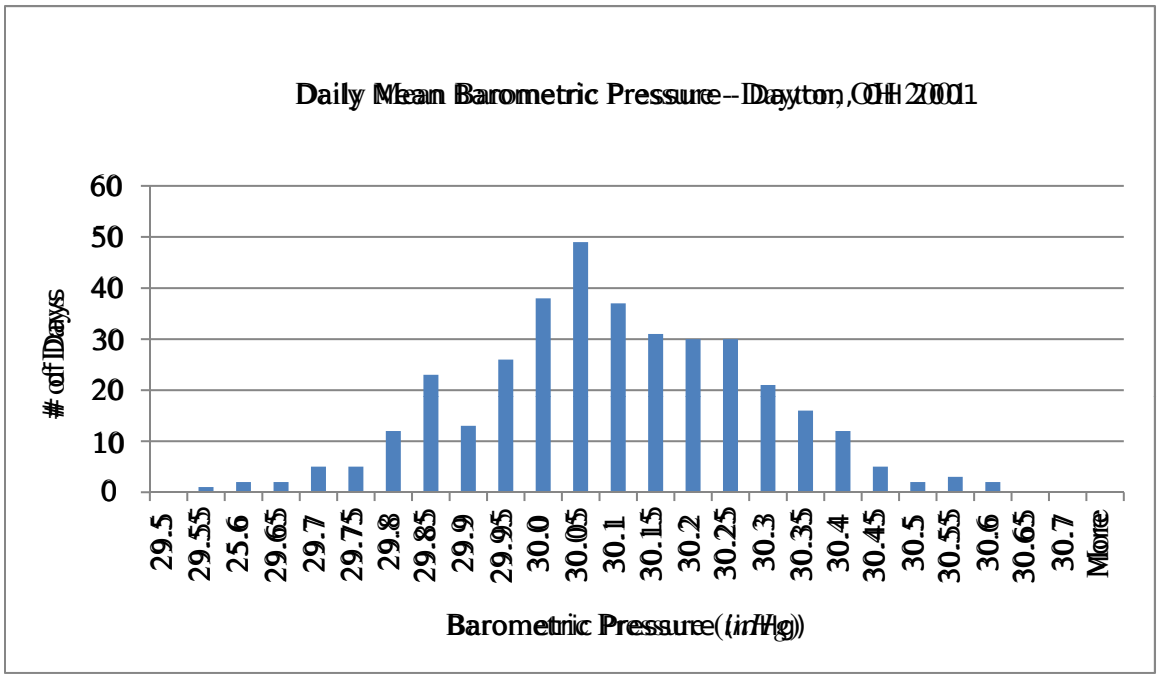

Figure 3.9: Distribution of daily average sea level pressure in Dayton, OH in 2001

average was between 30.44 inHg and 29.7 inHg approximately 95% of the days. Accordingly, on these days, the altimeter would see an error of up to 415 ft. If on the other hand, the altimeter could be adjusted for the sea level pressure at its location just once at the beginning of the day, then the error would be up to 230 ft. When adjusted for current sea level pressure settings, baro-altimeters can have an accuracy between 2 ft and 3 ft [32]. There are some combination GPS/baro-altimeters that have an altimeter accuracy of 10 ft with a resolution of one foot [10].

3.11 Unmanned Aerial Vehicle Simulation

In order to simulate the flight of an autonomous UAV, an error state Kalman Filter is implemented with a very simple inertial navigation system (INS) error model and is updated with position updates from GPS or GPS augmented with foreign GNSSs. This

model is derived in [3]. In the Kalman Filter, there are 11 states:

$$
\begin{aligned}
x_1 &= \text{east position error} \\
x_2 &= \text{east velocity error} \\
x_3 &= \text{platform tilt about north axis} \\
x_4 &= \text{north position error} \\
x_5 &= \text{north velocity error} \\
x_6 &= \text{platform tilt about east axis} \\
x_7 &= \text{vertical position error} \\
x_8 &= \text{vertical velocity error} \\
x_9 &= \text{platform azimuth error} \\
x_{10} &= \text{range bias error due to GPS receiver clock} \\
x_{11} &= \text{range rate error due to GPS receiver clock}
\end{aligned}
\tag{3.44}
$$

These states propagate via the equation

$$\dot{\mathbf{x}} = \mathrm{F}\mathbf{x} + \mathrm{G}\mathbf{w} \tag{3.45}$$

The state transition matrix, F, is

$$F = \begin{bmatrix} 0 & 1 & 0 & 0 & 0 & 0 & 0 & 0 & 0 & 0 & 0 \\ 0 & 0 & -g & 0 & 0 & 0 & 0 & 0 & 0 & 0 & 0 \\ 0 & \frac{1}{R_e} & 0 & 0 & 0 & 0 & 0 & 0 & 0 & 0 & 0 \\ 0 & 0 & 0 & 0 & 1 & 0 & 0 & 0 & 0 & 0 & 0 \\ 0 & 0 & 0 & 0 & 0 & -g & 0 & 0 & 0 & 0 & 0 \\ 0 & 0 & 0 & 0 & \frac{1}{R_e} & 0 & 0 & 0 & 0 & 0 & 0 \\ 0 & 0 & 0 & 0 & 0 & 0 & 0 & 1 & 0 & 0 & 0 \\ 0 & 0 & 0 & 0 & 0 & 0 & 0 & 0 & 0 & 0 & 0 \\ 0 & 0 & 0 & 0 & 0 & 0 & 0 & 0 & 0 & 0 & 0 \\ 0 & 0 & 0 & 0 & 0 & 0 & 0 & 0 & 0 & 0 & 1 \\ 0 & 0 & 0 & 0 & 0 & 0 & 0 & 0 & 0 & 0 & 0 \end{bmatrix} \tag{3.46}$$

The matrix G is

$$G = \begin{bmatrix} 0 & 0 & 0 & 0 & 0 & 0 & 0 & 0 \\ 1 & 0 & 0 & 0 & 0 & 0 & 0 & 0 \\ 0 & 1 & 0 & 0 & 0 & 0 & 0 & 0 \\ 0 & 0 & 0 & 0 & 0 & 0 & 0 & 0 \\ 0 & 0 & 1 & 0 & 0 & 0 & 0 & 0 \\ 0 & 0 & 0 & 1 & 0 & 0 & 0 & 0 \\ 0 & 0 & 0 & 0 & 0 & 0 & 0 & 0 \\ 0 & 0 & 0 & 0 & 1 & 0 & 0 & 0 \\ 0 & 0 & 0 & 0 & 0 & 1 & 0 & 0 \\ 0 & 0 & 0 & 0 & 0 & 0 & 1 & 0 \\ 0 & 0 & 0 & 0 & 0 & 0 & 0 & 1 \end{bmatrix} \tag{3.47}$$

The matrix Q is made up of the strengths of the white noise driving the errors in the states. The values that populate the Q matrix come from [3] and characterize the errors in the

accelerometers and gyroscopes. The Q matrix is

$$Q = \begin{bmatrix} 2.25e-6 & 0 & 0 & 0 & 0 & 0 & 0 & 0 \\ 0 & 3.0625e-8 & 0 & 0 & 0 & 0 & 0 & 0 \\ 0 & 0 & 2.25e-6 & 0 & 0 & 0 & 0 & 0 \\ 0 & 0 & 0 & 3.0625e-8 & 0 & 0 & 0 & 0 \\ 0 & 0 & 0 & 0 & 2.25e-6 & 0 & 0 & 0 \\ 0 & 0 & 0 & 0 & 0 & 3.0625e-8 & 0 & 0 \\ 0 & 0 & 0 & 0 & 0 & 0 & 0.003 & 0 \\ 0 & 0 & 0 & 0 & 0 & 0 & 0 & 0.0118 \end{bmatrix} \quad (3.48)$$

The measurement matrix H is

$$H = \begin{bmatrix} 1 & 0 & 0 & 0 & 0 & 0 & 0 & 0 & 0 & 0 & 0 \\ 0 & 1 & 0 & 0 & 0 & 0 & 0 & 0 & 0 & 0 & 0 \\ 0 & 0 & 0 & 1 & 0 & 0 & 0 & 0 & 0 & 0 & 0 \\ 0 & 0 & 0 & 0 & 1 & 0 & 0 & 0 & 0 & 0 & 0 \\ 0 & 0 & 0 & 0 & 0 & 0 & 1 & 0 & 0 & 0 & 0 \\ 0 & 0 & 0 & 0 & 0 & 0 & 0 & 1 & 0 & 0 & 0 \\ 0 & 0 & 0 & 0 & 0 & 0 & 0 & 0 & 0 & 1 & 0 \\ 0 & 0 & 0 & 0 & 0 & 0 & 0 & 0 & 0 & 0 & 1 \end{bmatrix} \quad (3.49)$$

When a position solution is available, the update is incorporated by way of the dilution of precision matrix multiplied by random values that follow a Gaussian distribution with zero mean and a standard deviation equal to the σ_{UERE} of GPS in order to simulate the "measurement errors" in the position and velocity update from GPS in terms of east, north, and up quantities.

The discrete time Kalman Filtering equations are given in Equations 3.50-3.56.

$$K_k = P_k^- H^T (H P_k^- H^T + R_k)^{-1} \tag{3.50}$$

$$\hat{x}_k = \hat{x}_k^- + K_k(z_k - H\hat{x}_k^-) \tag{3.51}$$

$$\hat{x}_k = \hat{x}_k^- \tag{3.52}$$

$$P_k = (I - K_k H) P_k^- \tag{3.53}$$

$$P_k = P_k^- \tag{3.54}$$

$$\hat{x}_{k+1}^- = \Phi \hat{x}_k \tag{3.55}$$

$$P_{k+1}^- = \Phi P_k \Phi^T + Q \tag{3.56}$$

$$\tag{3.57}$$

In the Kalman Filtering equations, subscript k denotes the time step and a minus sign in the exponent indicates an update has not been incorporated. The hat on $\hat{x}$ denotes that this is the Kalman filter's estimate of the the state vector x. Φ is the state transition matrix which is the F matrix converted for use in a discrete time algorithm. The Q matrix in Equation 3.56 has also been converted to discrete time. The matrix P is the covariance matrix of the state estimate and the matrix R is the covariance of the measurement noise, which in this case is the DOP matrix multiplied by the σ_{UERE} for GPS.

Equation 3.50 gives what is known as the Kalman gain. This is used to weight subsequent measurement updates as well as in calculating the post-update covariance. Measurements, z_k, are incorporated using Equation 3.51. If no update is available, Equation 3.52 is used instead. Equation 3.53 updates the covariance of the state estimate when a measurement is incorporated. Otherwise, when no measurement update is available, Equation 3.54 is used. Equations 3.55 and 3.56 propagate the state estimate and covariance forward in time to the next time step and the cycle is repeated.

3.12 Summary

This chapter began by going over the simulation used in this research. It outlined the scenario, and delved into the assumptions made as well as a description of the simulation. In Section 3.5, finding position and velocity from pseudorange measurements was discussed. Following this, Sections 3.6 and 3.7 discussed calculating the DOP and applying weighted least squares. In Section 3.8 the method of combining multiple systems together was examined. Then, Section 3.9 discussed an alternative method of selecting augmentation satellites. Section 3.10 discussed the accuracy associated with barometric altimeters and Section 3.11 closed out the chapter with details of the UAV simulation.

4 Results and Analysis

4.1 Overview

This chapter presents and examines the results of the simulation. Section 4.2 contains the results of the simulation using only GPS which is used as a baseline for comparison to the rest of the results. Then, the next sections will deliver the results of the GPS constellation combined with the other global navigation systems and a barometric altimeter. Finally the results of the UAV navigation scenario will be discussed in Section 4.8.

4.2 GPS Results

The GPS constellation has global coverage yet buildings and other obstructions can block the sight lines to many satellites causing a disruption of positioning service. Figure 4.1 shows the ground tracks of all GPS satellites over the course of 24 hours on 4 July 2011. The colored tracks in the figure show where the satellites are visible to a receiver in Dayton, OH with an unobstructed view of the sky.

Contrasting the clear view of the sky is the partially obstructed view of the sky. Figure 4.2 shows the line of sight to a large portion of the sky is blocked by uniformly sized buildings yielding a more limited area of the sky to view satellites. The buildings in this figure are from a UTZ Type II consisting of widely spaced high-rise office buildings.

The symmetric UTZ models do not provide a realistic urban canyon with there uniformity. The Dayton city model, while not extremely accurate, does roughly model the real city buildings found in downtown Dayton and, thus, gives a higher degree of realism to the simulation. Figure 4.3 shows the GPS coverage in the Dayton city model. The coverage is viewed from the location shown in Figure 4.4.

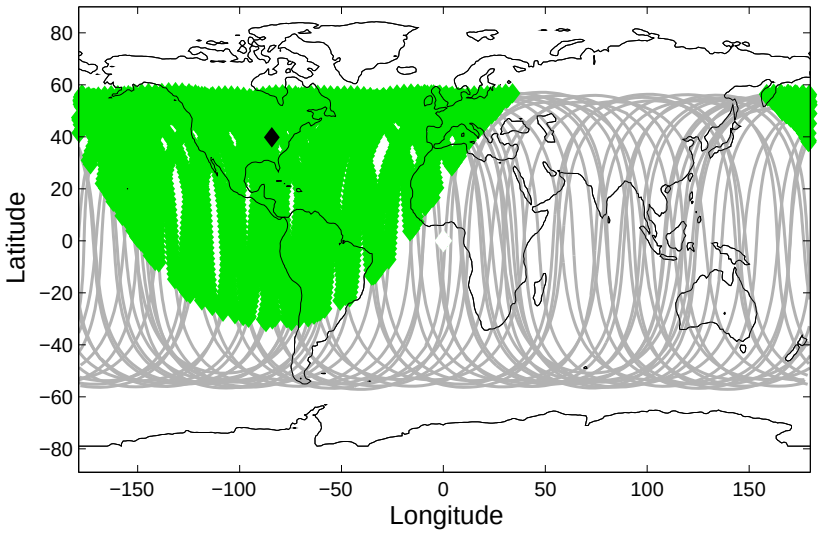

Figure 4.1: Unobstructed GPS visibility in Dayton, OH

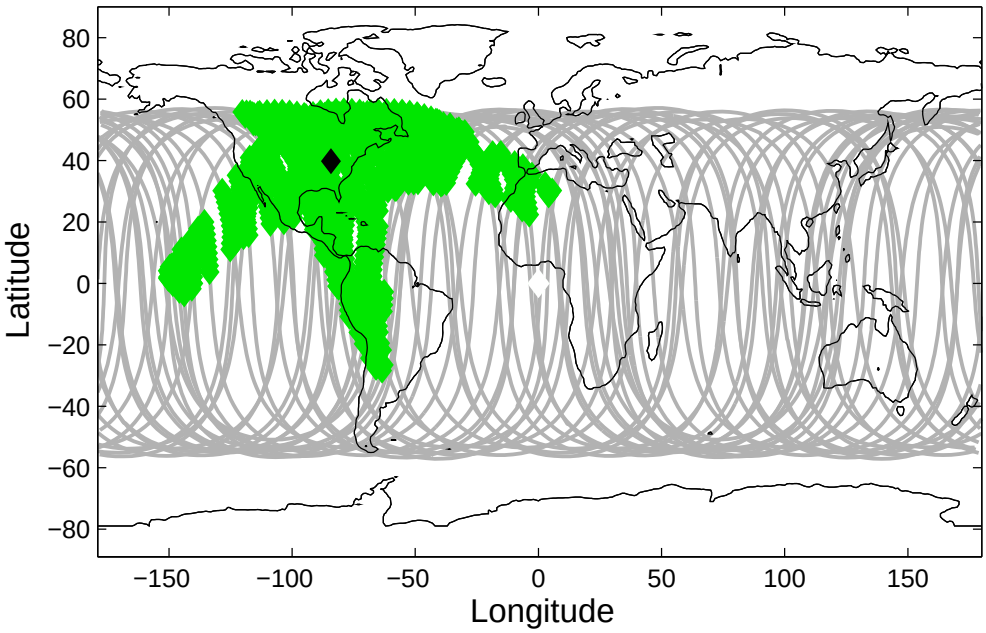

Figure 4.2: Obstructed GPS visibility in Dayton, OH

When there are no obstructions, GPS alone has an excellent PDOP as shown in Figure 4.5. The PDOP acceptability threshold is marked with a dashed red line in all

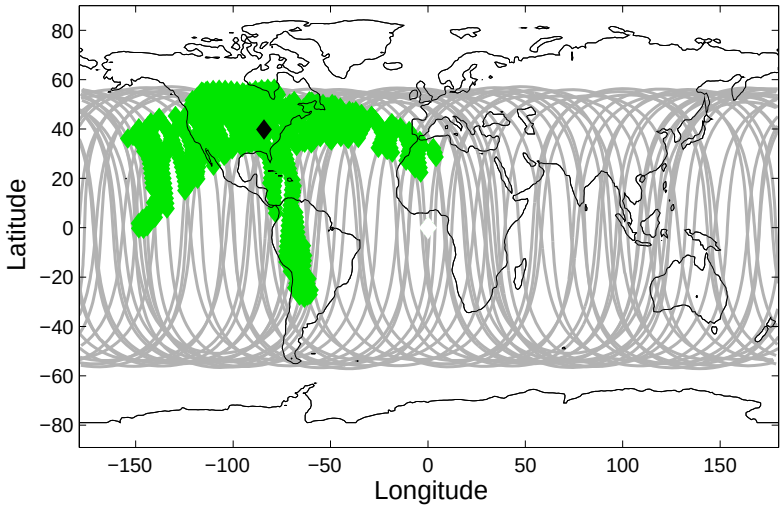

Figure 4.3: Obstructed GPS visibility from Dayton city model

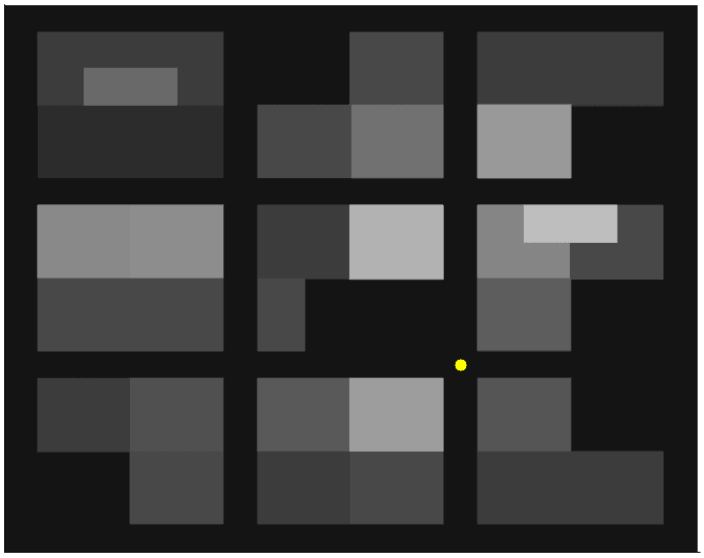

Figure 4.4: Location in Dayton city model

PDOP plots and the number of GPS satellites is shown by the blue color and the red color denotes the number of non-GPS satellites. Figure 4.6 shows that when the location has

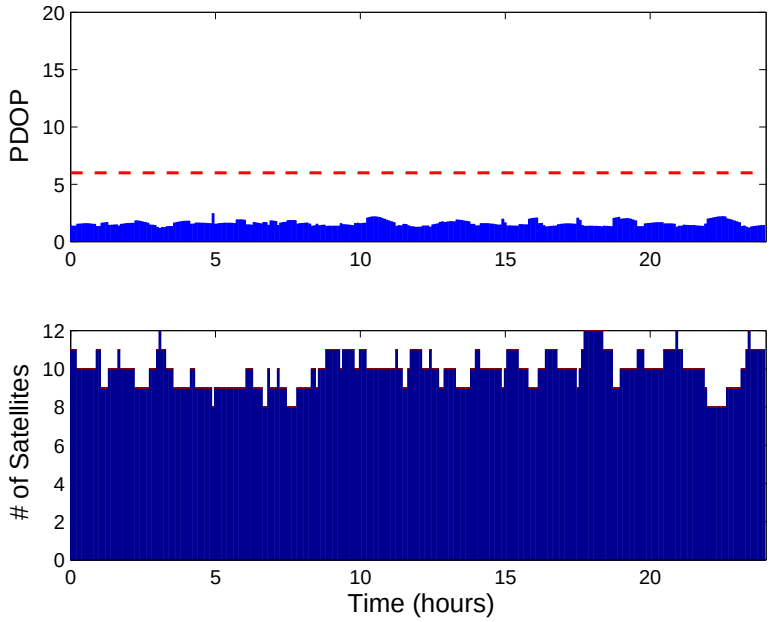

Figure 4.5: PDOP when using only GPS without obstructions

obstructions, like at an intersection in the UTZ Type II model, performance drops significantly. There is similar performance when the model is changed to the Dayton city model with the receiver at the location given in Figure 4.4.

The simulation was run in all seven UTZ models as well as the Dayton city model and the collected data was put into Table 4.1. The simulation calculates the percentage of availability over the course of 24 hours where the PDOP is less than 6. Clearly, in most

Table 4.1: Availability using only GPS

Model	Type I	Type II	Type III	Type IV	Type V	Type VI	Type VII	Dayton
Availability	0%	28.47%	100%	100%	100%	100%	100%	13.19%

situations, GPS alone yields an acceptable solution so these scenarios are not the focus of

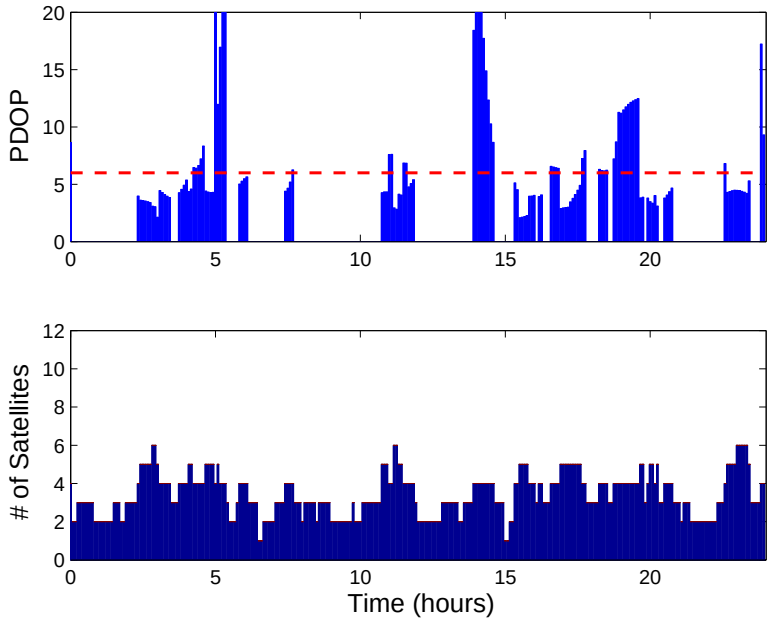

Figure 4.6: PDOP when using only GPS in the UTZ Type II model

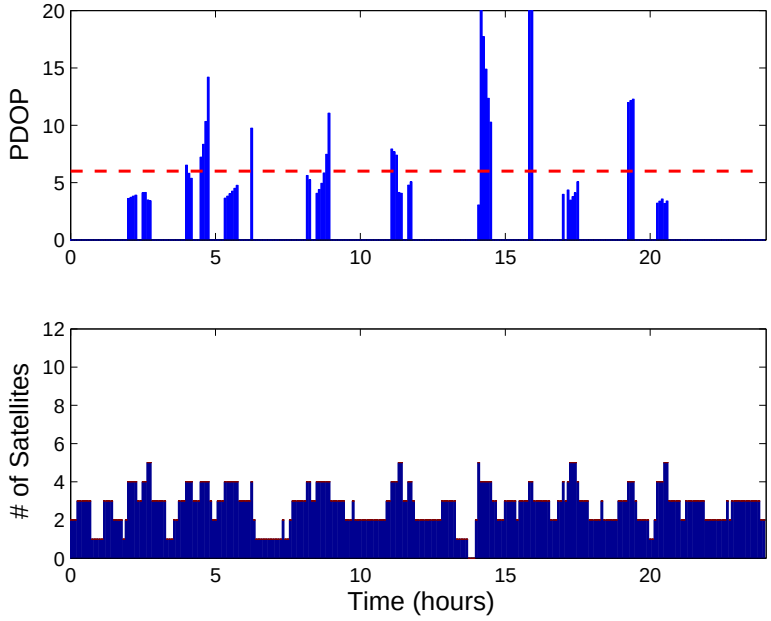

Figure 4.7: PDOP when using only GPS in the Dayton city model

the results. Instead, the results will focus on the UTZ Type II model and the Dayton city model.

4.3 Combined GPS/GLONASS Results

When GLONASS augments the GPS constellation, the number of satellites in orbit almost doubles. The increase in satellites should correspond to an increase in availability which is exactly what is seen in the simulation. In Figure 4.8, the all-in-view selection scheme is used to calculate the PDOP for a receiver at the same location in the UTZ Type II model and the Dayton city model. For this combination and location, an acceptable

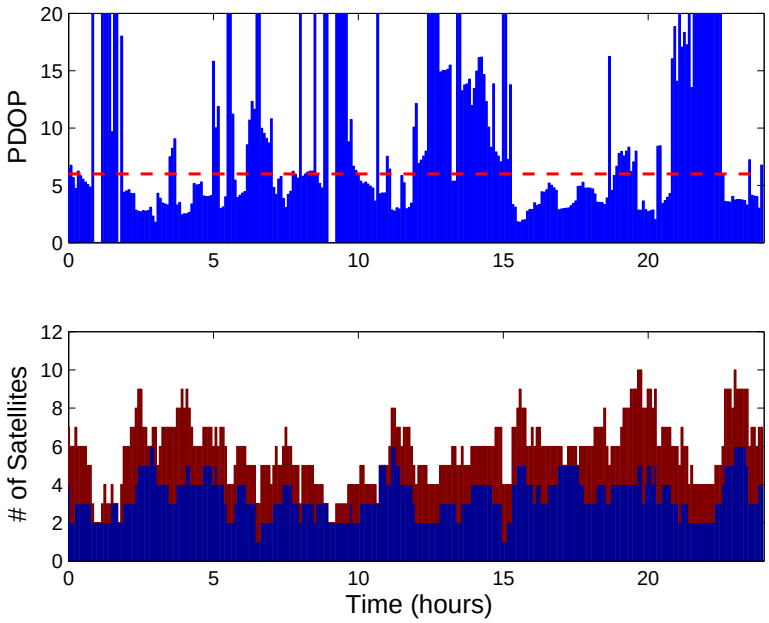

Figure 4.8: PDOP when using GPS and all-in-view GLONASS in the UTZ Type II model

PDOP is present 53.8% of the time which is a jump of more than 25 percent over the GPS only case. Figure 4.8 shows that there are more than 4 satellites in view sometimes but the PDOP still exceeds the threshold invalidating the solution. The PDOP would be better if the GLONASS satellites were equivalent in performance to GPS satellites, but they do have degraded accuracy so while they may be in view, the may not be accurate enough or have too poor geometry to get the PDOP below 6. The selective augmentation scheme has

the same availability as the all-in-view scheme but uses less satellites if possible. The difference in satellites used can be seen in Figure 4.9. Similar results are recorded when the Dayton city model is implemented in Figures 4.10 and 4.11. There is an available solution 33% of the time.

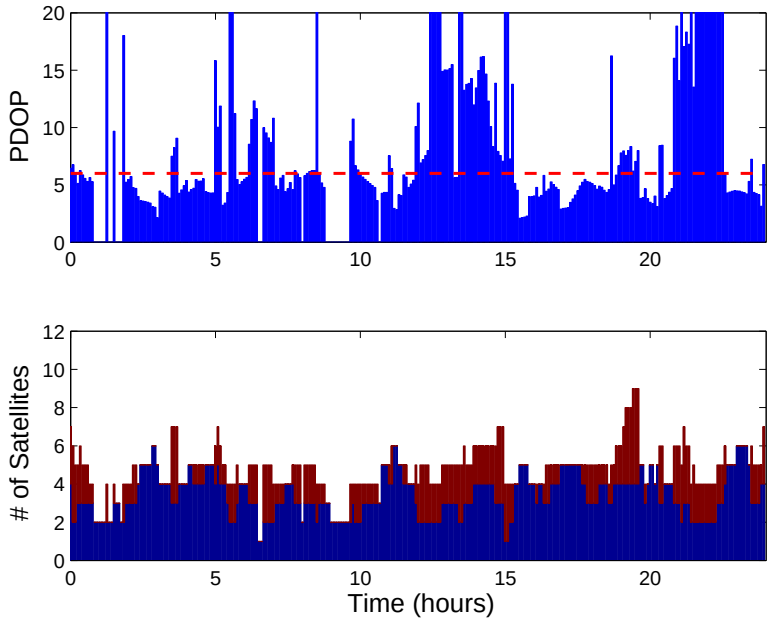

Figure 4.9: PDOP when using GPS and selective augmentation with GLONASS in the UTZ Type II model

The results from combining GPS and GLONASS are summarized in Table 4.2.

Table 4.2: Availability of combined GPS/GLONASS

	UTZ Type II	Dayton
GPS Only	28.5%	13.2%
GPS + GLONASS	53.8%	33%

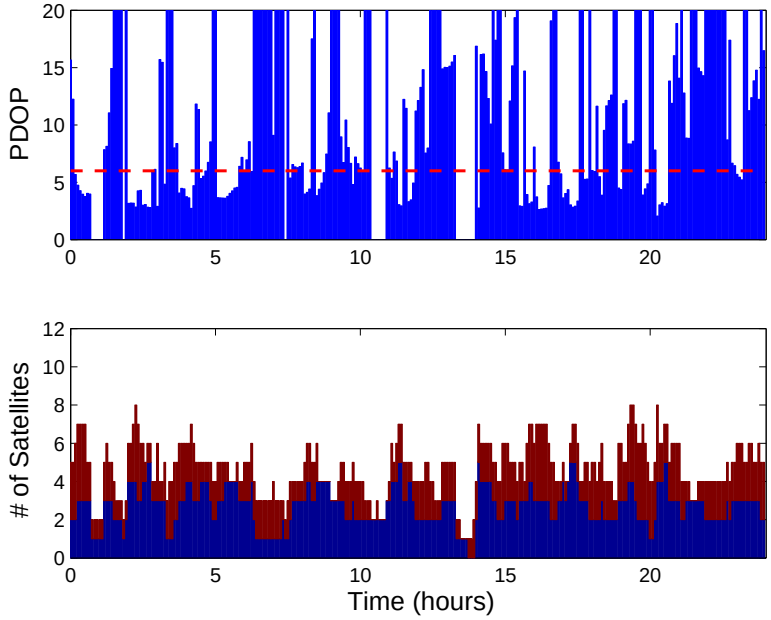

Figure 4.10: PDOP when using GPS and all-in-view GLONASS in the Dayton model

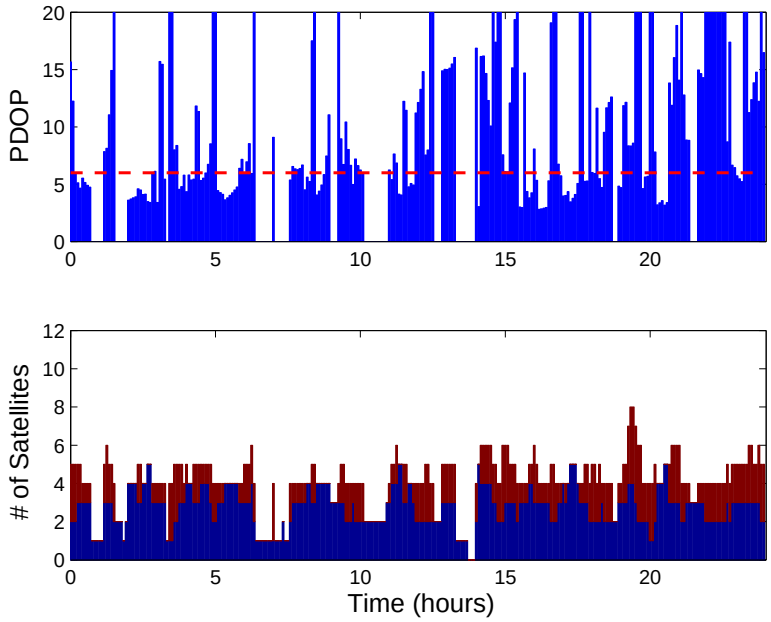

Figure 4.11: PDOP when using GPS and selective augmentation with GLONASS in the Dayton model

4.4 Combined GPS/Galileo Results

Galileo plans to eventually have 30 satellites in orbit. Furthermore, the specifications show that they will have better accuracy than GPS. Combining Galileo with GPS showed greater availability over combining GLONASS with GPS yielding an acceptable solution 69.8% of the time in the UTZ Type II model. Figure 4.12 shows the all-in-view augmentation results, and Figure 4.13 shows the selective augmentation results when using the UTZ Type II model. The results from the Dayton model, which had an availability of 59.4%, are presented in Figures 4.14 and 4.15.

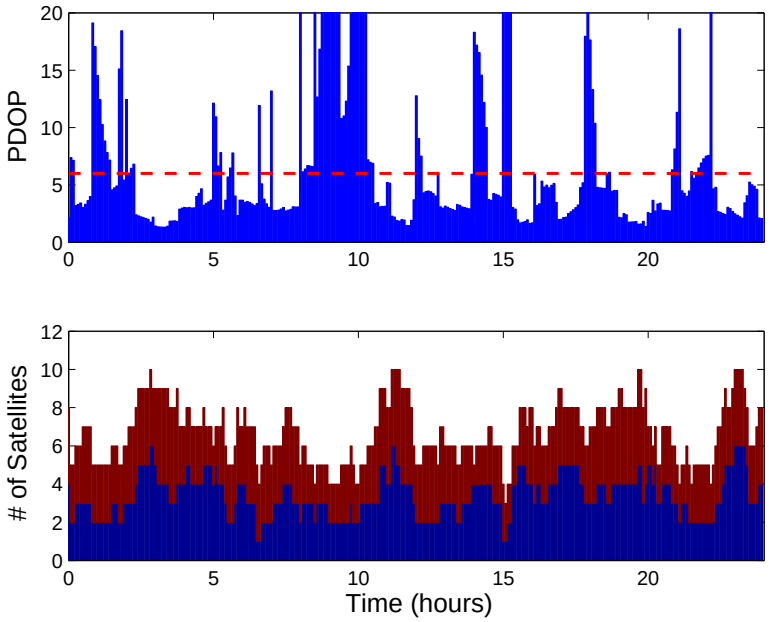

Figure 4.12: PDOP when using GPS and all-in-view Galileo in the UTZ Type II model

The results from combining GPS and Galileo are summarized in Table 4.3.

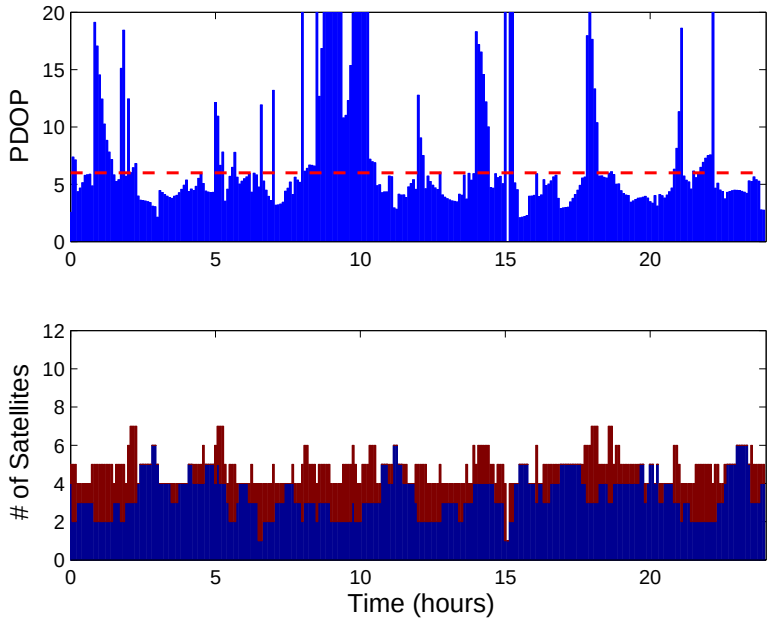

Figure 4.13: PDOP when using GPS and selective augmentation with Galileo in the UTZ Type II model

Table 4.3: Availability of combined GPS/Galileo

	UTZ Type II	Dayton
GPS Only	28.5%	13.2%
GPS + Galileo	69.8%	59.4%

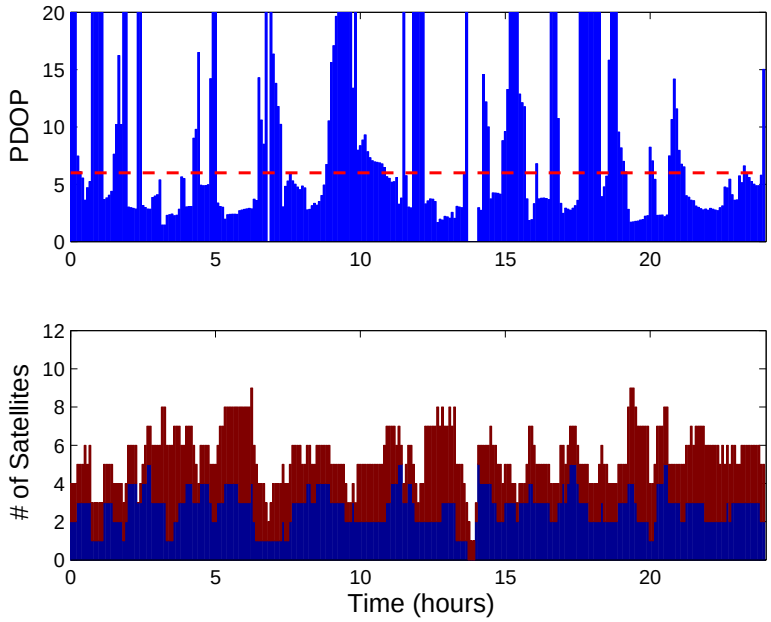

Figure 4.14: PDOP when using GPS and all-in-view Galileo in the Dayton model

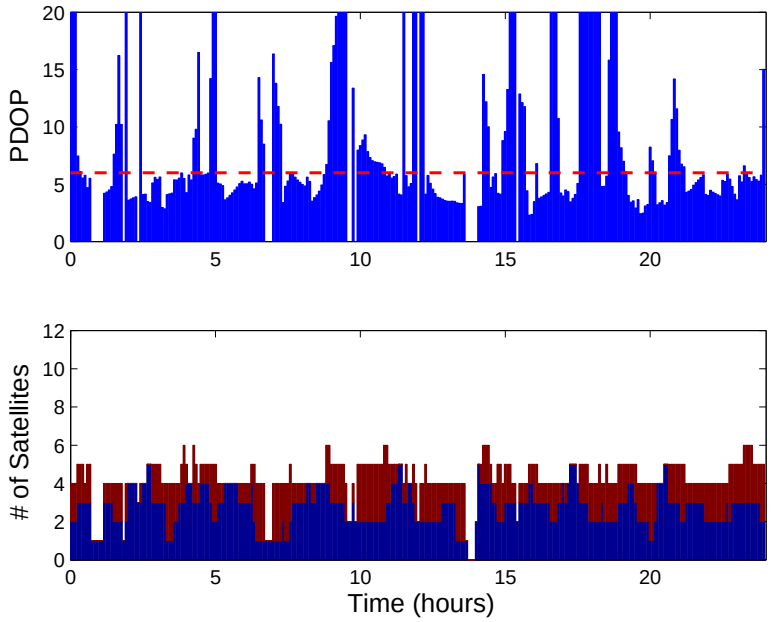

Figure 4.15: PDOP when using GPS and selective augmentation with Galileo in the Dayton model

4.5 Combined GPS/Compass Results

Compass plans to have 35 satellites in orbit, although only 30 of these satellites will have global coverage, the other 5 satellites will sit in geostationary orbits over China. Combining Compass with GPS showed slightly better availability than combining GLONASS with GPS but less than Galileo with GPS, yielding an acceptable solution 56.6% of the time with the UTZ Type II model. Figure 4.12 shows the all-in-view augmentation results and Figure 4.13 shows the selective augmentation results when using the UTZ Type II model. The results from the Dayton model, which had an availability of 40.6%, are presented in Figures 4.14 and 4.15.

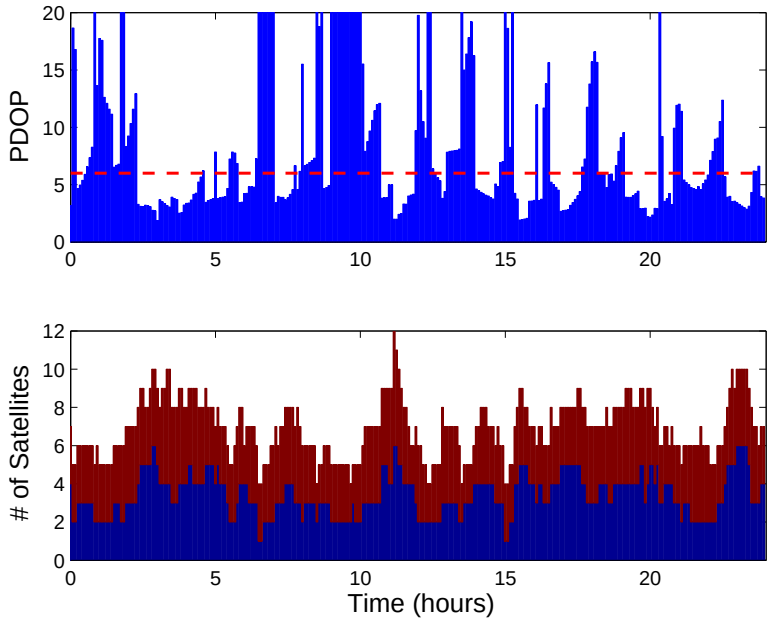

Figure 4.16: PDOP when using GPS and all-in-view Compass in the UTZ Type II model

The results from combining GPS and Compass are summarized in Table 4.4.

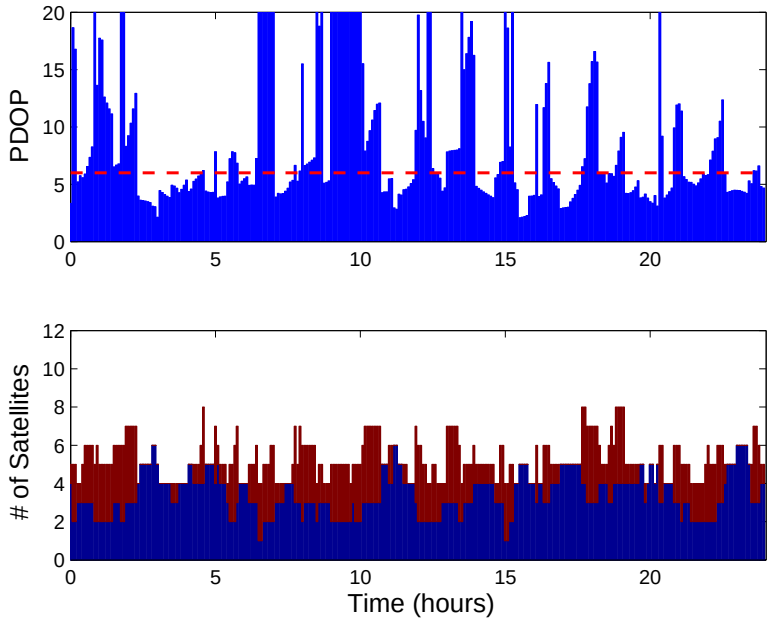

Figure 4.17: PDOP when using GPS and selective augmentation with Compass in the UTZ Type II model

Table 4.4: Availability of combined GPS/Compass

	UTZ Type II	Dayton
GPS Only	28.5%	13.2%
GPS + COMPASS	56.6%	40.6%

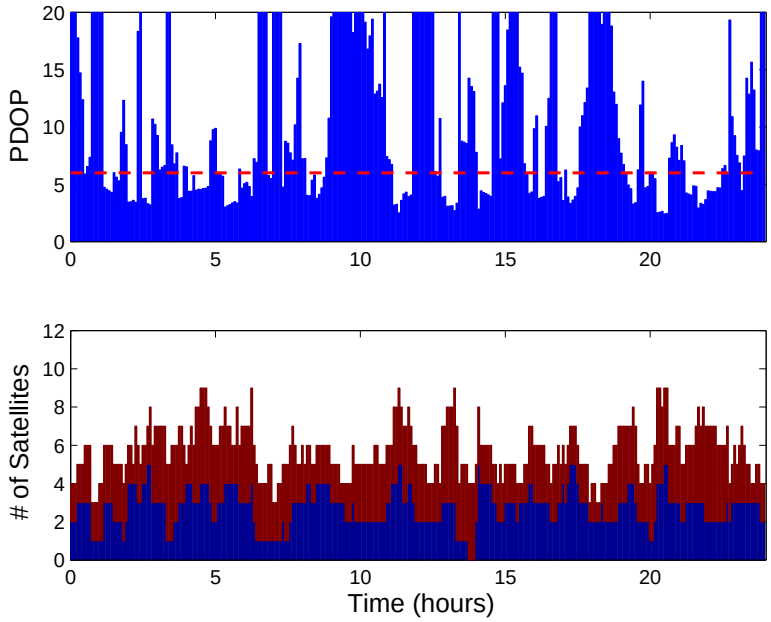

Figure 4.18: PDOP when using GPS and all-in-view Compass in the Dayton model

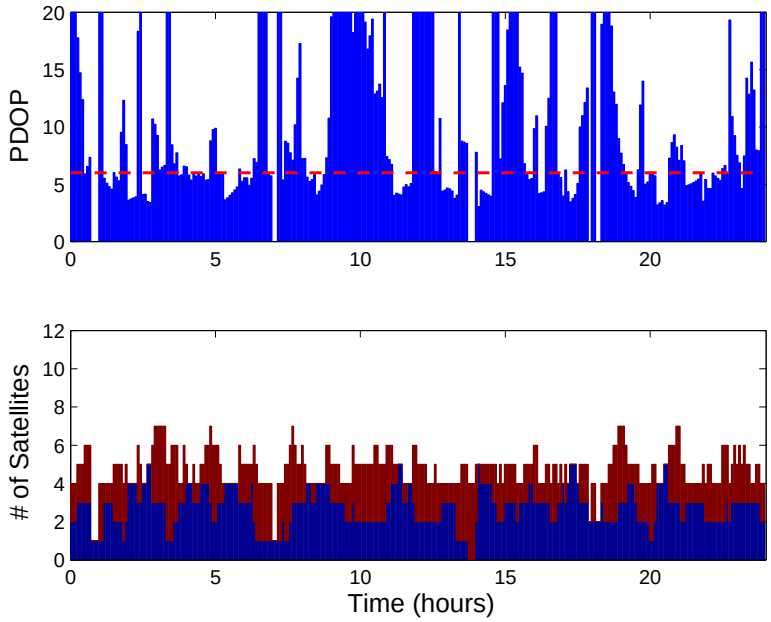

Figure 4.19: PDOP when using GPS and selective augmentation with Compass in the Dayton model

4.6 Multi-System Augmentation Results

Increasing the number of augmentation systems continues to improve the availability of an acceptable position solution in a degraded reception environment. More systems means more available satellites which means that there are more opportunities to find a satellite close to the optimal location which will yield a better PDOP. The complete results showing the PDOP and number of satellites used for all the system combinations are included in Appendix A. Table 4.5 summarizes the results from GPS with multiple augmentation systems.

Table 4.5: Availability with multiple augmentation systems

Systems	UTZ Type II	Dayton
GPS Only	28.5%	13.2%
GPS/GLO/GAL	85.4%	74.3%
GPS/GLO/COM	78.8%	65.3%
GPS/GAL/COM	79.9%	69.8%
GPS/GLO/GAL/COM	92%	84.4%

Because the Dayton city model is not uniform, running the PDOP simulation from a single location in the city does not accurately portray the availability of a position solution throughout the city. In order to more accurately characterize the availability, the PDOP simulations were run not from a single location, but from 116 locations evenly spread out around the central city block in the Dayton model. The availability for all the locations was averaged to get a single value which can be compared between all the augmentation combinations. Table 4.6 shows the average PDOP from the locations throughout the Dayton city model for each augmentation combination.

Table 4.6: Average availability for all the system combinations throughout the Dayton city model

Systems	Dayton
GPS Only	4.6%
GPS/GLO	12.4%
GPS/GAL	20.9%
GPS/COM	12.8%
GPS/GLO/GAL	30.6%
GPS/GLO/COM	23%
GPS/GAL/COM	26.3%
GPS/GLO/GAL/COM	36.6%

4.7 Barometric Altimeter Results

Adding the barometric altimeter into the system yielded better results for all combinations of augmentation and standalone GPS. The results of the simulation without the altimeter are condensed into a single table and reprinted in Table 4.7 for convenience of comparison.

Table 4.8 shows the improved availability from including a barometric altimeter when the altimeter is set to the current sea level pressure for its location.

As an example, Figure 4.20 shows the PDOP using the all-in-view scheme without the altimeter when GPS is augmented with the Galileo system and Figure 4.21 shows the same scenario but with the altimeter included. The altimeter is counted as a GPS satellite in the figures. Also of note, adding the altimeter greatly reduces the VDOP. Figure 4.22 shows GDOP, PDOP, HDOP, and VDOP for the previous scenario without the altimeter

Table 4.7: Availability for all the system combinations

Systems	UTZ Type II	Dayton
GPS Only	28.5%	13.2%
GPS/GLO	53.8%	33%
GPS/GAL	69.8%	59.4%
GPS/COM	56.6%	40.6%
GPS/GLO/GAL	85.4%	74.3%
GPS/GLO/COM	78.8%	65.3%
GPS/GAL/COM	79.9%	69.8%
GPS/GLO/GAL/COM	92%	84.4%

Table 4.8: Availability for all the system combinations when using a barometric altimeter

Systems	UTZ Type II	Dayton
GPS Only	28.5%	13.2%
GPS/Alt	70.8%	46.2%
GPS/GLO/Alt	86.1%	70.8%
GPS/GAL/Alt	95.8%	86.8%
GPS/COM/Alt	93.4%	81.6%
GPS/GLO/GAL/Alt	98.3%	93.8%
GPS/GLO/COM/Alt	97.9%	95.8%
GPS/GAL/COM/Alt	99.3%	91.3%
GPS/GLO/GAL/COM/Alt	100%	97.9%

and Figure 4.23 shows the same but with the altimeter and ensuing greatly diminished VDOP values.

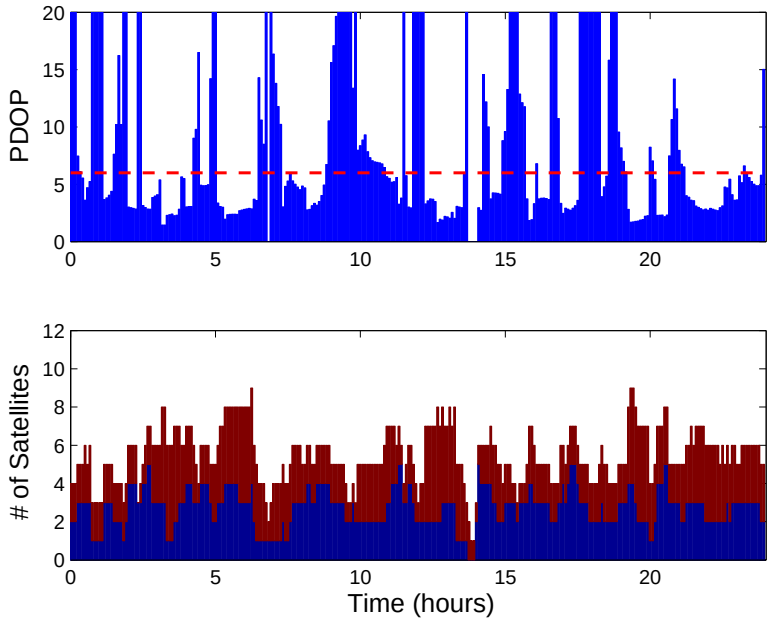

Figure 4.20: PDOP without using an altimeter

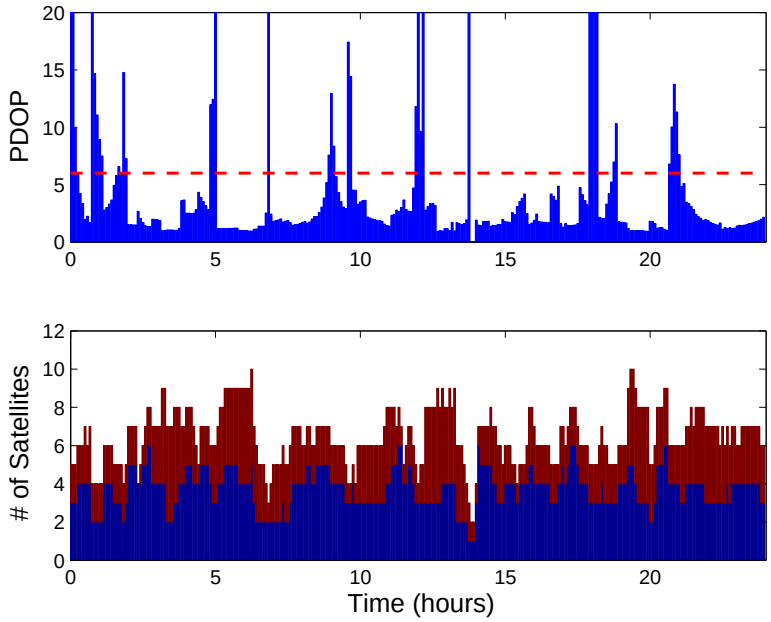

Figure 4.21: PDOP using an altimeter

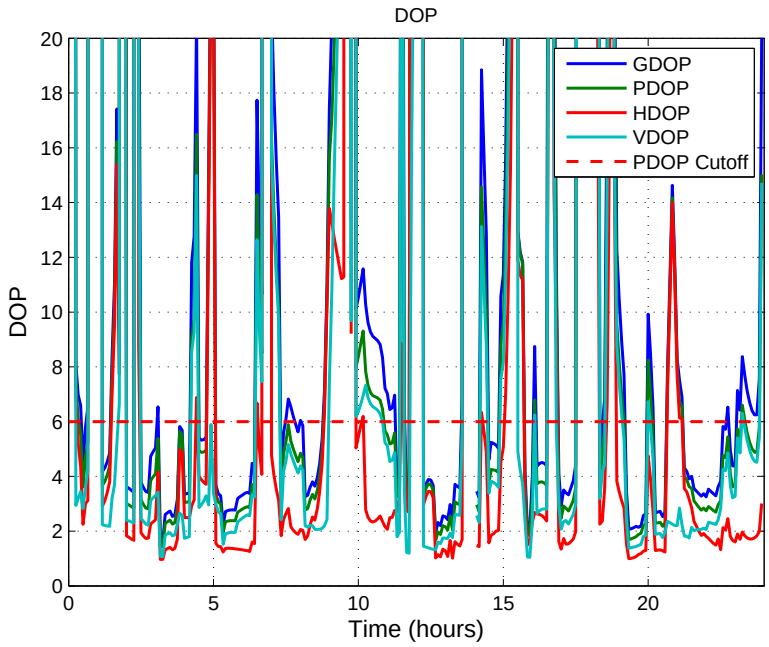

Figure 4.22: All DOPs without using an altimeter

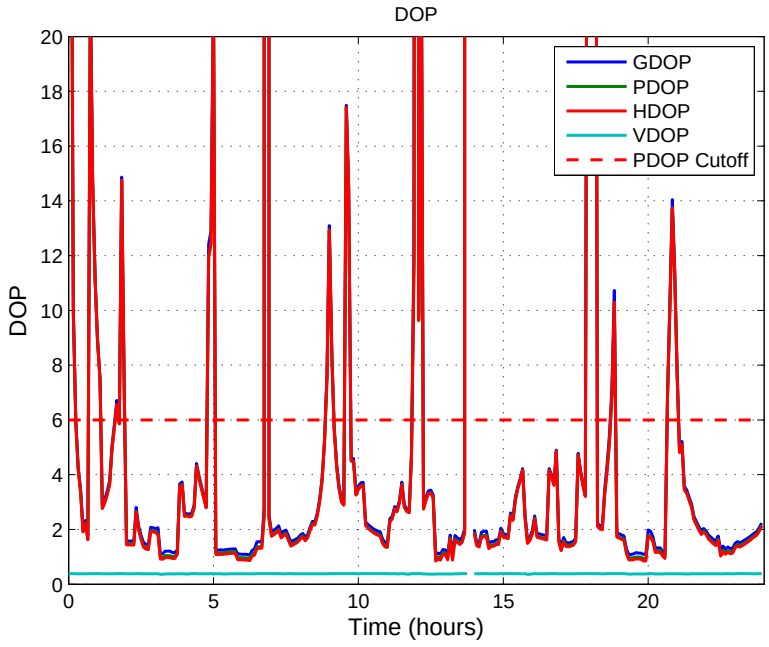

Figure 4.23: All DOPs when using an altimeter

As before, the simulation was run over 116 locations throughout the Dayton city model. The results of the average availability throughout the Dayton city model, both with and without using a barometric altimeter, are summarized in Table 4.9.

Table 4.9: Average availability for all the system combinations throughout the Dayton city model

Systems	No Altimeter	With Altimeter
GPS Only	4.6%	19.3%
GPS/GLO	12.4%	34.2%
GPS/GAL	20.9%	47.1%
GPS/COM	12.8%	37%
GPS/GLO/GAL	30.6%	58.5%
GPS/GLO/COM	23%	50.8%
GPS/GAL/COM	26.3%	54%
GPS/GLO/GAL/COM	36.6%	64.2%

4.8 UAV Kalman Filter Simulation Results

To apply the augmentation of GPS to a real world scenario, a micro-UAV simulation was created where the UAV autonomously navigates through the Dayton city model. In the simulation, the UAV is outfitted with low quality gyroscopes and accelerometers. The gyroscopes had a simulated white noise parameter of $0.001^{\circ}/\text{sec}/\sqrt{\text{Hz}}$ and the accelerometers had a white noise parameter of $99\mu\text{g}/\sqrt{\text{Hz}}$. The inertial sensors were combined with the GPS measurements in a Kalman Filter as described in Section 3.11. In the simulation, the UAV ideally would travel in a counter-clockwise path around the central block as shown in Figure 4.24.

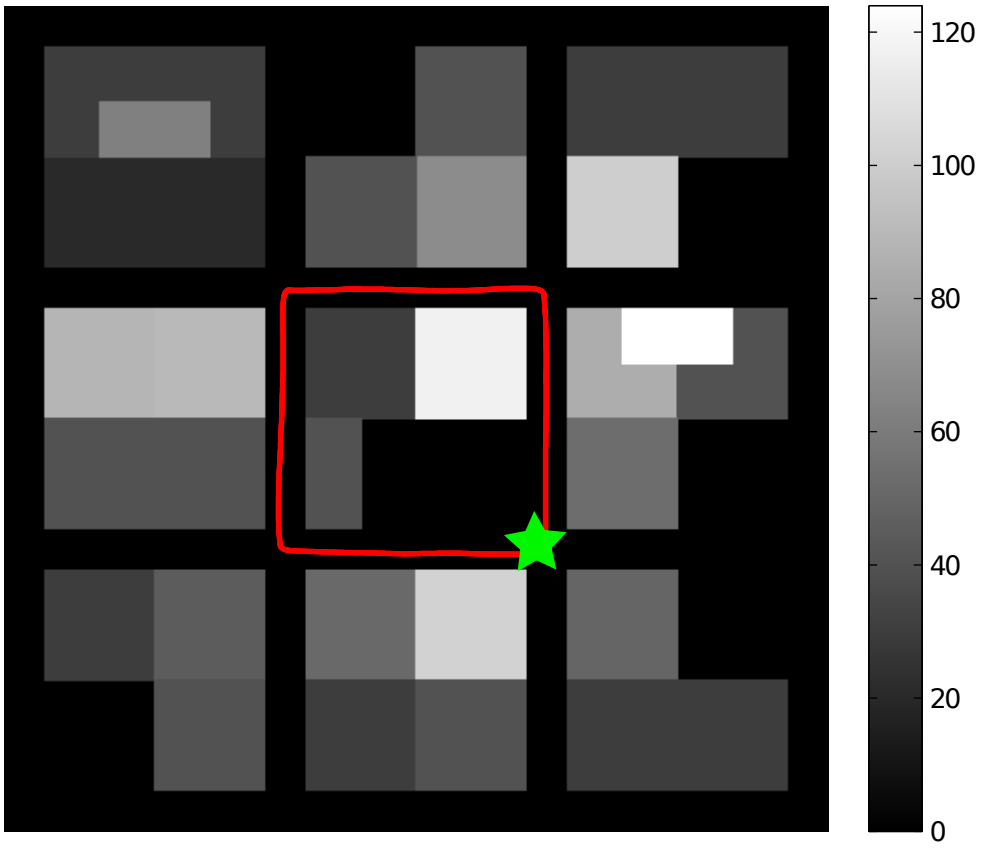

Figure 4.24: Ideal path of UAV around the city

Starting in the lower right-hand corner, the UAV navigates by using the estimate of it's location which is returned by the Kalman Filter. The UAV then computes the appropriate control inputs so that it moves with a velocity of 4 m/s in the direction of the unit vector between it's position estimate and the location of the next waypoint. The waypoints are located at the intersections at the corners of the middle city block. When the UAV gets to each waypoint, it moves on to the next until it finishes its circuit around the block and stays at the starting position.

Because the buildings hinder satellite reception and the inertial sensors are low-quality, the Kalman Filter's position estimate is not always accurate limiting the UAV's ability to autonomously navigate. An example run of the error prone navigation is shown in Figure 4.25. The true path of the vehicle is shown by the red line and the

Kalman Filter's estimate is shown by the yellow line. The colors of the blocks in the city denote building height in meters.

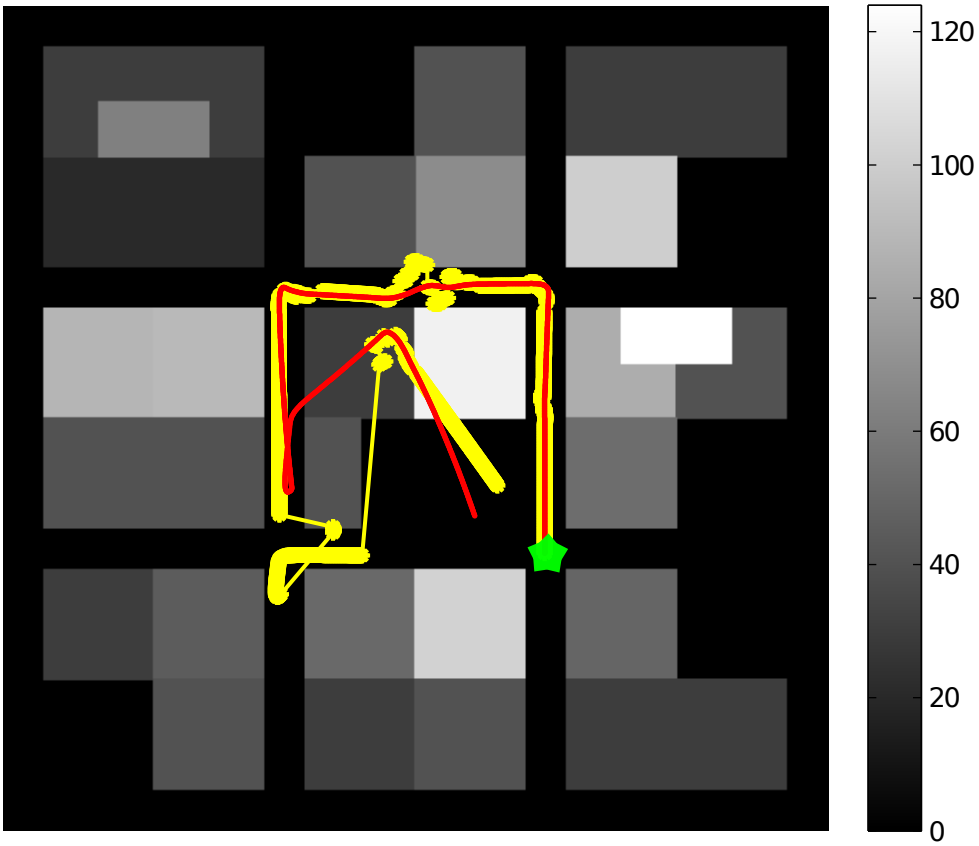

Figure 4.25: Path of UAV around the city using un-augmented GPS

Errors in the perceived location of the UAV will render it unable to complete its mission. Augmenting the GPS constellation gives more visible satellites so an accurate position solution is more often available yielding smaller position errors. Smaller position errors mean that the UAV can accurately get to the waypoints without colliding with the buildings. Figure 4.26 shows the UAV navigating the city using GLONASS, Galileo, and Compass augmenting GPS. While not pretty like the ideal case, the UAV is successful in making it around the block via all four waypoints.

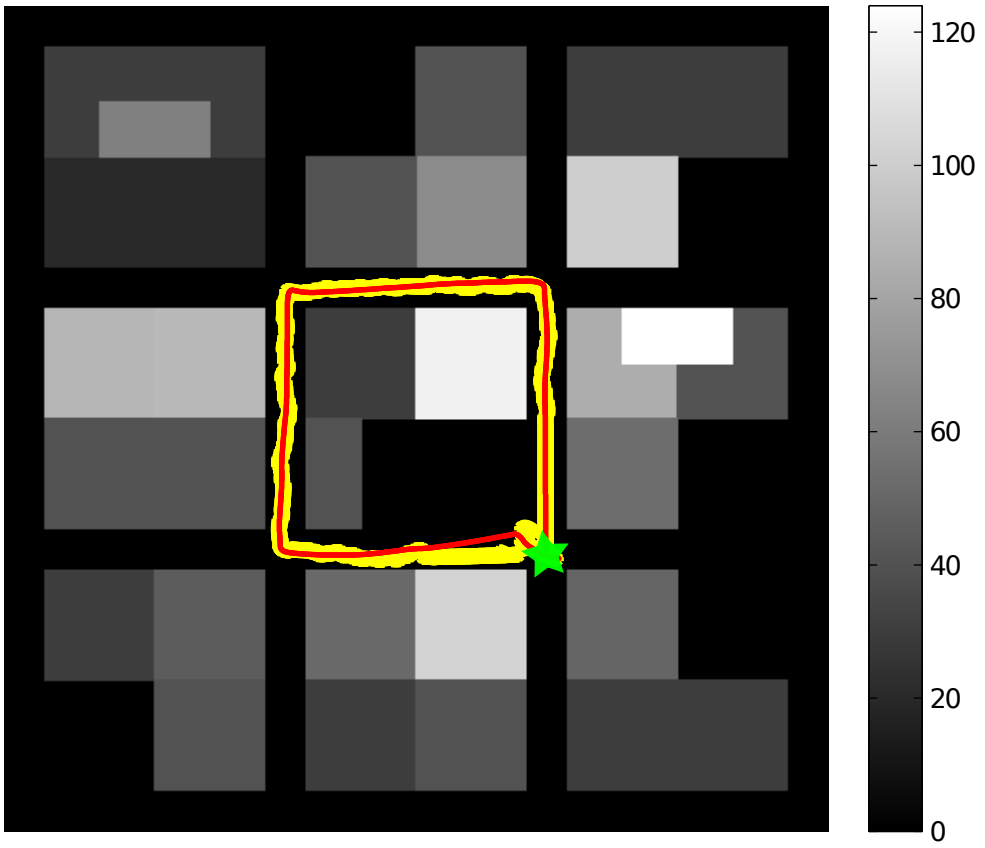

Figure 4.26: Example of a UAV navigating with the augmented GPS constellation

By the random nature of the errors, a single run of the simulation cannot accurately characterize potential performance nor allow for comparison between differing augmentation scenarios. To that end, a Monte Carlo analysis was performed. This analysis executed 240 runs of the simulation: 10 runs at 24 separate times throughout the 24 hours of satellite data. The data shown in Figure **??** comes from using only GPS. It shows the mean radial spherical error (MRSE) of the 240 samples over the 150 seconds of the simulation.

This data is also hard to compare so again the average was taken, this time over the length of the simulation. This average MRSE gives a single number which can be used to

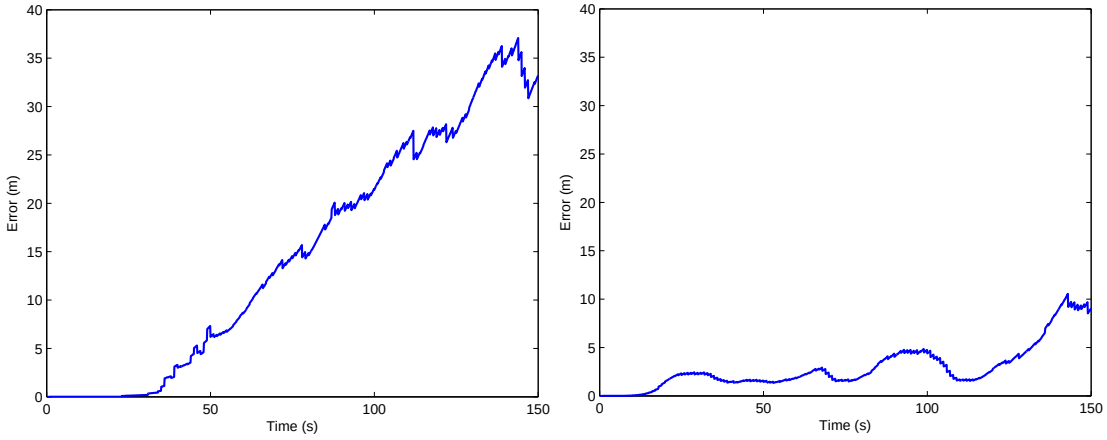

(a) Unaugmented GPS (b) Augmented GPS

Figure 4.27: MRSE comparison

compare between scenarios. Table 4.10 displays the results of the average MRSE for each of the augmentation scenarios.

Table 4.10: Average MRSE

Systems	Error - No Alt (m)	Error - With Alt (m)
GPS Only	14.8	13.2
GPS/GAL	12.7	7
GPS/GLO	11.9	5.7
GPS/COM	9	5
GPS/GAL/GLO	6.9	4.3
GPS/GAL/COM	8.6	4.1
GPS/GLO/COM	5.4	3.6
GPS/GAL/GLO/COM	5.1	2.8

An average MRSE of 14 m will not allow for autonomous navigation on a street that is 15 m wide. However, with augmentation, the value drops all the way down to 2.8 m which will allow the vehicle to navigate the city without hitting buildings. This is shown graphically in Figure 4.28.

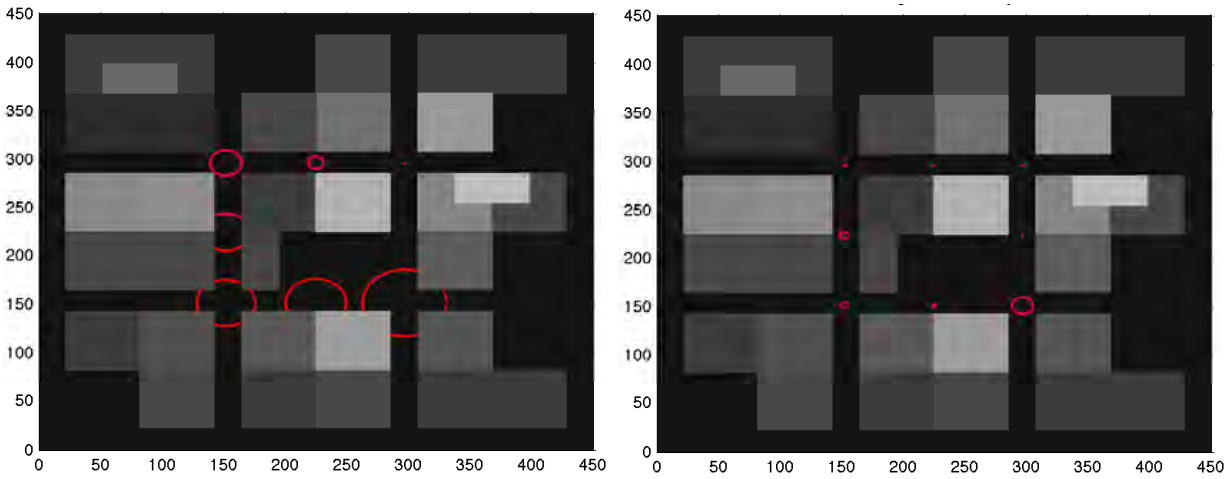

(a) Unaugmented GPS

(b) Augmented GPS

Figure 4.28: Alternate MRSE comparison

4.9 Summary

This chapter presented the results of the simulation. Section 4.2 contains the results of the simulation using only GPS which was used as a baseline for comparison to the rest of the results. Then, the next sections delivered the results of the GPS constellation combined with the other global navigation systems and a barometric altimeter. Finally the results of the UAV navigation scenario were discussed in Section 4.8.

5 Conclusions

This thesis investigated augmenting the GPS constellation with foreign GNSSs as well as inertial and barometric sensors in an effort to improve the accuracy and availability of a position solution in a degraded satellite signal reception environment. This chapter concludes the thesis with a final assessment of the methods as well as recommendations for future research.

5.1 Conclusions

According to the data from this research, situations with a limited view of the sky present real problems for users of GPS receivers. This includes the urban canyon scenario of the downtown area in a population center. While these areas are just a small portion of the overall city, they are centers of activity and contain many of the points of interest in a military operation.

The model of Dayton, Ohio proved that even the modest buildings of an average-sized city are capable of rendering GPS services unavailable. Augmenting the GPS constellation with the foreign navigation satellites and a barometric altimeter alleviated much of this availability issues. This is because the greater number of satellites in orbit means that there will likely be more visible satellites in the open patches of sky while in an urban canyon. Aiding with a barometric altimeter further increased the availability of a position solution.

When it is desirable to limit the dependency on foreign systems as much as possible, a selective-augmentation algorithm can be implemented which will not use all of the foreign satellites in view, but instead utilize only the minimum number necessary to get a satisfactory position solution. This selective augmentation technique has exactly the same availability as the all-in-view scheme all the while minimizing the dependence on foreign services.

An autonomous UAV in the simulation using only a GPS receiver could not navigate through the city model. Furthermore, using low-quality inertial sensors blended with the GPS receiver in a Kalman Filter failed to yield successful autonomous navigation due to excessive errors in the inertial measurements and the limited availability of a GPS-only position solution to update and reset the Kalman Filter errors. When augmented with the foreign systems and a barometric altimeter, the accuracy improved enough to allow successful navigation in the urban canyon scenario.

This research provides a simulation environment to test the availability and usefulness of satellite navigation in an urban canyon and has shown improved performance allowing the successful navigation of a UAV in a degraded reception environment. This could allow more accurate and dependable position information for friendly forces on the ground as well as open up a new environment of operation for autonomously navigating vehicles.

5.2 Recommendations

Following are some recommendations for continued research in this field of study.

- Loose integration of the GPS and INS was used in this study. Tighter integration between the GPS and the INS in the Kalman Filter can be implemented where not a position solution from the receiver (requiring at least 4 satellites) is used as the measurement but instead the pseudoranges from the individual satellites are used as the measurements.

- A more accurate and descriptive model of the INS errors can be used in the Kalman Filter to improve the estimation accuracy of the algorithm.

- When the European and Chinese systems become operational, the study can be updated to use complete operational data for the satellite orbits as well as error statistics for the systems.

Appendix A: Multiple Augmentation System Results

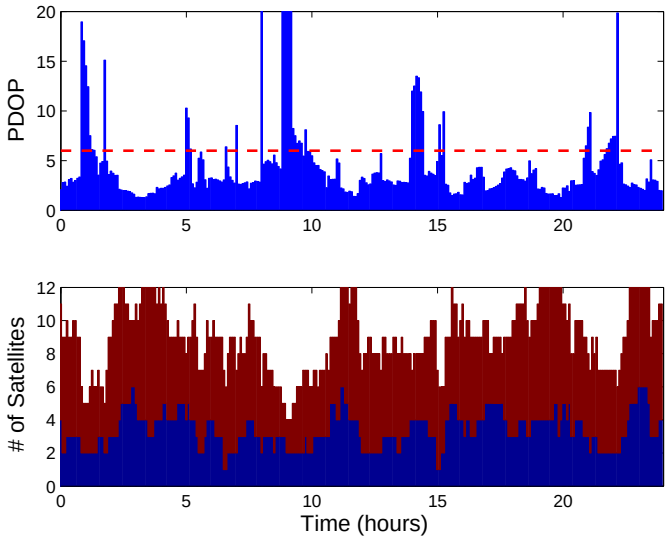

Figure A.1: GPS/Galileo/Glonass all-in-view in the UTZ Type II model

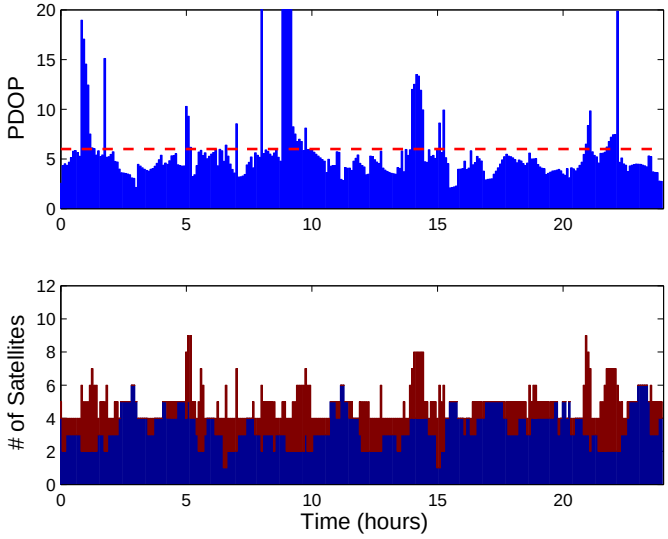

Figure A.2: GPS/Galileo/Glonass and selective augmentation in the UTZ Type II model

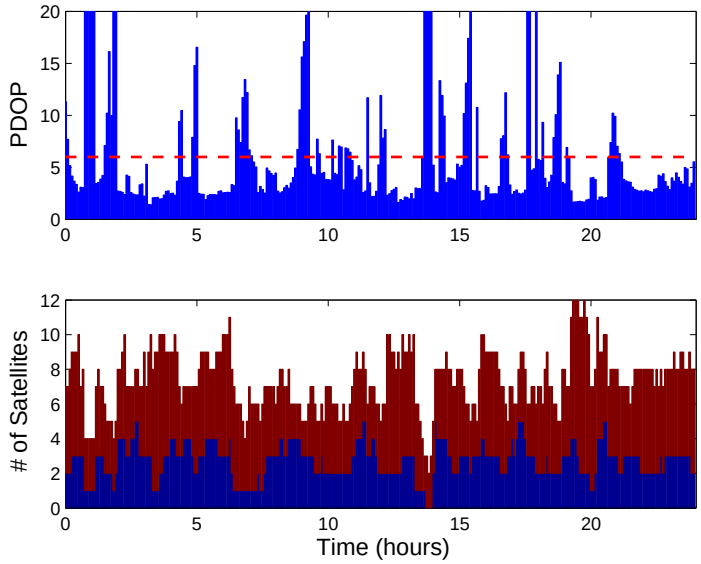

Figure A.3: GPS/Galileo/Glonass all-in-view in the Dayton model

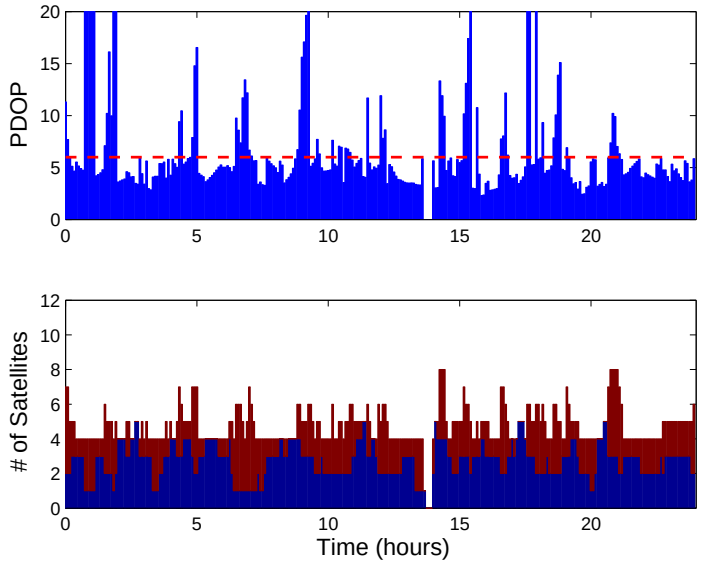

Figure A.4: GPS/Galileo/Glonass and selective augmentation in the Dayton model

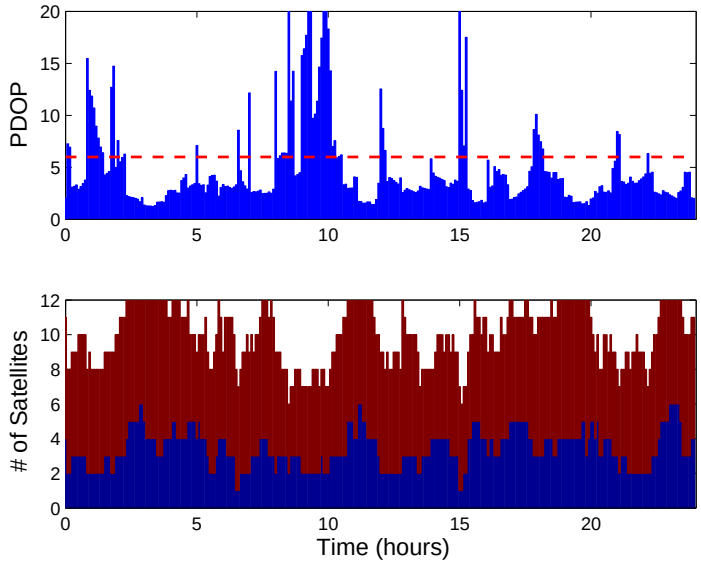

Figure A.5: GPS/Galileo/Compass all-in-view in the UTZ Type II model

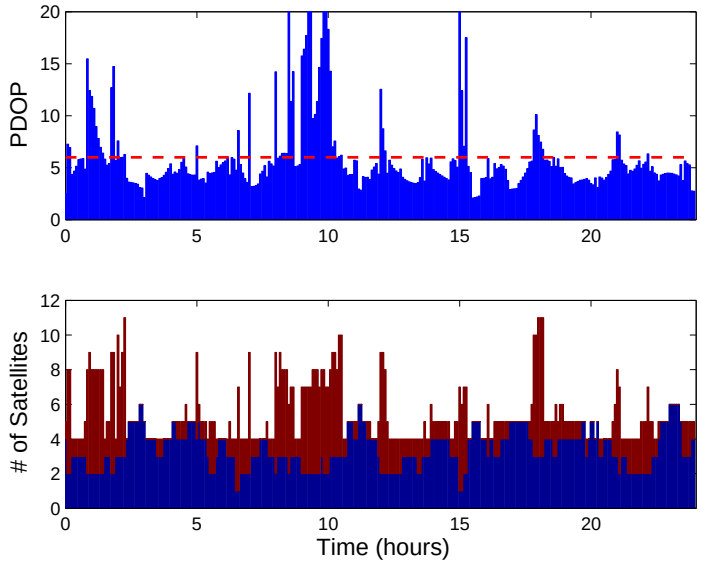

Figure A.6: GPS/Galileo/Compass and selective augmentation in the UTZ Type II model

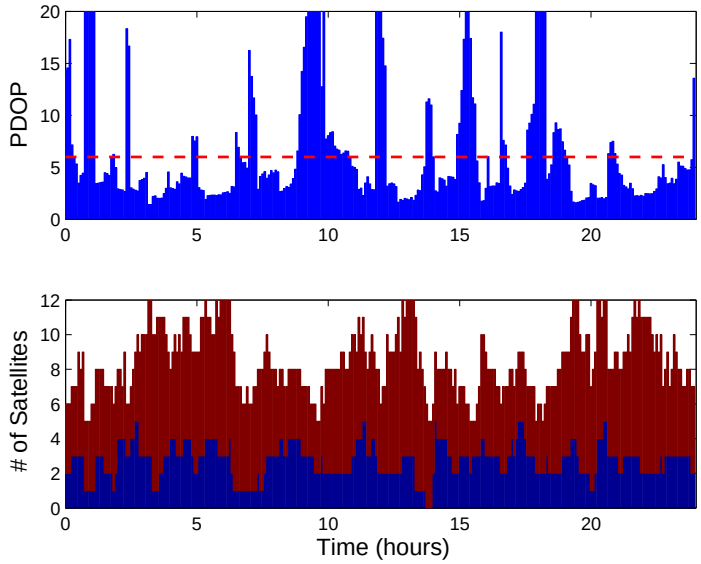

Figure A.7: GPS/Galileo/Compass all-in-view in the Dayton model

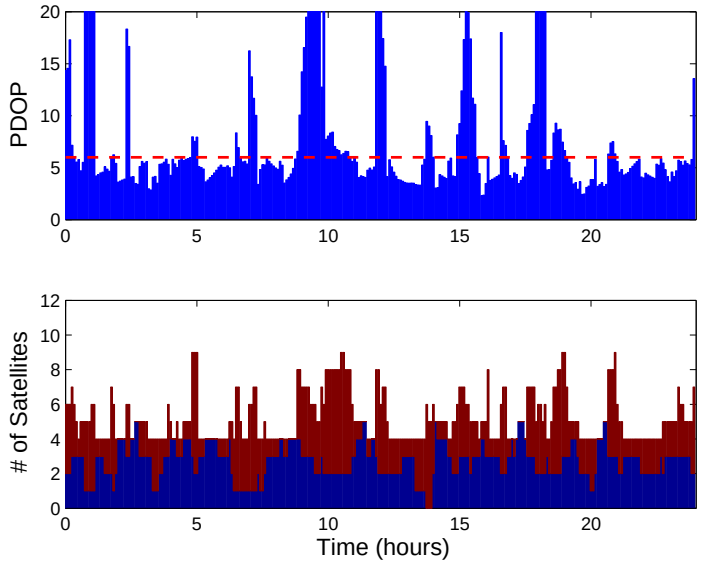

Figure A.8: GPS/Galileo/Compass and selective augmentation in the Dayton model

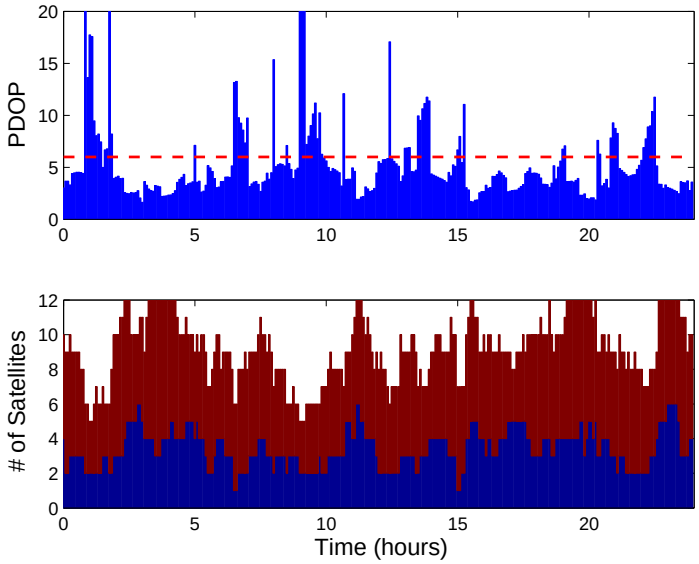

Figure A.9: GPS/Glonass/Compass all-in-view in the UTZ Type II model

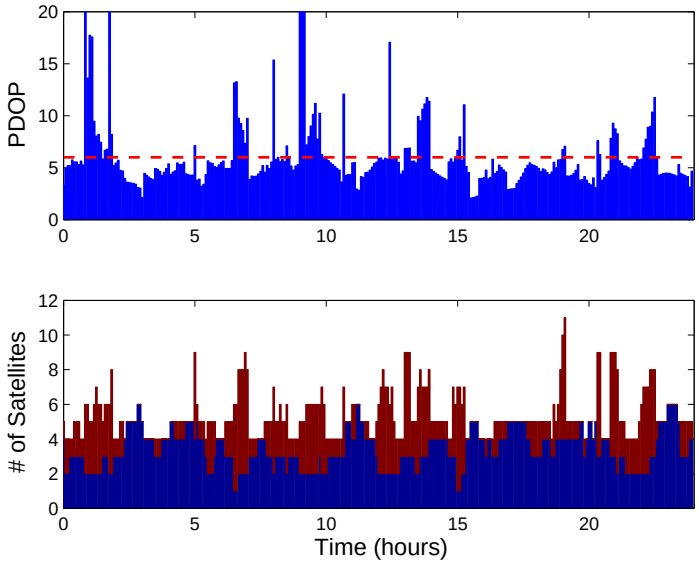

Figure A.10: GPS/Glonass/Compass and selective augmentation in the UTZ Type II model

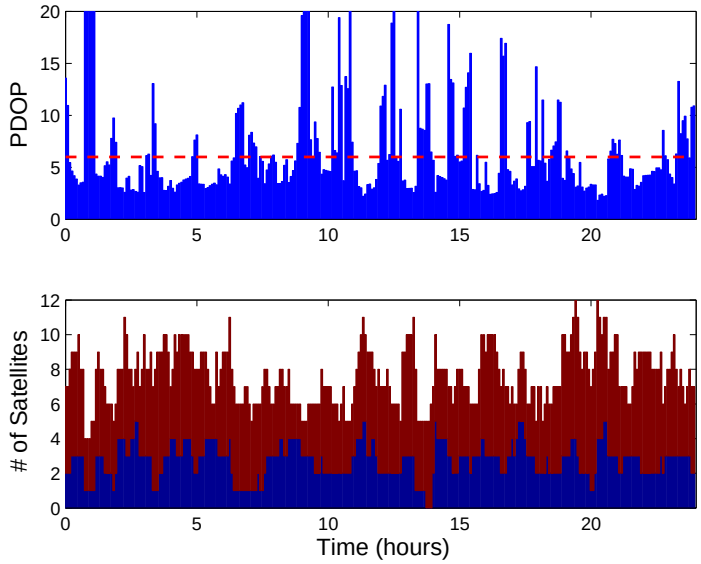

Figure A.11: GPS/Glonass/Compass all-in-view in the Dayton model

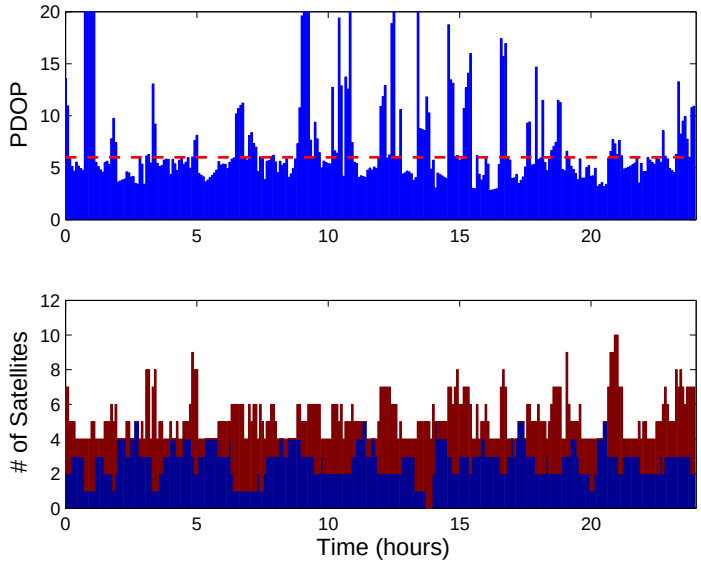

Figure A.12: GPS/Glonass/Compass and selective augmentation in the Dayton model

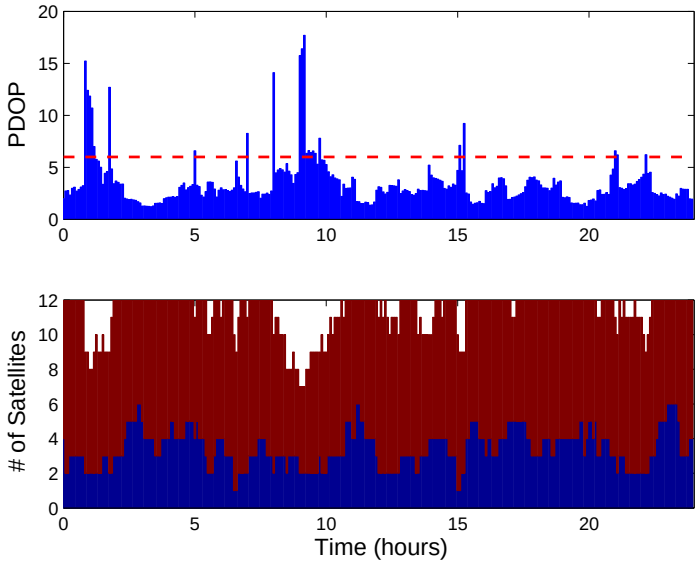

Figure A.13: GPS/Galileo/Glonass/Compass all-in-view in the UTZ Type II model

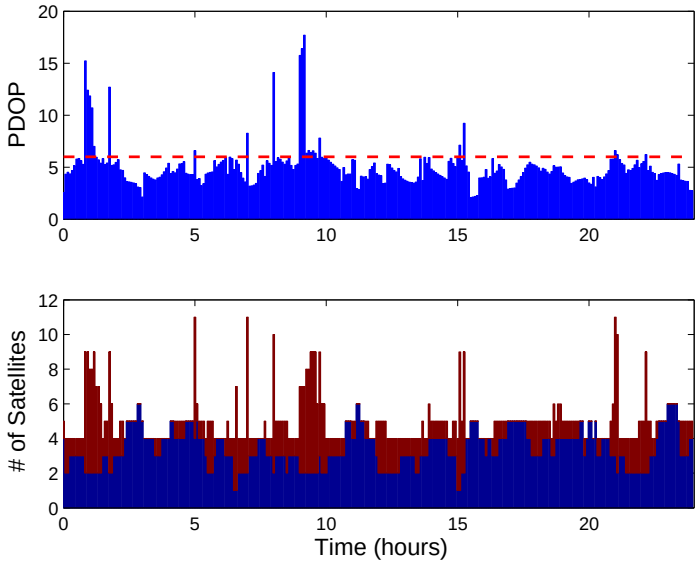

Figure A.14: GPS/Galileo/Glonass/Compass and selective augmentation in the UTZ Type II model

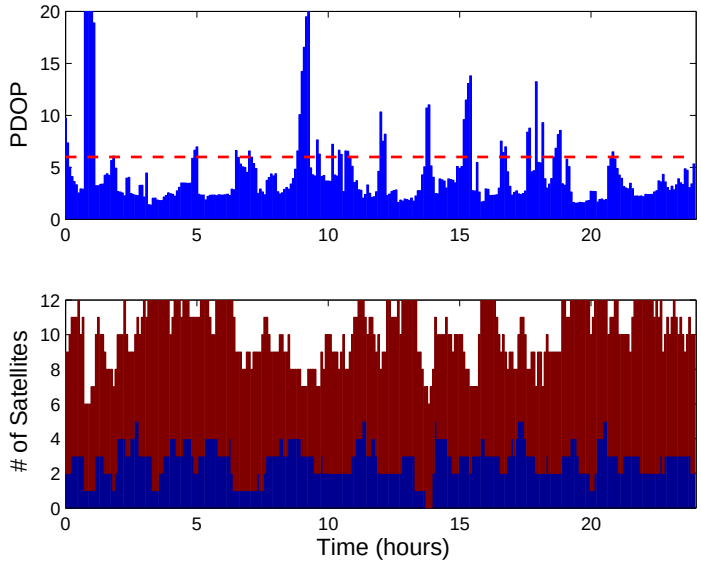

Figure A.15: GPS/Galileo/Glonass/Compass all-in-view in the Dayton model

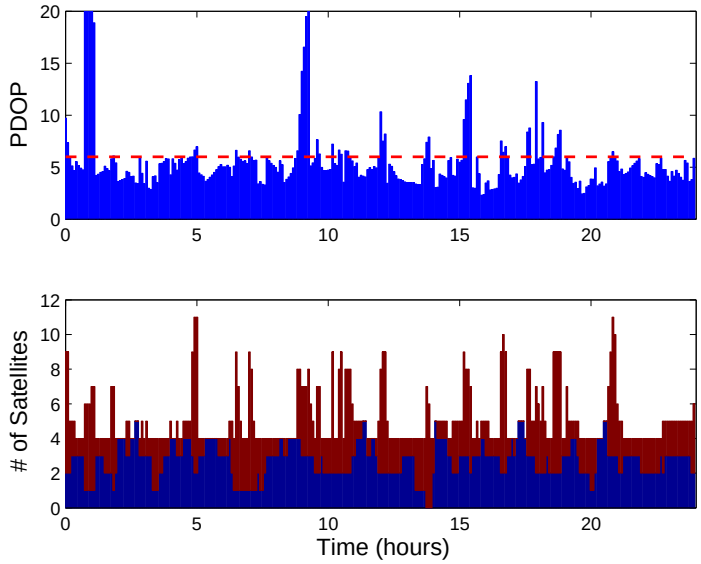

Figure A.16: GPS/Galileo/Glonass/Compass and selective augmentation in the Dayton model

Appendix B: Augmentation Results Including the Barometric Altimeter

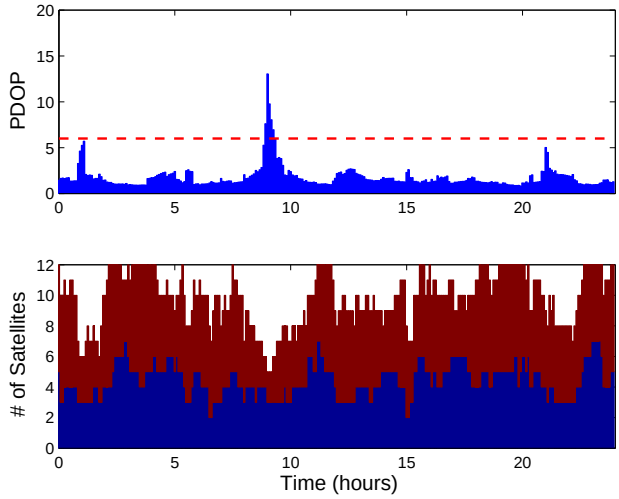

Figure B.1: GPS/Galileo/Glonass/Altimeter all-in-view in the UTZ Type II model

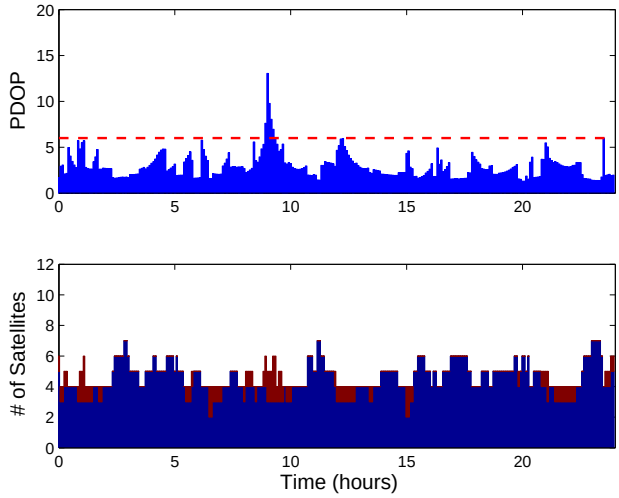

Figure B.2: GPS/Galileo/Glonass/Altimeter and selective augmentation in the UTZ Type II model

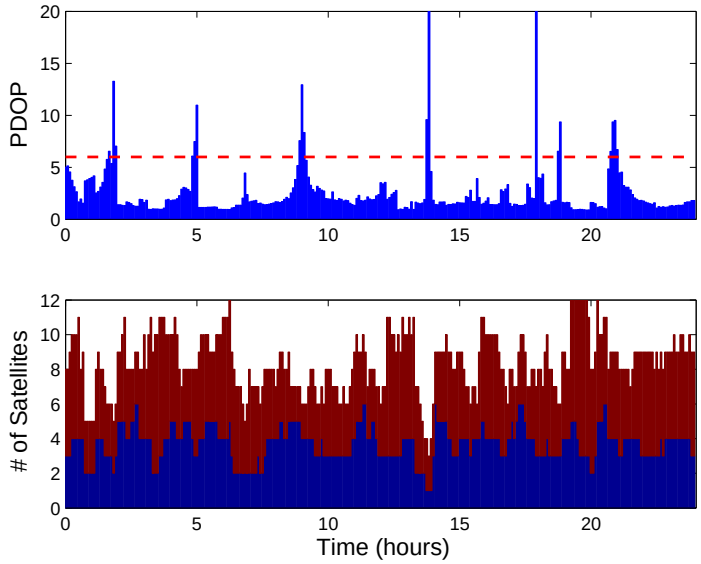

Figure B.3: GPS/Galileo/Glonass/Altimeter all-in-view in the Dayton model

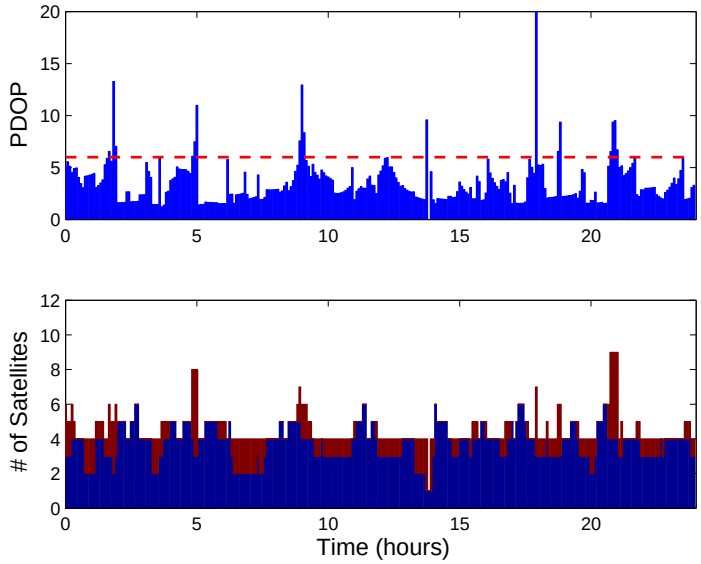

Figure B.4: GPS/Galileo/Glonass/Altimeter and selective augmentation in the Dayton model

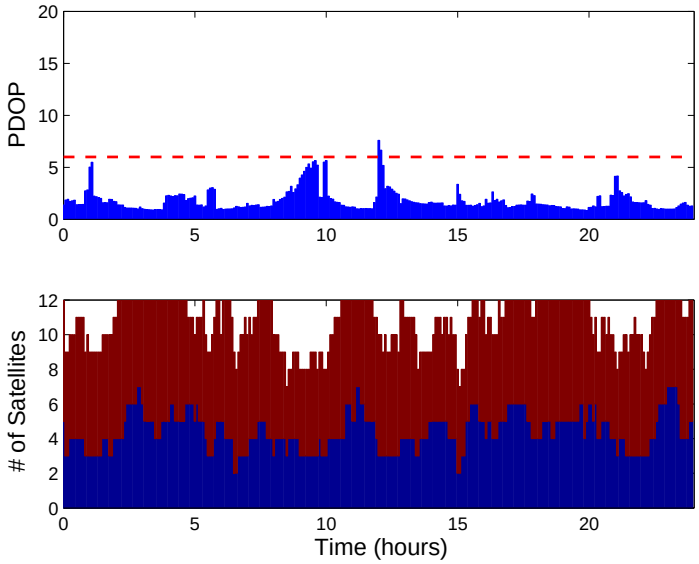

Figure B.5: GPS/Galileo/Compass/Altimeter all-in-view in the UTZ Type II model

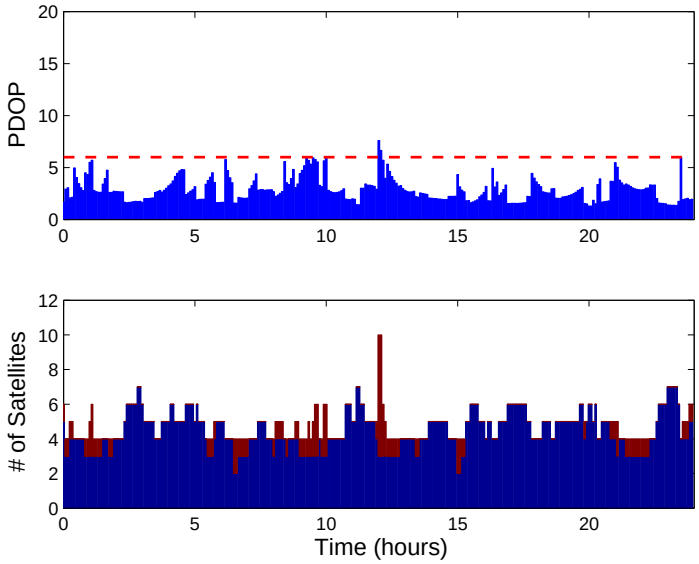

Figure B.6: GPS/Galileo/Compass/Altimeter and selective augmentation in the UTZ Type II model

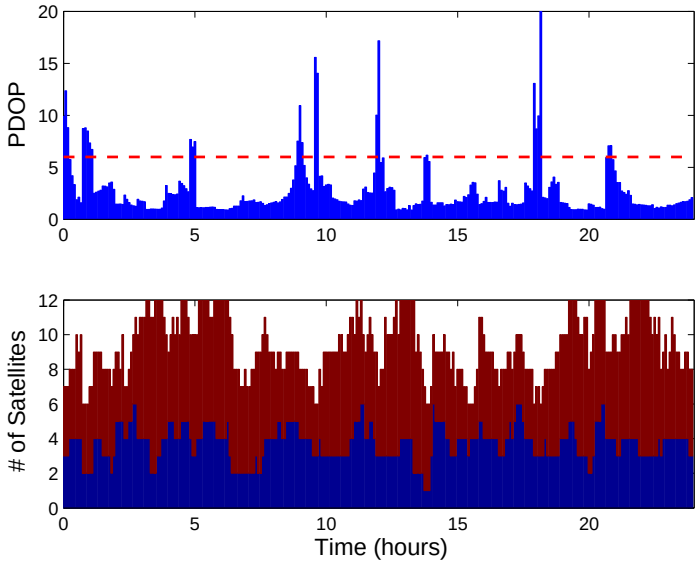

Figure B.7: GPS/Galileo/Compass/Altimeter all-in-view in the Dayton model

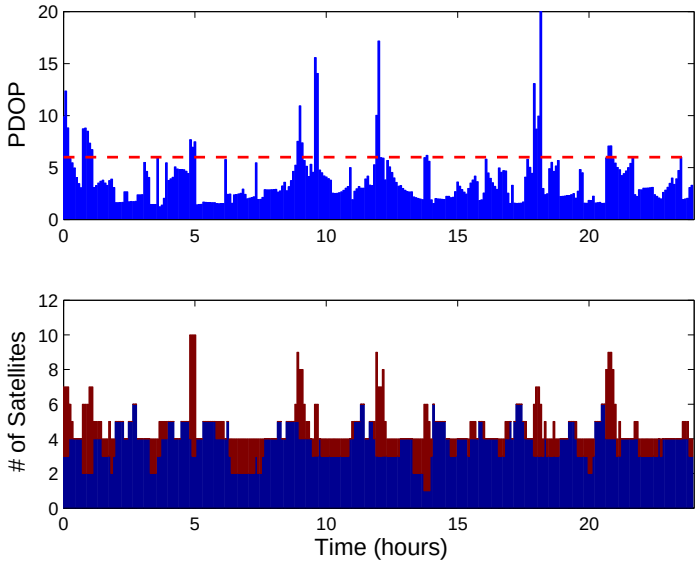

Figure B.8: GPS/Galileo/Compass/Altimeter and selective augmentation in the Dayton model

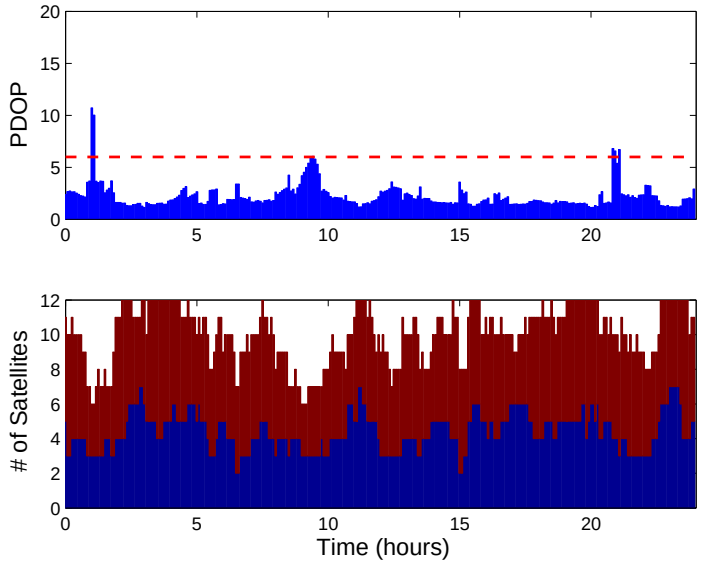

Figure B.9: GPS/Glonass/Compass/Altimeter all-in-view in the UTZ Type II model

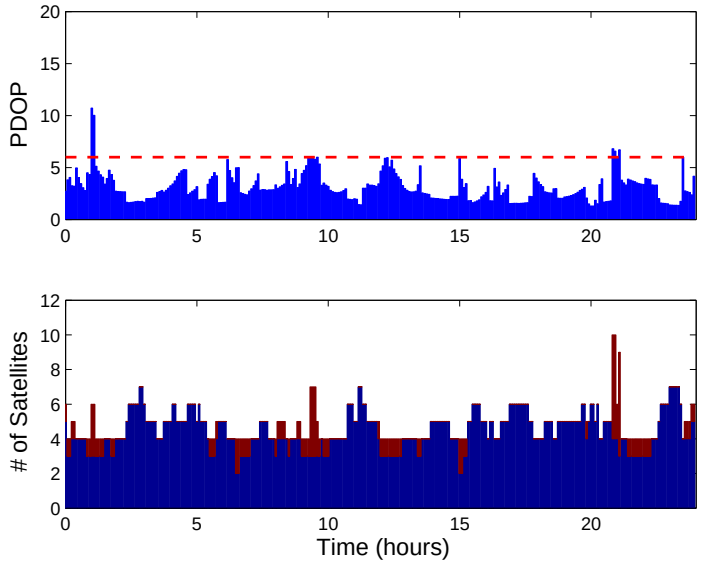

Figure B.10: GPS/Glonass/Compass/Altimeter and selective augmentation in the UTZ Type II model

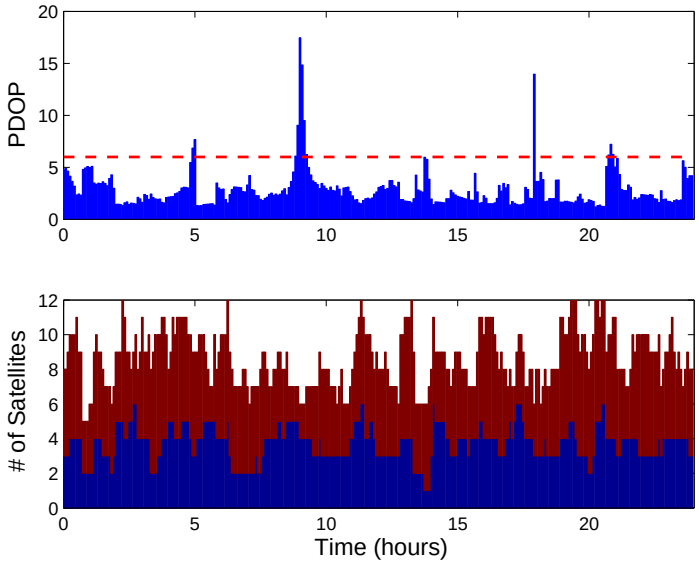

Figure B.11: GPS/Glonass/Compass/Altimeter all-in-view in the Dayton model

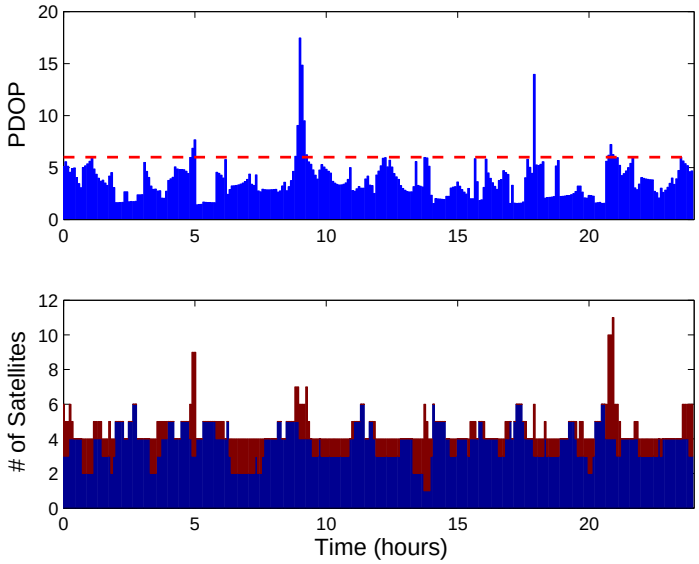

Figure B.12: GPS/Glonass/Compass/Altimeter and selective augmentation in the Dayton model

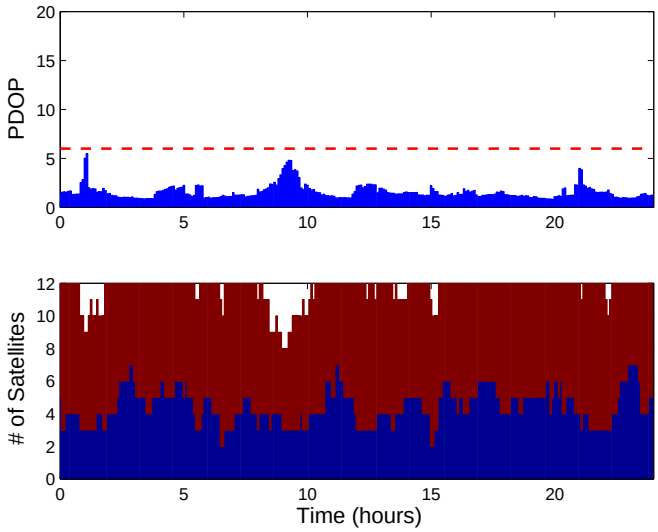

Figure B.13: GPS/Galileo/Glonass/Compass/Altimeter all-in-view in the UTZ Type II model

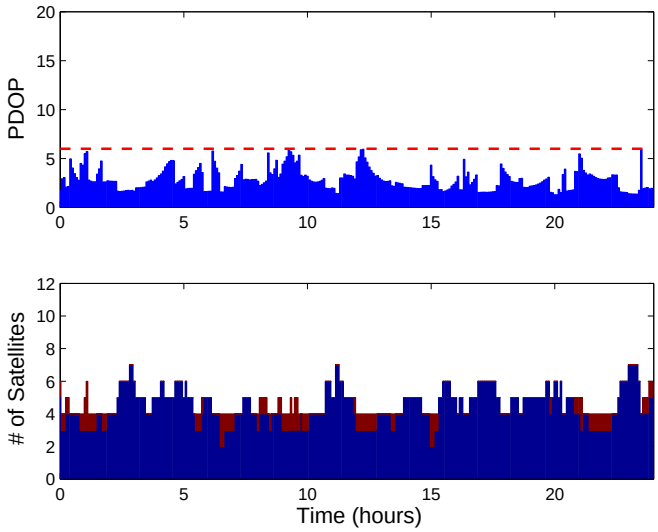

Figure B.14: GPS/Galileo/Glonass/Compass/Altimeter and selective augmentation in the UTZ Type II model

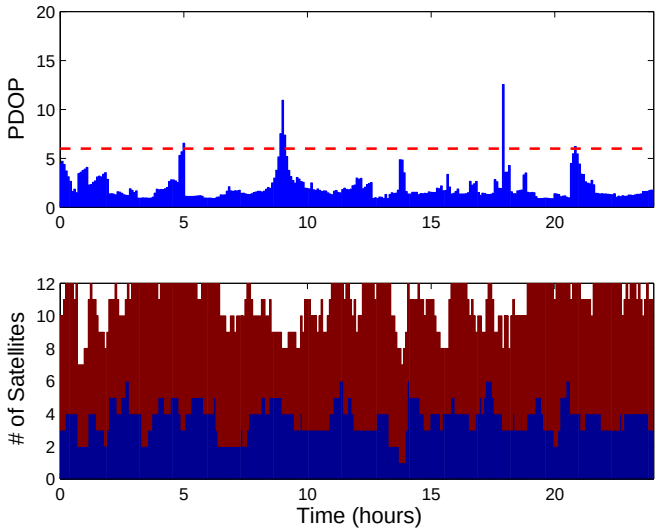

Figure B.15: GPS/Galileo/Glonass/Compass/Altimeter all-in-view in the Dayton model

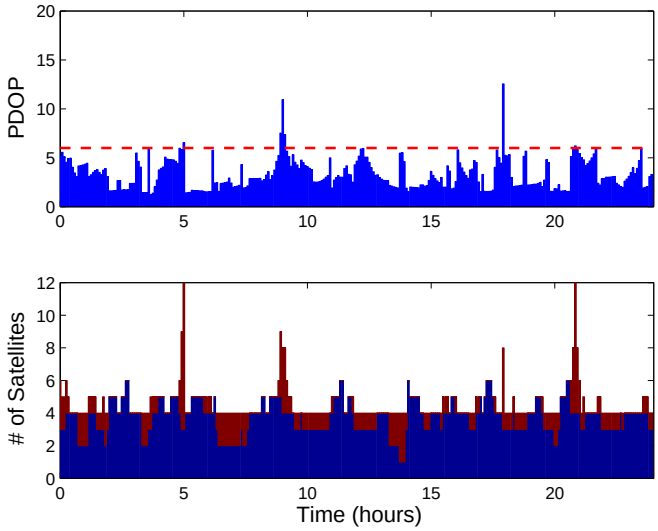

Figure B.16: GPS/Galileo/Glonass/Compass/Altimeter and selective augmentation in the Dayton model

Bibliography

[1] September 2011. URL ftp://ftp.glonass-ianc.rsa.ru/MCC/PRODUCTS.

[2] Bo, X. and B. Shao. "Satellite selection algorithm for combined GPS-Galileo navigation receiver". *4th International Conference on Autonomous Robots and Agents*, 149–154. ICARA, 2009.

[3] Brown, Robrt Grover and Patrick Y.C. Hwang. *Introduction to Random Signals and Applied Kalman Filtering*. John Wiley and Sons, 1997.

[4] Dutt, Srilatha Indira, G. Sasi Bhushana Rao, S. Swapna Rani, Swarna Ravindra Babu, Rajkumar Goswami, and CH. Usha Kumari. "Investigation of GDOP for Precise user Position Computation with all Satellites in view and Optimum four Satellite Configurations". *J. Ind. Geophys. Union*, 13(3):139–148, July 2009.

[5] Eissfeller, B., G. Ameres, V. Kropp, and D. Sanroma. "Performance of GPS, GLONASS and Galileo". 185–199, 2007.

[6] European Space Agency. *European GNSS Open Service Signal In Space Interface Control Document*. Technical report, European Union, September 2010.

[7] European Space Agency. "Galileo Fact Sheet", January 2011.

[8] European Space Agency. "Galileo Full Operational Capability Procurement", July 2011.

[9] Gao, Grace Xingxin, Alan Chen, Sherman Lo, David De Lorenzo, Todd Walter, and Per Enge. "Compass-M1 Broadcast Codes and Their Application to Acquisition and Tracking". *Proceedings of the 2008 National Technical Meeting of the Institute of Navigation*. 2008.

[10] Garmin. "Oregon Series Owner's Manual", September 2010.

[11] Gibbons, Glen. "China GNSS 101". *Inside GNSS*, January 2008.

[12] Gibbons, Glen. "China Will Release Draft Compass/Beidou-2 ICD on 'Step-by-Step' Basis". *Inside GNSS*, October 2009.

[13] GPS Joint Program Office. "NAVSTAR Global Positioning System Interface Specification", March 2006.

[14] GPS Joint Program Office. "Global Positioning System Precise Positioning Service Performance Standard", February 2007.

[15] GPS Joint Program Office. "Global Positioning System Standard Positioning Service Performance Standard", September 2008.

[16] Hegarty, Christopher J. and Eric Chatre. "Evolution of the Global Navigation Satellite System (GNSS)". *Proceedings of the IEEE*, 96(12):1902–1917, 2008.

[17] Kaya, F. and M. Saritas. "A Computer Simulation of Dilution of Precision in the Global Positioning System Using Matlab". 2005.

[18] Kihara, M. "Study of a GPS satellite selection policy to improve positioning accuracy". *Position Location and Navigation Symposium*, 267–273. IEEE, 1994.

[19] Langley, Richard B. "GLONASS: Review and Update". *GPS World*, 8(7):46–51, 1997.

[20] Langley, Richard B. "Dilution of precision". *GPS world*, 10(5):52–59, 1999.

[21] Maybeck, Peter S. *Stochastic Models, Estimation, and Control Volume 1*. Navtech Book and Software Store, 1994.

[22] Maybeck, Peter S. *Stochastic Models, Estimation, and Control Volume 2*. Navtech Book and Software Store, 1994.

[23] McKay, JB and M. Pachter. "Geometry optimization for GPS navigation". *Decision and Control, 1997., Proceedings of the 36th IEEE Conference on*, volume 5, 4695–4699. IEEE, 1997.

[24] Misra, P., B.P. Burke, and M.M. Pratt. "GPS performance in navigation". *Proceedings of the IEEE*, 87(1):65–85, 1999.

[25] Misra, Pratap and Per Enge. *Global Positioning System: Signals, Measurements and Performance*. Ganga-Jamuna Press, December 2001.

[26] Moudrak, A. *Timing Aspects of GPS-Galileo Interoperability: Challenges and Solutions*. Technical report, DTIC Document, 2004.

[27] Mutlu, Yasin A. *Aiding GPS with Additional Satellite Navigation Services*. Master's thesis, Air Force Intitute of Technology, March 2010.

[28] Oktay, Halit. *Airborne Pseudolites in a Global Positioning System Degraded Environment*. Master's thesis, Air Force Intitute of Technology, March 2011.

[29] Revnivykh, Sergey. "GLONASS Status and Progress", September 2010.

[30] Sairo, H., D. Akopian, and J. Takala. "Weighted dilution of precision as quality measure in satellite positioning". *Radar, Sonar and Navigation*, volume 150, 430–436. IET, 2003.

[31] Scientific Information Center. *GLONASS Interface Control Document*. Technical report, Russian Space Force, 1998.

[32] Tang, Wang, Gene Howell, and Yi-Hsueh Tsai. “Barometric Altimeter Short-Term Accuracy Analysis”. *Aerospace and Electronic Systems, IEEE*, 20(12):24–26, 2005.

[33] of the United States, The President. “National Space Policy of the United States of America”, June 2010.

[34] Vick, Alan, John Stillion, David R. Frelinger, Joel Kvitky, Benjamin S. Lambeth, Jefferson P. Marquis, and Matthew C. Waxman. *Aerospace Operations in Urban Environments Exploring New Concepts*. RAND, 2000.

[35] Yarlagadda, R., I. Ali, N. Al-Dhahir, and J. Hershey. “GPS GDOP metric”. *Radar, Sonar and Navigation*, volume 147, 259–264. IET, 2000.

[36] Yong, Yang and Miao Lingjuan. “GDOP results in all-in-view positioning and in four optimum satellites positioning with GPS PRN codes ranging”. *Position Location and Navigation Symposium*, 723–727. IEEE, 2004.

Vita

Second Lieutenant Brett Killion was born in Lubbock, Texas. He was appointed to the United States Air Force Academy in 2006. On 26 May 2010 he graduated as a Distinguished Graduate with a Bachelor of Science degree in Electrical Engineering and was commissioned as a second lieutenant. His first assignment was to the Air Force Institute of Technology at Wright-Patterson Air Force Base. Following graduation, 2^{d} Lt Killion will move to Ft. Meade, Maryland for his follow-on assignment at the National Security Agency.

REPORT DOCUMENTATION PAGE

Form Approved
OMB No. 0704-0188

PLEASE DO NOT RETURN YOUR FORM TO THE ABOVE ADDRESS.

1. REPORT DATE *(DD-MM-YYYY)*	2. REPORT TYPE	3. DATES COVERED *(From - To)*
22-03-2012	Master's Thesis	Sep 2010 - Mar 2012

4. TITLE AND SUBTITLE

Augmenting the Global Positioning System with Foreign Navigation Systems and Alternative Sensors

5a. CONTRACT NUMBER

5b. GRANT NUMBER

5c. PROGRAM ELEMENT NUMBER

6. AUTHOR(S)

Killion, Christopher B, 2d Lt

5d. PROJECT NUMBER

5e. TASK NUMBER

5f. WORK UNIT NUMBER

7. PERFORMING ORGANIZATION NAME(S) AND ADDRESS(ES)

Air Force Institute of Technology
Graduate School of Engineering and Management (AFIT/EN)
2950 Hobson Way
Wright-Patterson AFB OH 45433-7765

8. PERFORMING ORGANIZATION REPORT NUMBER

AFIT/GE/ENG/12-24

9. SPONSORING/MONITORING AGENCY NAME(S) AND ADDRESS(ES)

Intentionally Left Blank

10. SPONSOR/MONITOR'S ACRONYM(S)

11. SPONSOR/MONITOR'S REPORT NUMBER(S)

12. DISTRIBUTION/AVAILABILITY STATEMENT

Approved for Public Release; Distribution Unlimited

13. SUPPLEMENTARY NOTES

This material is declared a work of the U.S. Government and is not subject to copyright protection in the United States.

14. ABSTRACT

The United States Global Positioning System receives extensive use throughout the world. In areas with limited or partially obstructed views of the sky, a position solution can be difficult or impossible to obtain. Augmenting the GPS constellation by receiving signals from foreign satellite navigation systems as well using measurements from inertial and barometric sensors can increase the availability of a position solution in a degraded reception environment. This thesis investigates combining the GPS system with foreign navigation systems, a barometric altimeter, and inertial sensors. A model of downtown Dayton, OH was used as the simulated urban environment. A simulation was also made for an autonomous aerial vehicle flight through the model using a Kalman filter to combine the various sensors with GPS. Augmenting GPS showed great improvements in availability throughout the model of downtown Dayton. Furthermore, augmenting the GPS system with foreign systems allowed the autonomous aerial vehicle to successfully navigate in the simulation. This opens up the urban environment to more robust navigation solutions.

15. SUBJECT TERMS

^GPS, Augmentation, Kalman filter, urban environment

16. SECURITY CLASSIFICATION OF:			17. LIMITATION OF ABSTRACT	18. NUMBER OF PAGES	19a. NAME OF RESPONSIBLE PERSON
a. REPORT	b. ABSTRACT	c. THIS PAGE			Lt Col Michael J. Stepaniak
U	U	U	UU	124	19b. TELEPHONE NUMBER *(Include area code)* (937) 255-3636 x4603 michael.stepaniak@afit.edu

Reset

Standard Form 298 (Rev. 8/98)
Prescribed by ANSI Std. Z39.18